AD-A110 686 ROCKWELL INTERNATIONAL EL SEGUNDO CA NORTH AMERICAN --ETC F/8 1/3
SUPERSONIC CRUISE/TRANSONIC MANEUVER WING SECTION DEVELOPMENT S--ETC(U)
JUN 80 E BONNER, P GINGRICH F33615-77-C-3066
UNCLASSIFIED AFWAL-TR-80-3047 NL

END
DATE
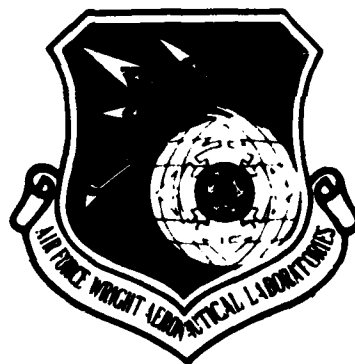FILMED
3 82
DTIC

MICROCOPY RESOLUTION TEST CHART

LEVEL

AFWAL-TR-80-3047

AD A110686

SUPERSONIC CRUISE/TRANSONIC MANEUVER WING SECTION DEVELOPMENT STUDY

Ellwood Bonner
Philip Gingrich

Rockwell International
North American Aircraft Division
P.O. Box 92098
Los Angeles, California

June 1980

DTIC
SELECTED
FEB 1 0 1982
H

Approved for public release; distribution unlimited

82 02 09 107
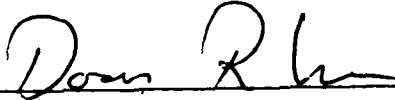
When Government drawings, specifications, or other data are used for any purpose. other than in connection with a definitely related Government procurement operation, the United States Government thereby incurs no responsibility nor any obligation whatsoever; and the fact that the government may have formulated, furnished, or in any way supplied the said drawings, specifications, or other data, is not to be regarded by implication or otherwise as in any manner licensing the holder or any other person or corporation, or conveying any rights or permission to manufacture use, or sell any patented invention that may in any way be related thereto.
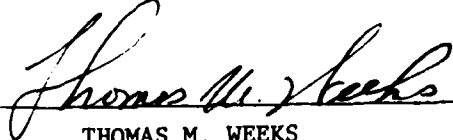
This report has been reviewed by the Office of Public Affairs (ASD/PA) and is releasable to the National Technical Information Service (NTIS). At NTIS, it will be available to the general public, including foreign nations.

This technical report has been reviewed and is approved for publication.

DOON R. LEE
Aerospace Engineer
Forward Swept Wing
Advanced Development Program Office

FOR THE COMMANDER

THOMAS M. WEEKS
Program Manager
Forward Swept Wing
Advanced Development Program Office

"If your address has changed, if you wish to be removed from our mailing list, or .if the addressee is no longer employed by your organization please notify AFWAL/FIF , W-PAFB, OH 45433 to help us maintain a current mailing list".

Copies of this report should not be returned unless return is required by security considerations, contractual obligations, or notice on a specific document.

REPORT DOCUMENTATION PAGE		READ INSTRUCTIONS BEFORE COMPLETING FORM
1. REPORT NUMBER AFWAL-TR-80-3047	2. GOVT ACCESSION NO. AD-A110686	3. RECIPIENT'S CATALOG NUMBER
4. TITLE (and Subtitle) Supersonic Cruise/Transonic Maneuver Wing Section Development		5. TYPE OF REPORT & PERIOD COVERED FINAL REPORT Aug 1977 - Nov 1979
		6. PERFORMING ORG. REPORT NUMBER
7. AUTHOR(s) Ellwood Bonner Philip Gingrich		8. CONTRACT OR GRANT NUMBER(s) F33615-77-C-3066
9. PERFORMING ORGANIZATION NAME AND ADDRESS Rockwell International, NAAD PO Box 92098 Los Angeles, CA 90009		10. PROGRAM ELEMENT, PROJECT, TASK AREA & WORK UNIT NUMBERS 62201F 2404 10 04
11. CONTROLLING OFFICE NAME AND ADDRESS Flight Dynamics Laboratory Air Force Wright Aeronautical Laboratories Air Force Systems Command, WPAFB, OH 45433		12. REPORT DATE June 1980
		13. NUMBER OF PAGES 67
14. MONITORING AGENCY NAME & ADDRESS(if different from Controlling Office)		15. SECURITY CLASS. (of this report) Unclassified
		15a. DECLASSIFICATION/DOWNGRADING SCHEDULE

16. DISTRIBUTION STATEMENT (of this Report)

Approved for public release, distribution unlimited

17. DISTRIBUTION STATEMENT (of the abstract entered in Block 20, if different from Report)

18. SUPPLEMENTARY NOTES

19. KEY WORDS (Continue on reverse side if necessary and identify by block number)

wing design, supersonic cruise, supercritical flow, transonic maneuver,
variable camber, aeroelastic tailoring

20. ABSTRACT (Continue on reverse side if necessary and identify by block number)

Computational aerodynamic design of advanced fighter wings with well-controlled transonic maneuver flow and high supersonic cruise efficiency is described.

DD FORM 1473 1 JAN 73   EDITION OF 1 NOV 65 IS OBSOLETE

PREFACE

This report documents the results of Flight Dynamics Laboratory contract F33615-77-C-3066, "Supersonic Cruise/Transonic Maneuver Wing Section Design Study," project 2404 10 04.

The Air Force study manager was Mr. Doon R. Lee AFWAL/FIMM. Mr. C. Wiler was the Rockwell program manager. Principal investigators were E. Bonner and P. Gingrich, of the Aerodynamics Group, with additional contributions by M. Crehan, K. M. Dunn, W. T. Karger, and S. White.

TABLE OF CONTENTS

LIST OF ILLUSTRATIONS

NOMENCLATURE

AR	Aspect ratio
b	Span
c	Chord
CG	Center of gravity
$\bar{c}$	Mean aerodynamic chord
C_D	Drag coefficient
CL	Lift coefficient
C_ℓ	Section lift coefficient or rolling moment coefficient
C_M	Moment coefficient
C_n	Yawing moment coefficient
CP	Pressure coefficient
C_P^*	Critical pressure coefficient
h, H	Altitude
M	Mach number
N_Z	Normal load factor
P_S	Specific excess power
$\overline{q^2}$	Mean-square fluctuating velocity
R_{ec}	Chord Reynolds number
S, SREF	Wing area
T	Thrust
t	Thickness
UDP	Unified distributed panel theory
W	Weight
X,Y,Z	Cartesian Coordinates (axial, vertical, and lateral)
α	Angle of attack

β	Angle of sideslip
β_w	Wall flow angle relative to local inviscid streamline
Γ	Dihedral
δ	Deflection
δ^*	Displacement thickness
ϵ	Downwash
η	Semispan fraction
θ	Twist
Λ	Sweep
λ	Taper ratio
ρ	Density
τ	Shear stress

SUBSCRIPTS

c	Camber or canard
cp	Center of pressure
D	Design
f	*Flap*
F	Fuel
L	Left
N	Normal to local wing generator
TO	Takeoff
t	Total
v	Vertical
w	Wing, wave, or wall
α, β	Differentiation with respect to α or β
$\perp$	Perpendicular
∞	Free-stream conditions
u	Upper
R	Root

INTRODUCTION

The vehicle characteristics required for supersonic cruise/transonic maneuvering missions are conflicting in both overall technology integration and configuration arrangement concepts; and on wing section design philosophies for a given configuration. The opposing requirements of efficient supersonic cruise (high sweep, fineness ratio, and wing loading) versus transonic maneuvering performance (moderate aspect ratio, reduced sweep, and low wing loading) must be addressed by the proper integration of advanced technologies.

The purpose of this study was to develop a design approach for multiple-design point tactical aircraft through the use of state-of-the-art computational methods. This inherently iterative process commenced with the definition of two basepoint designs, one tailored for supersonic cruise flight and the other for transonic maneuvers. Each was optimized to best accommodate the other role. At the conclusion of this dual design phase, it was determined that the mixed mission requirements can best be accomplished starting with a design configured for supersonic cruise.

This approach was then followed in the development of a compromise design tailored for both mission requirements. A systematic design approach is defined and exercised to develop a wing section with characteristics significantly improved from that of the Rockwell HiMAT design, which is used as a benchmark. Much of this improvement is due to the use of numerical methods that were not available for the HiMAT design, and the use of a supercruise design as a starting point, which was not required by the HiMAT mission.

During this study, several computational deficiencies were identified which should serve as targets for future methodology development.

SECTION I

APPROACH

GENERAL

The initial task of the study is to define two configurations designed for transonic maneuver and supersonic cruise, respectively. The off-design performance for each is then to be maximized. The results of task I were used to develop an approach for defining a compromise configuration having optimized performance at two design conditions: supersonic cruise and transonic maneuver. A schematic of the major tasks of the study is shown in Figure 1.

```
|←————— Task 1 —————→|←————————Task II————————→|

                     Phase I

Technology           Supercruise bias
   data                                          Phase III
   bank
                                                 Compromise design

                     Phase II

                     Maneuver bias
```
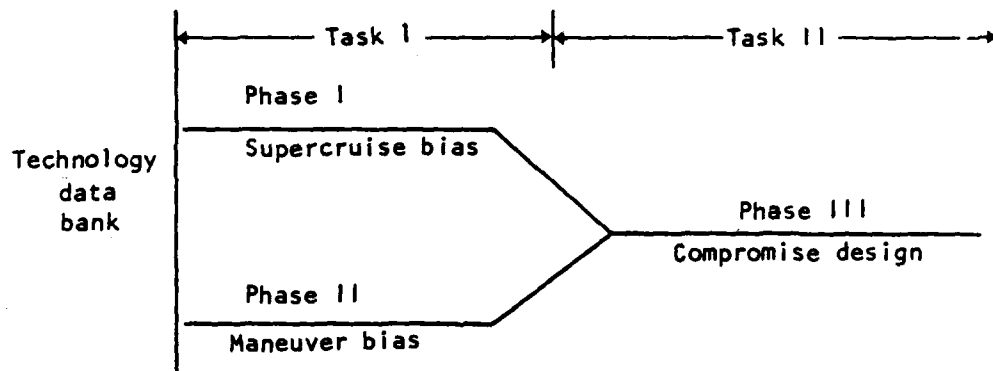
Figure 1. Study task effort.

The emphasis of the effort is the design and analysis of high-performance wings rather than conducting configuration studies. In order to assure the relevance of the designs, however, it is desirable to select missions and baseline vehicles that are consistent with current and projected Air Force requirements for tactical fighters. Basic missions are defined for separate supersonic cruise and transonic maneuver point designs, and currently existing designs selected for modification to meet the point design requirements and for maximization of off-design potential.

The selected baselines are used to define wing loading, thrust-to-weight ratio, and fuel fraction. This allows minimal sizing effort since this information is available from previous studies. It is noted that the study configurations will differ from their generic counterparts in order to obtain off-design improvements. That is, aspect ratio, sweep, component arrangement, and volume distribution, among other parameters, will be varied to establish the supersonic cruise and transonic maneuver baselines. However, the basic configuration characteristics (W/S, T/W, and W_F/W) will be retained so that the associated mission profiles will be appropriate.

METHODOLOGY

Linear potential flow analysis[1,2] is used to perform general configuration arrangement trade-offs and evaluation. Linear total configuration thickness and lifting solvers[3,4] are used to derive constrained subsonic vortex and supersonic pressure drag optimums.

Nonlinear potential flow analysis[5-9] is used at transonic maneuver conditions. Canard interference is approximated as a wing twist correction based on a downwash immersion philosophy. Design merit is judged on shockless or weak-shock supercritical flow considerations in conjunction with boundary layer[9-11] attached flow assessment.

The design methodology is summarized in Figure 2. Its application within the framework of specific supersonic bias, maneuver bias, and compromise configuration design cycles is detailed in the pertinent sections.

1. Three-dimensional linear potential theory

    a. Modal wave drag optimization
    b. Zero suction drag-due-to-life optimization
    c. Inverse solver

Sequential Application

2. Three-dimensional transonic potential theory

    a. Full-potential CONMIN inverse solver
    b. Modified Small Disturbance (MSD)
    c. Downwash immersion

3. Potential design boundary layer analysis
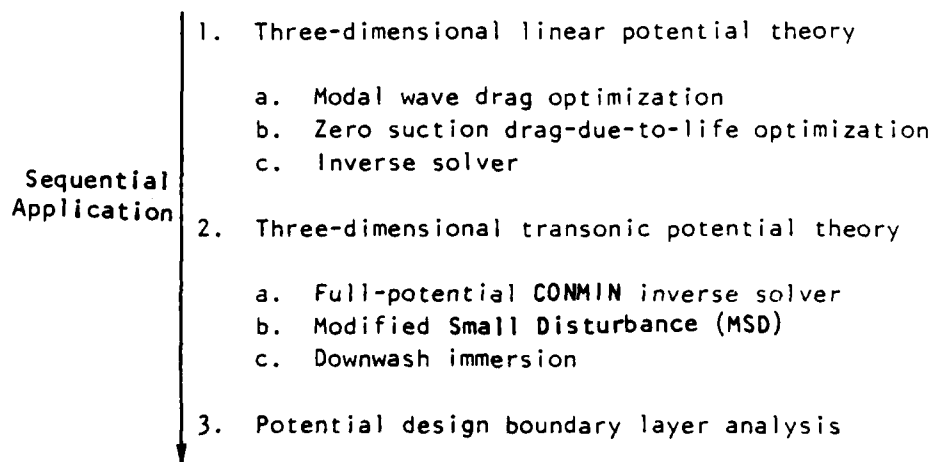
Figure 2. Design methodology.

SECTION II

SUPERSONIC CRUISE BIAS

BASELINE

The baseline configuration (Figure 3) and mission (Figure 4) selected for the supersonic bias design is the M = 1.6 NASA/Rockwell Supercruiser[12]. The vehicle performance is between a pure cruising and maneuvering fighter at supersonic conditions.

$$S_W = 185 \text{ ft}^2$$

$$W_{TO} = 15060 \text{ lb}$$

$$T/W_{TO} = .722$$

SEP at .9M/30K/5g = -157 fps

AR = 2.48
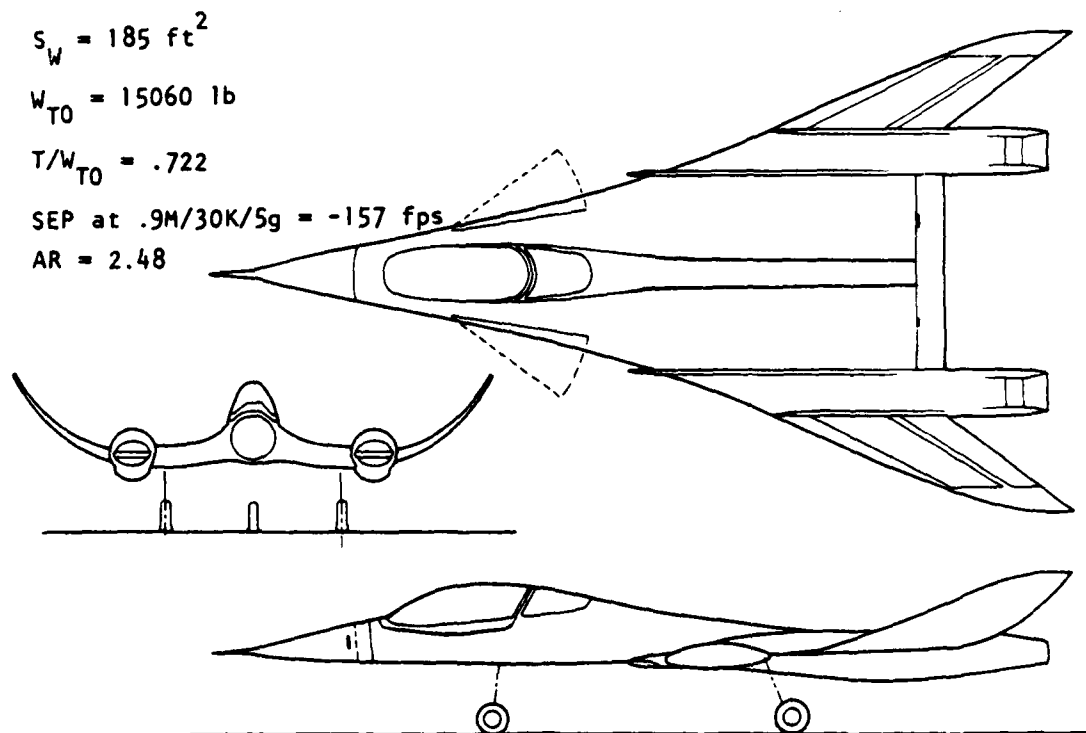
Figure 3. Rockwell Supercruise configuration.

A transonic maneuvering requirement was added to the supercruiser mission. A nominal condition of 4 g at M = 0.9, 30,000 feet was selected. Modification to the baseline will accordingly be made to improve the transonic aerodynamic maneuver potential.

CONFIGURATION DEVELOPMENT

The supersonic bias design retains the thrust-to-weight, wing loading, and basic mission profile of the Supercruiser configuration. The baseline modifications to improve transonic maneuverability are summarized in Figure 5.

Fuel allowance
for maneuver
at 30K, 1.6M

BCA, 1.6M

← 100.0 n mi → ← 200.0 n mi →
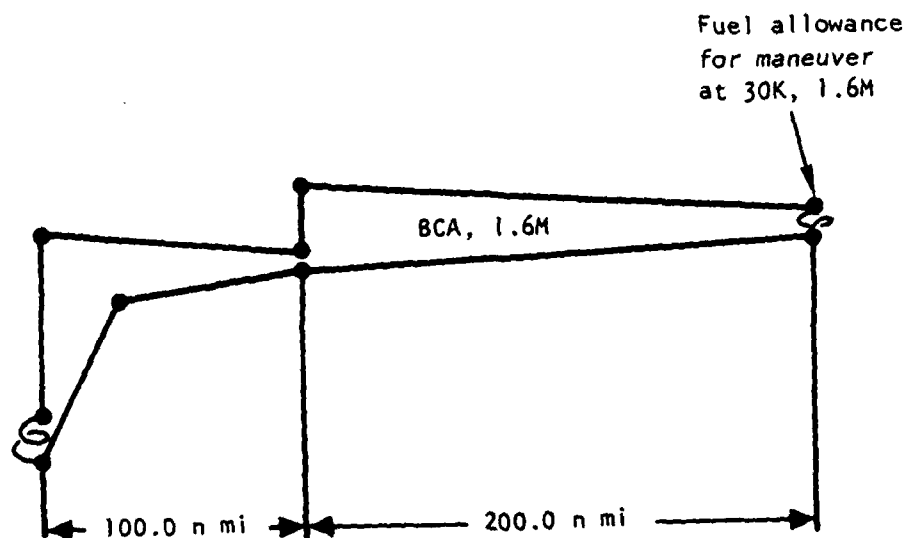
Figure 4.   Supercruise design mission.

D575-2A   D647-1   D647-2

High inlet   Low inlet

Upswept wings   Flat higher AR wing
No tail   Centerline Engine
Minimum wetted area   Canard
$AR, \lambda, \Lambda = 2.48, .32, 65$ Fuselage verticals
$S_w = 185$ $AR, \lambda, \Lambda = 3.5, .3, 55$
                           $S_w, S_c, S_v = 185, 35, 44$
$\dfrac{W_{TO}}{S} = 85$ $\dfrac{W_{TO}}{S} = 85$

Figure 5.   Supersonic bias configuration evolution.

4

The wing aspect ratio was increased from 2.48 to 3.5, and the leading edge sweep was reduced from 65 to 55 degrees. These modifications were made to increase the maneuver span load efficiency and reduce the perpendicular sectional lift (by one-third) for a given maneuver gross lift while retaining a subsonic leading edge at M = 1.6. A twin aft tail was incorporated for high angle-of-attack directional stability in place of the wingtip dihedral.
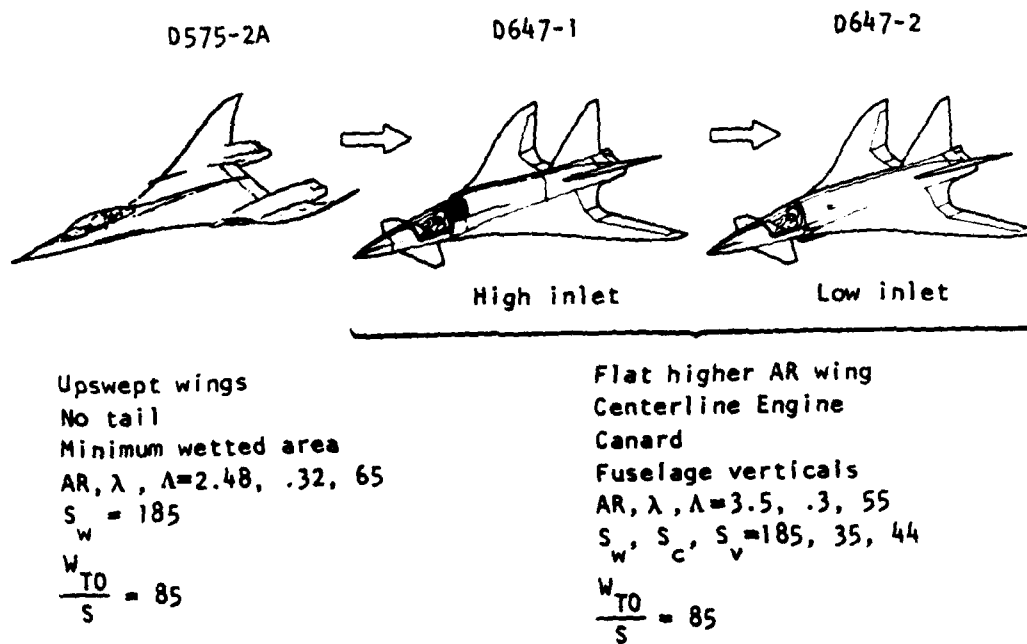
A simple centerline engine replaced the two midspan engines of the Supercruiser to provide more flexibility in the implementation of a variable camber system. The initial supersonic bias design, designated D647-1, was configured with an upper inlet. This placement allows reduced duct length, simplifies landing gear placement, and reduces foreign object damage, but is subject to high-angle-of-attack inlet distortion. A bottom inlet variant, designated D647-2, was subsequently developed. The duct was lengthened to position it ahead of the nosewheel, with gear loads taken out through a thin centerline divider in the duct. The inlet is contoured to fit the blended forebody and results in a high-aspect-ratio, minimum height duct which facilitates clearance of the nose gear and wing carry-through.

Wave drag analysis for both configurations was conducted, and the results are presented in Figure 6. The volumetric efficiency was not significantly different between the two arrangements. Thus, there was no preference so far as the wing design is concerned. Agreement with the Air Force study manager led to the selection of the lower inlet design, D647-2.
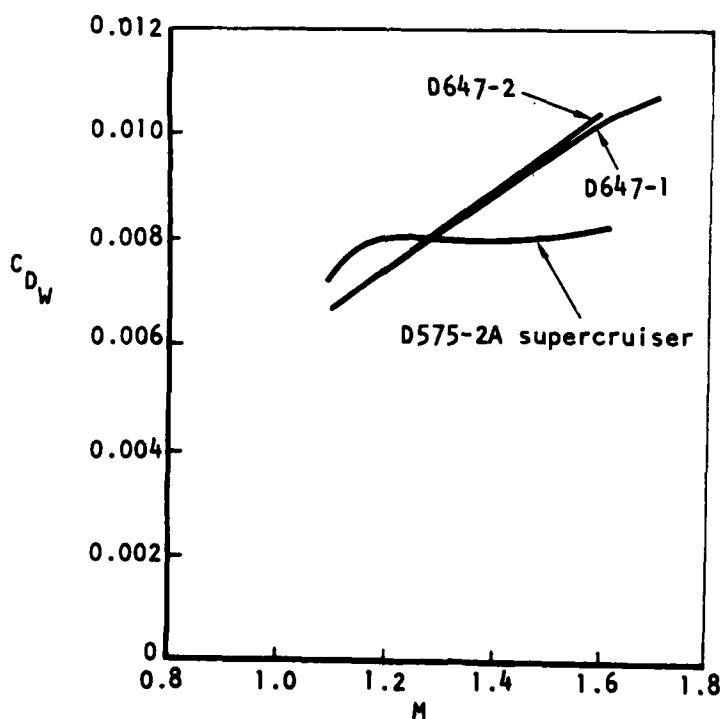

Figure 6. Supersonic bias wave drag.

The longitudinal stability was determined by using linear distributed panel analysis[1]. The stability variation with mach number is shown in Figure 7. To reduced supersonic trim drag, a 15-percent statically unstable balance was used at low speeds. The wing alone exhibits the typical stability shift. For the wing-canard-tail, a slight reversal is noted. An examination of the pressure distributions for the total configuration indicated a loss of tail effectiveness with increasing supersonic mach number. This circumstance can be used to advantage since it reduces the subsonic-supersonic stability shift. Several configuration modifications were made to determine the sensitivity of this stability reversal. For one case, the canard was vertically raised 7 inches. Although the shift from low speed to supersonic cruise was reduced, the potential pilot visibility problem indicated that the original baseline be retained.
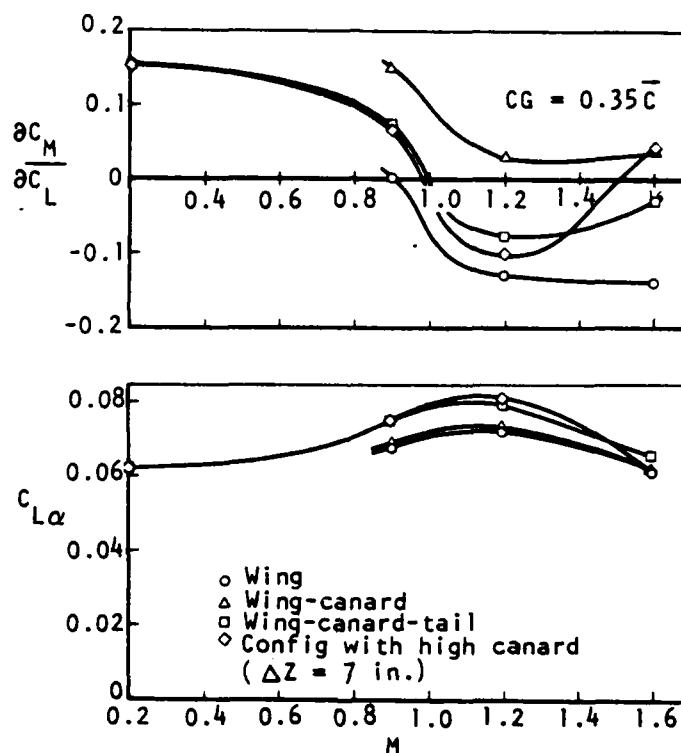

Figure 7. Supersonic bias longitudinal stability.

Having established the Supersonic Bias configuration general arrangement and balance, the wing design is initiated in accordance with Figure 8.

6
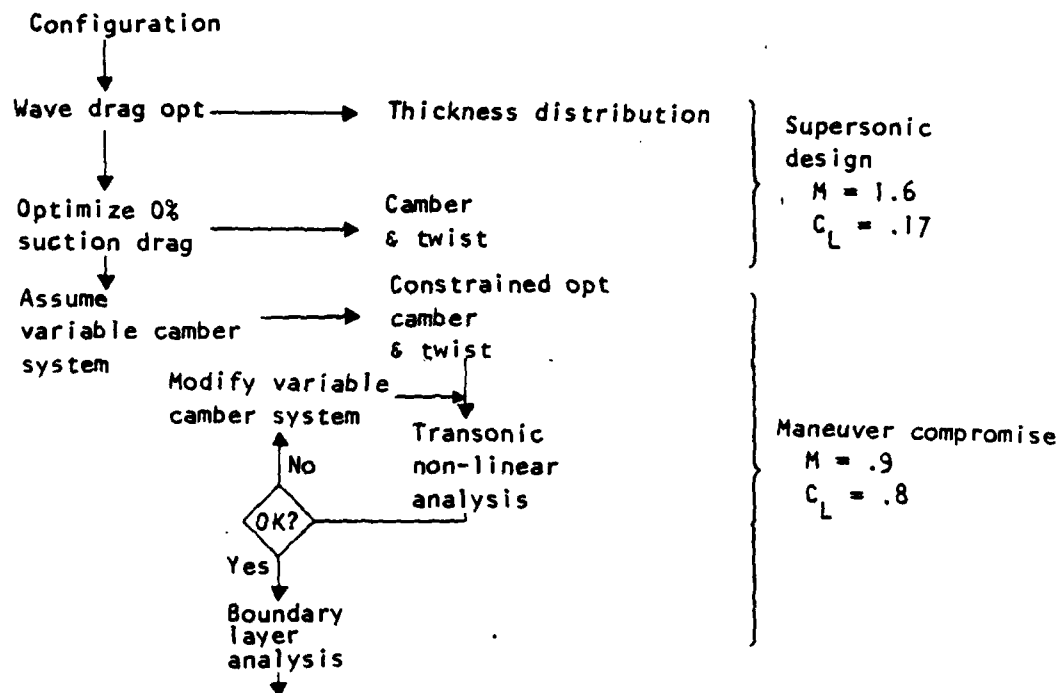
Figure 8. Supersonic bias design approach.

SUPERSONIC CRUISE DESIGN

The objective of the supersonic cruise design is to derive wing-body thickness and wing twist and camber for minimum drag at the M = 1.6 cruise point. The wave drag due to volume is minimized with the supersonic area rule[3] applied in a design mode. The geometry is perturbed by a set of harmonic functions. Lagrange's method for extremal problems with constraints is used. The constraints include cross-sectional area and wing thickness at arbitrary chordwise and spanwise positions. Drag-due-to-lift is minimized by a similar procedure[4]. This method uses the aerodynamic influence coefficients obtained with the unified distributed panel theory. The zero-percent suction drag is minimized subject to lift, moment, twist, camber over a specified region, and local section lift and moment constraints.

VOLUME OPTIMIZATION

The D647-2 configuration was simulated using the method of Reference 2. This simulation is shown in Figure 9. The wave drag of the baseline configuration is shown in Figure 10. The wing, canard, and tail surfaces were represented initially by 4-percent-thick airfoil sections. The optimization technique can minimize drag for each component separately or for a combination of components. Past experience has indicated that the best procedure is to optimize first the fuselage and then the lifting surfaces. The fuselage is usually 80 percent of the total volume. For lifting surfaces with small volume such as the canard and aft tail, optimization normally does not result in any significant drag reduction. The canard retained the baseline 64A004 section. The aft tail location exerted a significant influence on the wave drag and was reduced to 3-percent thickness.
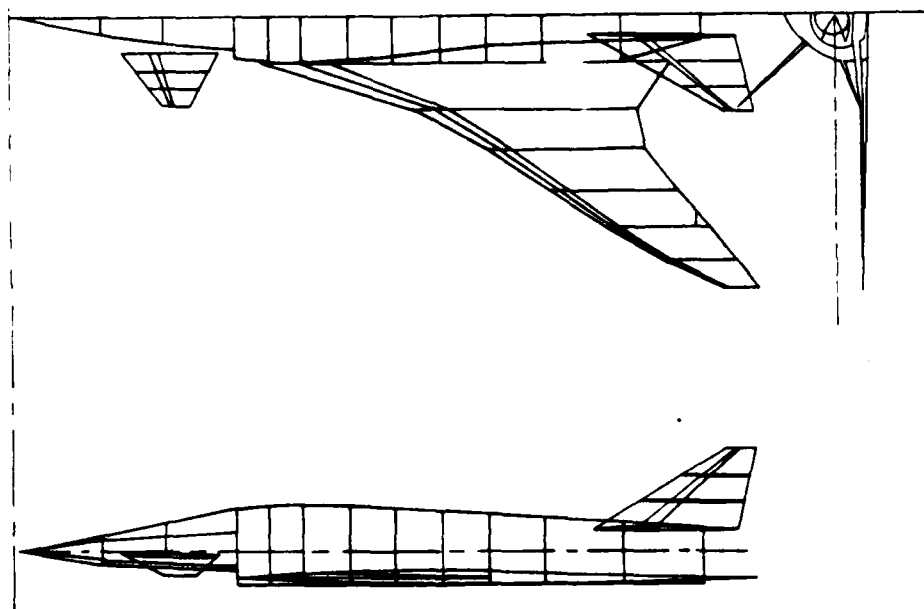
Figure 9. Linear analysis simulation.

The optimization procedure is summarized as:

1. Optimize the fuselage subject to constant volume and area (or height) constraints at the cockpit and inlet

2. Optimize the wing, and apply constraints sequentially until smooth spanwise and chordwise distributions are obtained

3. Reoptimize the fuselage with the revised wing

The fuselage was optimized at $M = 1.6$. The volume redistribution is shown in Figure 11. Wing optimizations were performed at $M = 1.4$ and 1.6. For some configurations, the wing, or even the wing-body, is optimized at a mach number lower than the design. Increased transonic acceleration capability is then traded with $M = 1.6$ cruise drag.

8

Figure 10. Supersonic bias optimized wave drag.

D647-2 LOWER INLET SUPERCRUISE
MACH= 1.600   DELTA VOLUME= 0.0

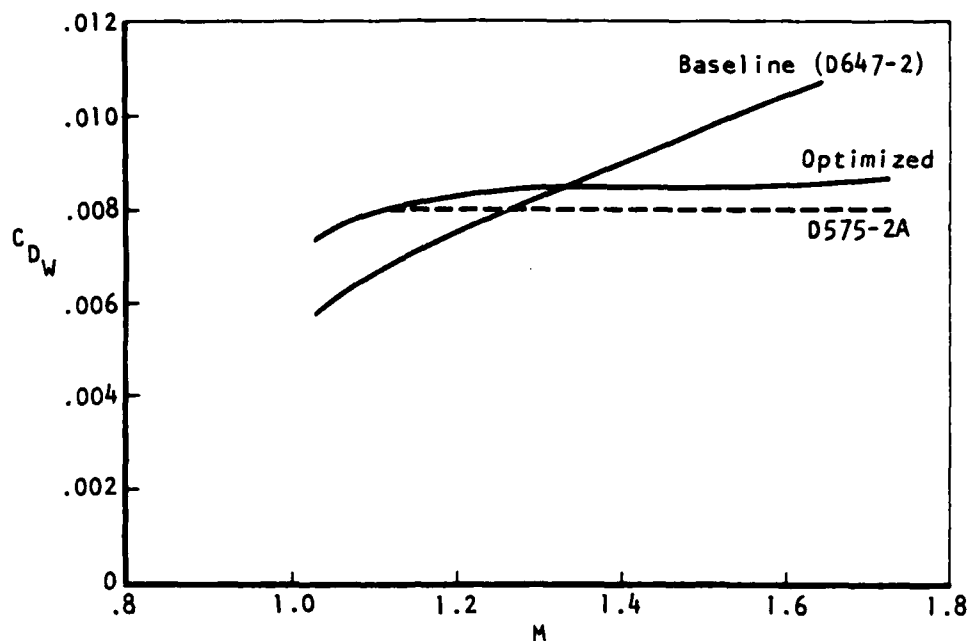| THETA	D/Q	OPT D/Q
-90.000	196.3729	196.J613
-45.000	230.3170	163.3929
0.0	274.8193	216.1028
45.000	243.8859	236.3040
90.000	386.4265	362.5640

TOTAL WAVE DRAG   245.7744   214.8765

| OPT H	OLD H	OPT A	OLD A	X	Y
0.000	0.000	0.0	0.0	91.286	0.0
9.699	9.384	362.866	351.732	140.934	0.0
12.684	12.306	733.534	695.238	174.950	0.0
17.168	17.168	1169.345	1168.338	213.673	0.0
21.032	21.032	1567.229	1567.229	213.572	0.0
21.152	21.662	1684.022	1724.612	231.611	0.0
20.735	21.910	1784.236	1893.825	250.390	0.0
19.376	21.491	1559.388	1729.623	276.115	0.0
18.133	20.710	1303.076	1579.612	303.615	0.0
19.023	19.941	1376.637	1443.193	326.977	0.0
20.165	19.210	1381.053	1315.646	352.044	0.0
21.250	18.488	1305.412	1130.857	382.657	0.0
18.658	17.238	1467.666	1012.158	426.078	0.0
15.708	15.708	918.381	918.383	470.301	0.0

——— Optimized
- - - - - Original
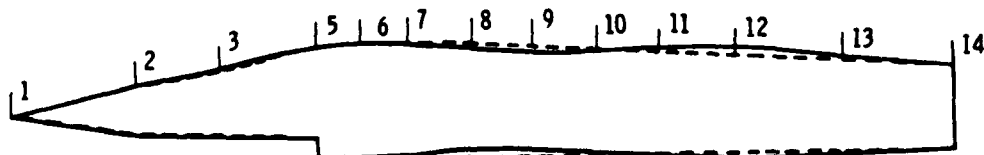
Figure 11. M = 1.6 fuselage optimization.
9

The derivation of wing thickness includes optimization of wave drag and then application of constraints at arbitrary spanwise and chordwise locations until smooth distributions are obtained. Results for the wing optimized at M = 1.4 are shown in Figure 12. Thickness distributions for optimum drag at M = 1.6 are shown in Figure 13. After the necessary constraints were added, the two thickness distributions were similar. The M = 1.6 wing design wave drag was 2 counts higher at M = 1.2 relative to the optimized M = 1.4 wing design. The M = 1.6 wing design was selected since the potential transonic acceleration improvement was small.
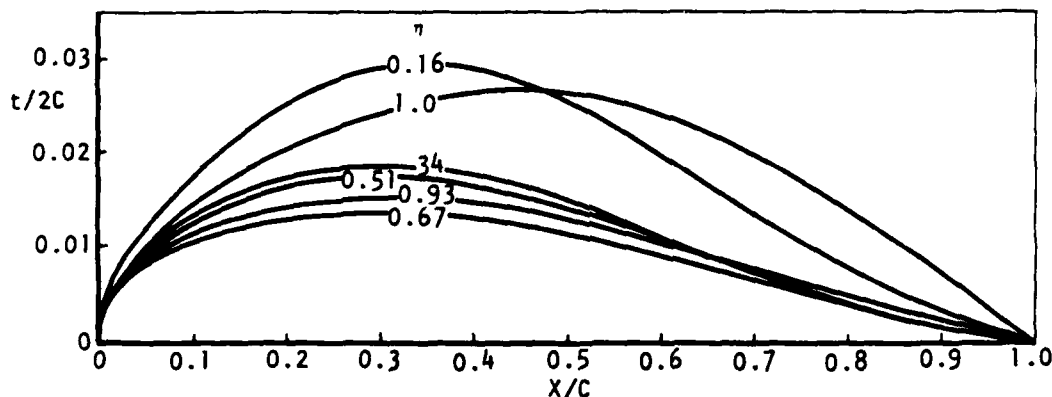

Figure 12. Wing thickness optimized at M = 1.4.

CAMBER OPTIMIZATION

Twist and camber for the lifting surfaces are derived with the linear theory optimization technique of Reference 4. A nominal cruise point was selected at M = 1.6, h = 50,000 feet. The lift coefficient is C_L = 0.169. The configuration was trimmed for the nominal center of gravity at $0.35\bar{c}$.

A solution was first obtained with no constraints except trim. The 0-percent suction drag polar is compared in Figure 14 with the flat-plate result. The wing twist is shown in Figure 15. This is a low wing configuration; therefore, the incidence change between the wing and body cannot be large.
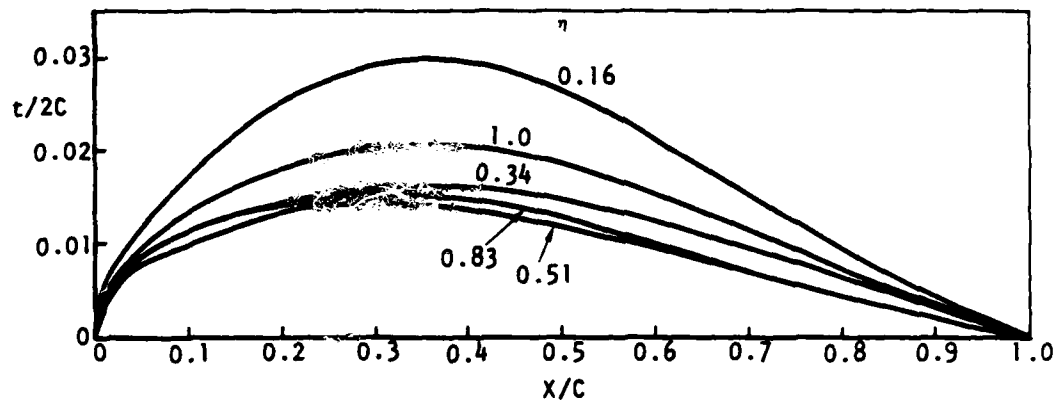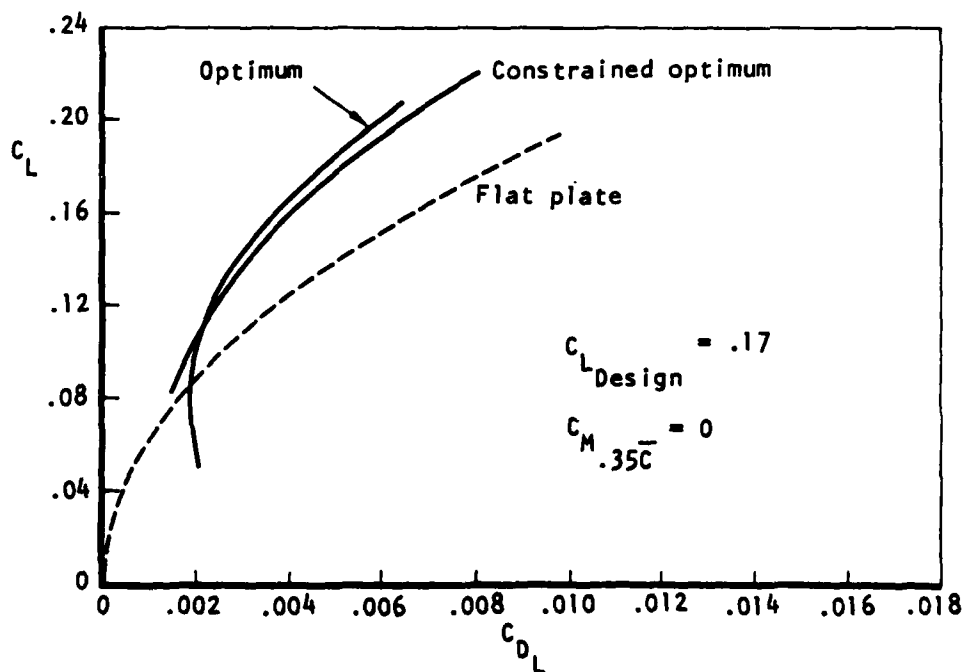
10

Figure 13. Wing thickness optimized at M = 1.6.

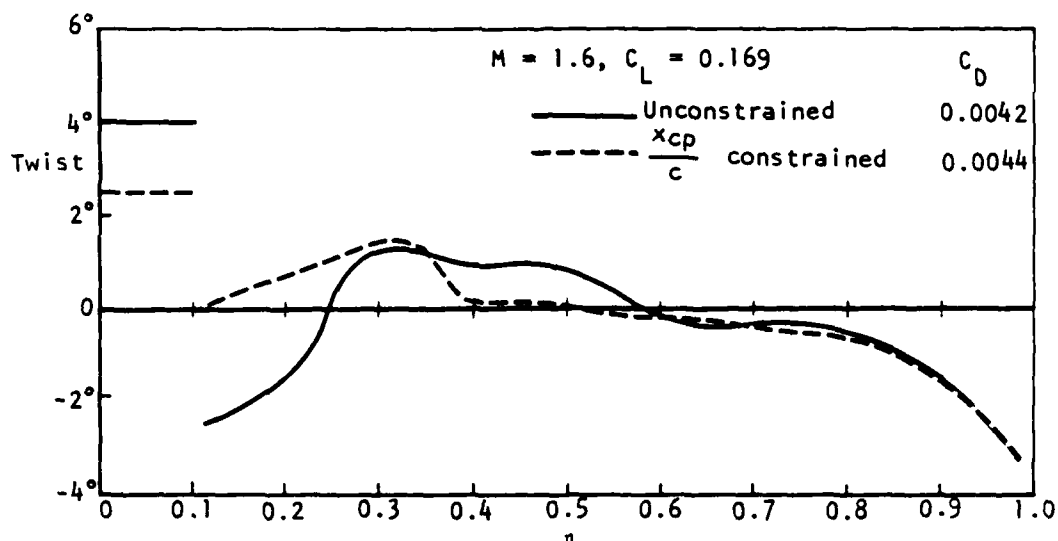Figure 14. Supersonic bias zero suction drag due to lift at M = 1.6.

Figure 15. Supersonic bias optimum wing twist.

Several solutions were obtained where constraints were sequentially added, first on the local center-of-pressure variation and then on the twist. An intermediate results is shown in Figure 15. Here, the $(X/C)_{Cp}$ was constrained to smooth the twist. Eventually, the wing root incidence and part of the twist were constrained. The final spanwise variations are shown in Figure 16. The camber for the canard and tail was small and was subsequently neglected without any perceptible drag penalty. The wing camber is shown in Figure 17. The drag polar is compared to the original optimum in Figure 14.

TRANSONIC MANEUVER DESIGN

In order to achieve the best maneuver performance at M = 0.9, a variable camber system was selected and evaluated with nonlinear potential theory methods. The variable camber is modified and reanalyzed until acceptable performance is obtained; i.e., the drag is minimized at the nominal maneuver lift coefficient.

For multisurface configurations, a transonic potential theory method is not available. The approach, as is discussed subsequently, is to consider each surface separately but to include the induced downwash. Thus, to minimize drag, the objectives are a spanload derived for minimum vortex drag, and transonic chordwise pressure distributions with, at most, weak shocks and only minor trailing edge separation.
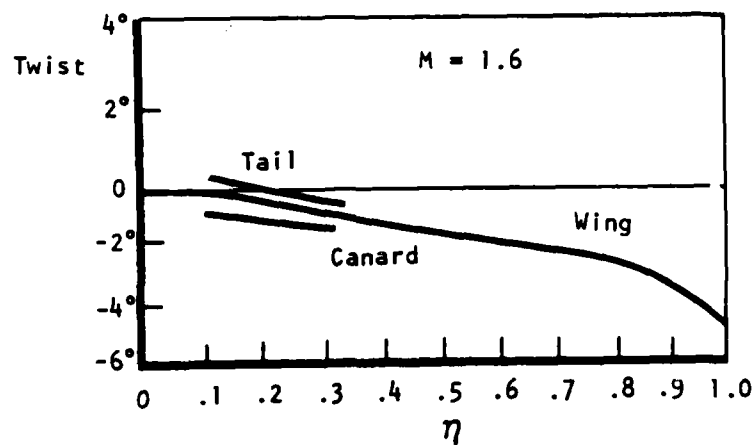
Figure 16. Supersonic design twist distributions.

a) Inboard

Figure 17. Supersonic optimum wing camber.

13
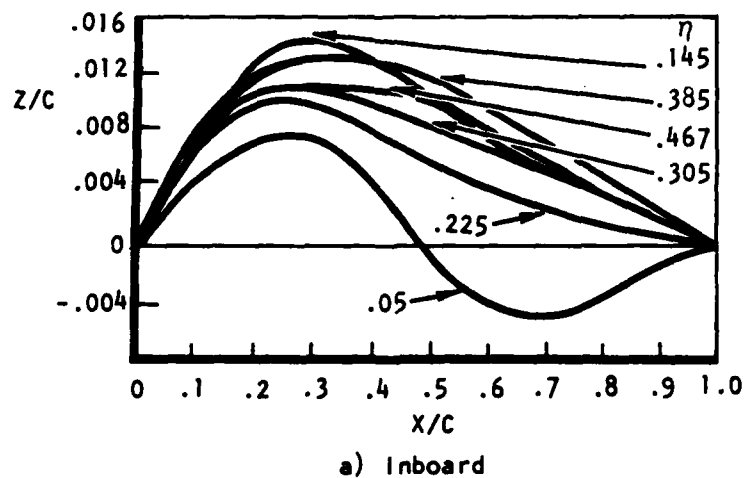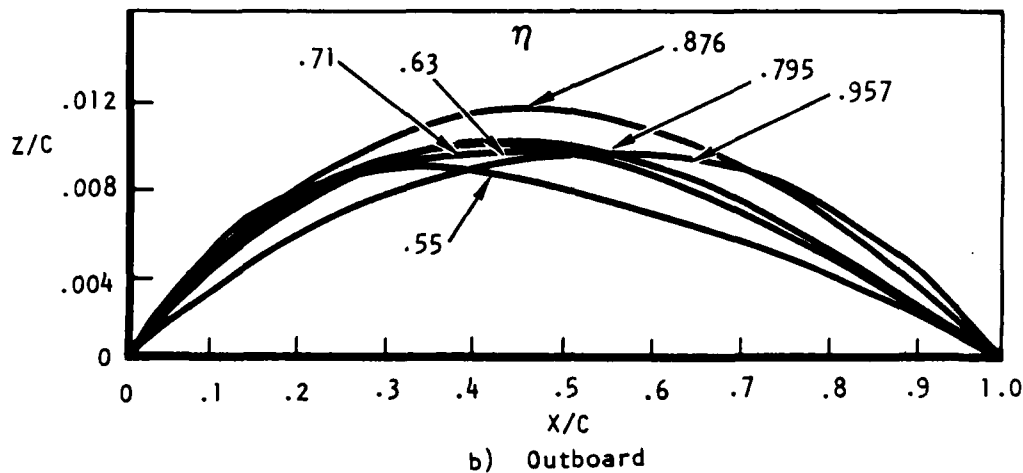
Figure 17. Supersonic optimum wing camber. (concluded)

The variable camber system considered includes wing leading and trailing edge devices, aeroelastic deformation, and an all-movable canard. The approach used was to select a particular variable camber system, solve for a linear theory optimum, and then analyze the wing with nonlinear potential methods. This procedure is summarized in Figure 8.

The configuration is modeled as shown in Figure 18, where certain planform regions are identified as deflectable surfaces. The supersonic design camber forms a set of constraints. The unknowns are the deflections and the twist at each span station. For each set of flaps, a solution is obtained for a given trimmed lift condition. The twist may then be constrained to limit the section lift on, for example, the wingtip or canard.

Figure 18. Linear analysis variable camber simulation.

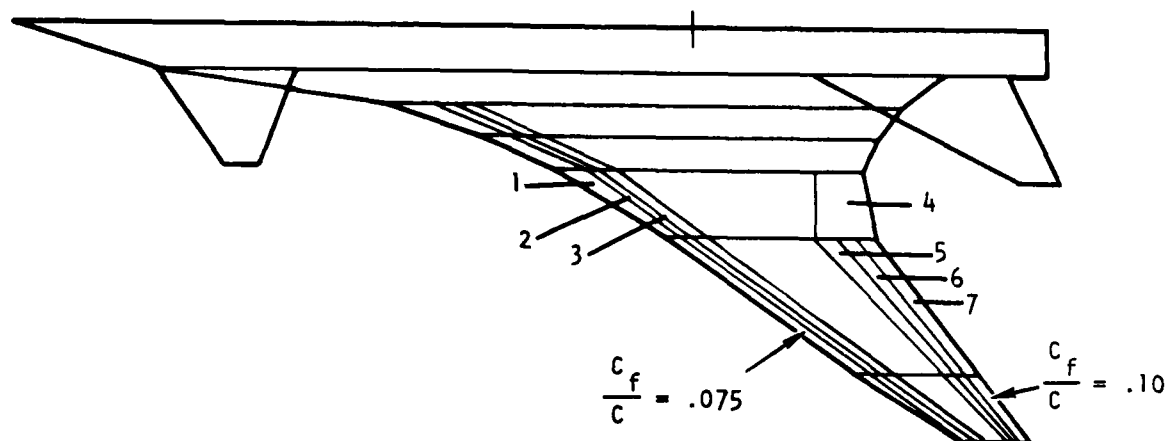The design condition at M = 0.9 was selected nominally at 4 g or a lift coefficient of C_L = 0.8. At this condition, the wing section lift was limited to C_ℓ ≤ 0.8. The linear theory designs were conducted at a C_L of 0.4. The drag and spanload are monitored for the C_L = 0.8 maneuver point. Optimizing at a lower lift does not significantly impact the vortex drag but does provide practical deflections of the variable camber devices.

In order to minimize the required aeroelastic twist increment, the first design considered only leading edge variable camber (flaps 1 through 3 of Figure 18). An optimization was obtained at M = 0.9 for a lift coefficient of C_L = 0.4. The wing twist and canard incidence were subsequently constrained to obtain smooth twist distributions and limit the loading on the canard and wingtip. The canard was assumed to be an all-movable device. The incidence was constrained so that the section lift on the canard was less than C_ℓ = 0.4 at the 4 g maneuver condition since the average sweep is low.

Section lift distributions for the wing and canard are shown in Figure 19 for a condition near the maneuver point, C_L = 0.77. The wing and canard twist distributions are shown in Figure 20. The optimization produced a set of deflections which, in addition to the supersonic camber, resulted in the camber distributions shown in Figure 21.

15
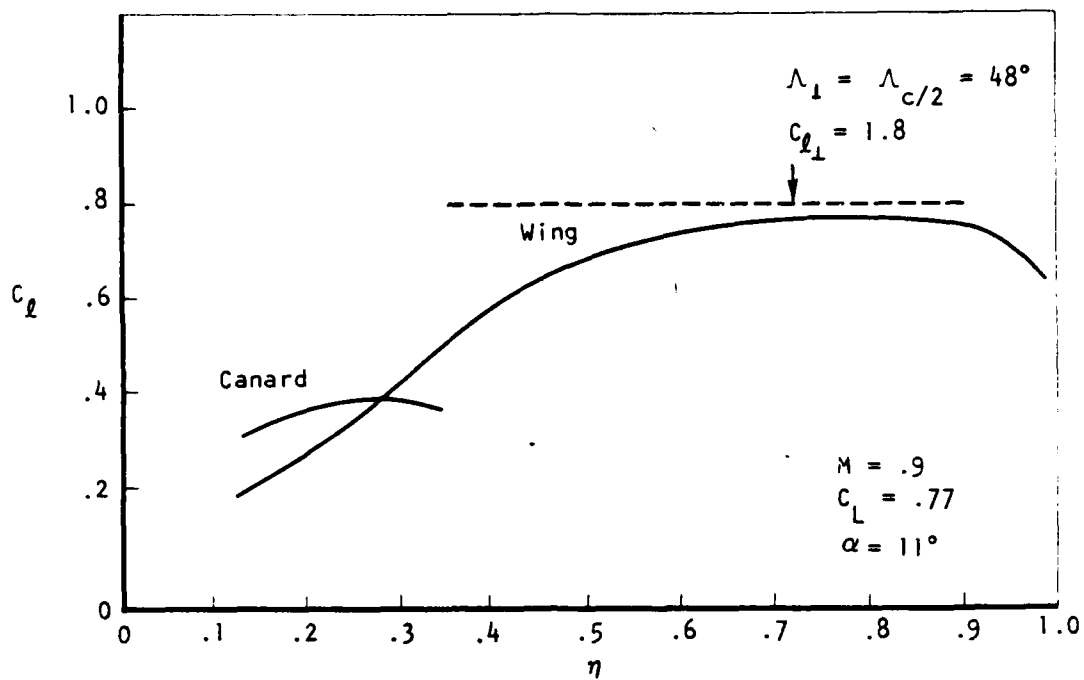
Figure 19. Linear theory section lift at maneuver design point.
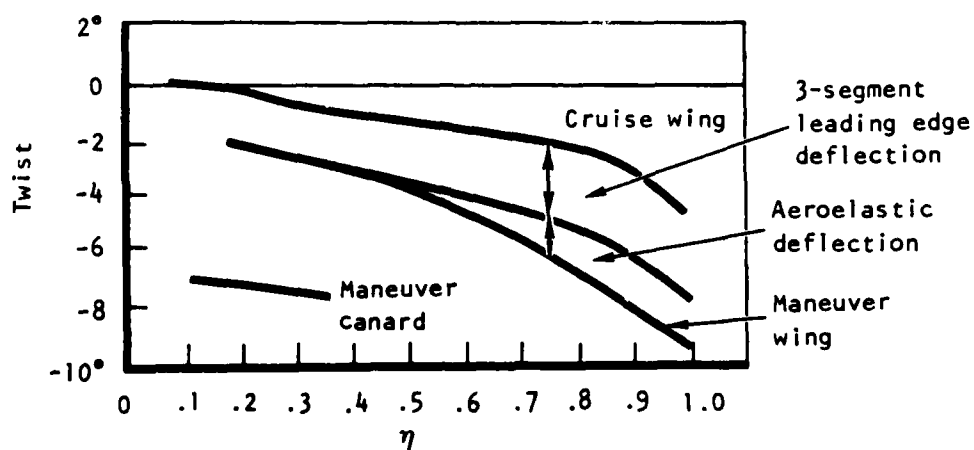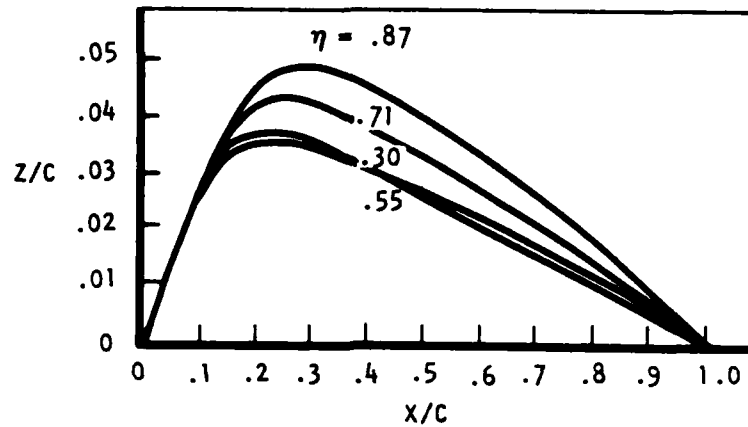

Figure 20. Maneuver twist requirements.

Figure 21. Supersonic bias maneuver camber.

An outboard wing section at $\eta = 0.71$ was analyzed with the transonic yawed wing program (5,10) to assess the flow quality. The upper surface pressure distribution is shown in Figure 22 for a lift of $C_\ell = 0.6$.
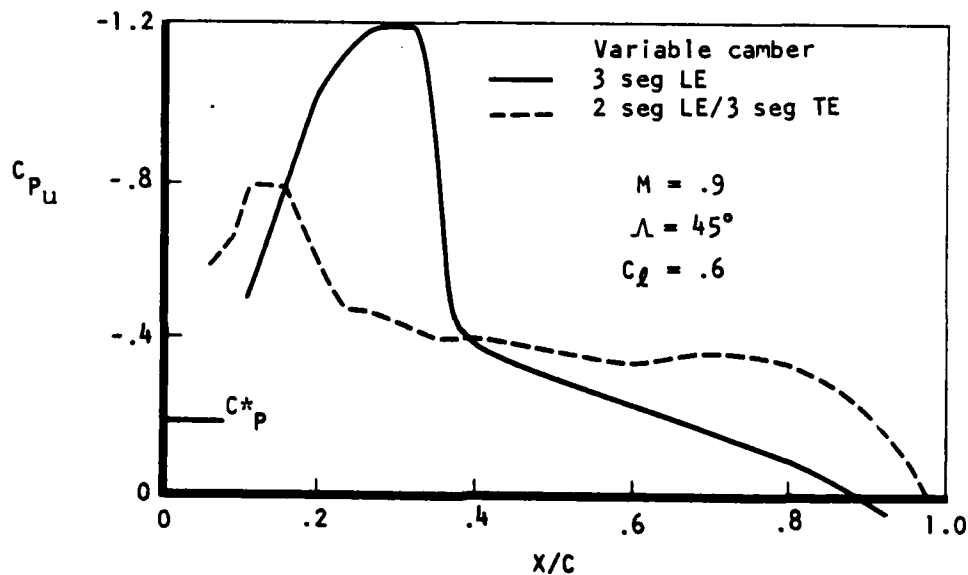

Figure 22. Transonic yawed wing analysis of wing section at $\eta = 0.71$.

A strong shock exists at 40-percent chord. This result indicated that trailing edge deflection would be required to increase the aft loading. Several optimizations were performed using various combinations of flap regions 1 through 7, as shown in Figure 18. The design selected for further analysis used all but flap 3. That is, the leading edge device extent was nominally 15-percent chord. This chordwise extent was selected initially as the probable minimum that would produce acceptable flow quality.

The camber that was derived is shown for a typical wing section, $\eta = 0.71$, in Figure 23. The supersonic camber is noted The twist between cruise and maneuver was similar to the previous result. However, the increment due to bending will be larger. A yawed wing calculation is compared with the first concept in Figure 22. This second design was selected for the initialization of the three-dimensional transonic design cycle.

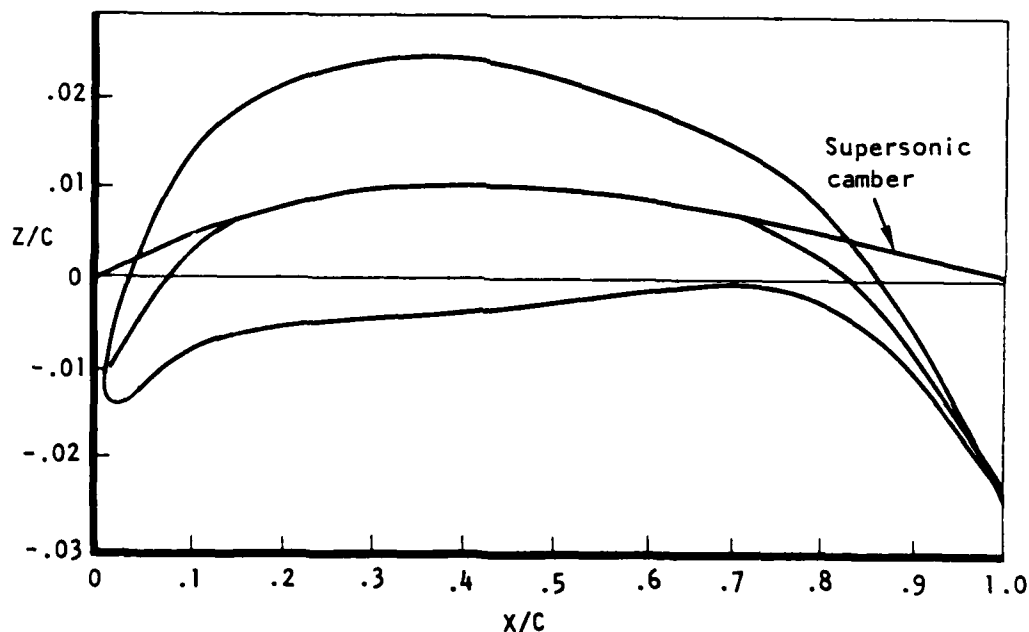Figure 23. Maneuver section at $\eta = .713$.

TRANSONIC DESIGN OF VARIABLE CAMBER SYSTEM

The design of the variable camber system for the M = 0.9 maneuver condition is accomplished with a design/analysis cycle using the conservative nonlinear full-potential code FLO27 [6]. The geometry is modified to obtain weak shocks and minor trailing edge separation by selecting alternate hinge lines and deflections.

In preparation for the nonlinear analysis, the canard-induced downwash was obtained with linear theory. This downwash is used to correct the wing twist distribution. The wing-alone transonic solution will then be indicative of the wing flow characteristics in the presence of the canard. The downwash is reasonably constant at any one spanwise location. The spanwise variation of the downwash is shown in Figure 24. The large discontinuity at the canard tip location is due to the close vertical proximity of the surfaces. A similar calculation was made to determine the induction effect of the tail. The effect on the wing was negligible.
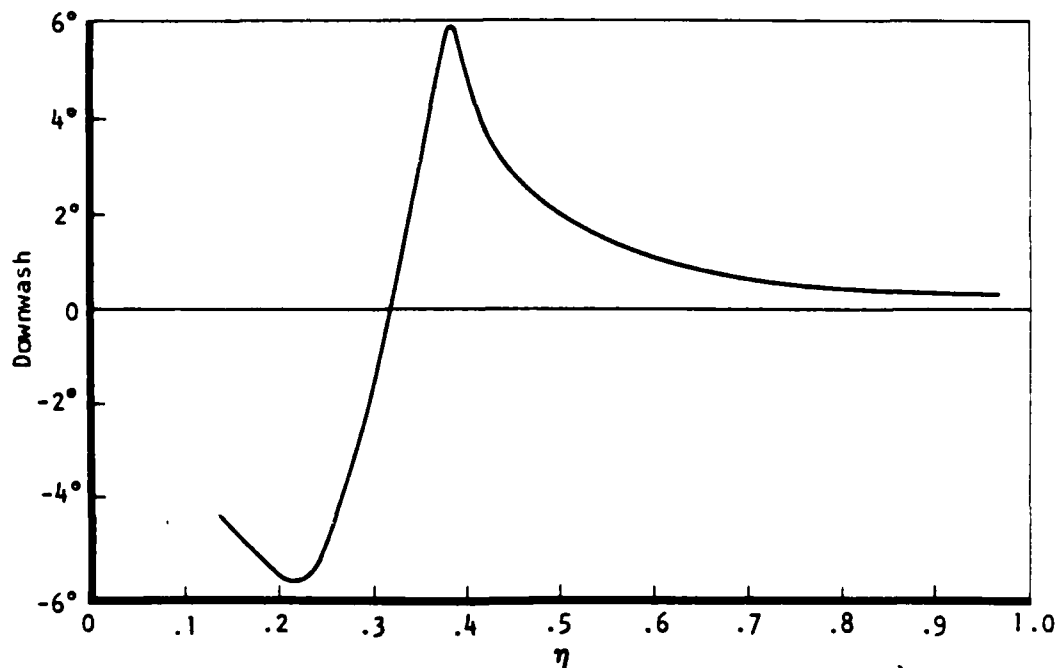

Figure 24. Canard induced downwash on wing plane.

The basic simulation was altered to a wing and canard extended to the centerline (Figure 25). The body loading is thus partitioned between the canard and wing. The wing is constructed with a given twist and deflection distribution.
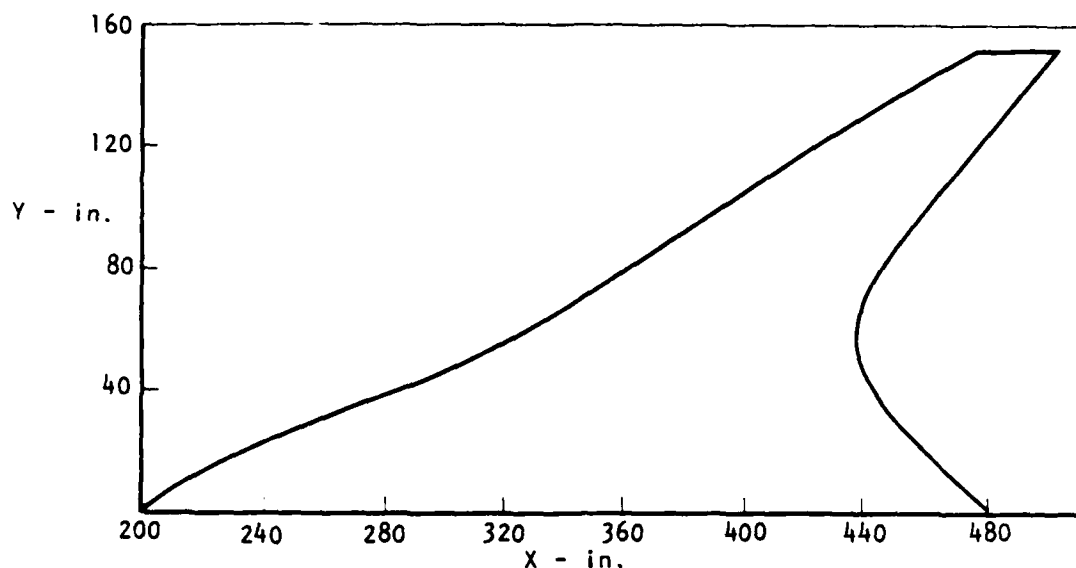
Figure 25. Maneuver computational planform.

The design was analyzed for a mesh of 80 by 8 by 16 grid points. Pressure distributions for the outboard wing are shown in Figure 26. For this mesh, the solution density for the streamwise coordinate is as indicated. The spanwise grid produces solutions at 10-percent span increments. No strong shocks were indicated except for the leading edge region. Separation was predicted by a viscous yawed wing analysis. Because of the high leading edge velocities, it was felt that a fine-grid solution would not be warranted at that time. The leading edge geometry would first be modified.

For the first modification (-A), the leading edge deflection was increased approximately 20 percent. The solution still indicated a large negative leading edge pressure peak. The second modification (-B) consisted of a still larger deflection, but the hinge line remained in the same position (approximately 15- to 20-percent chord). For the section at 71-percent span, the change in camber for the -B configuration is shown in Figure 27.

20

Figure 26. Pressure distribution for baseline variable camber.

Figure 27. Variable camber at $\eta = .71$ for maneuver condition.

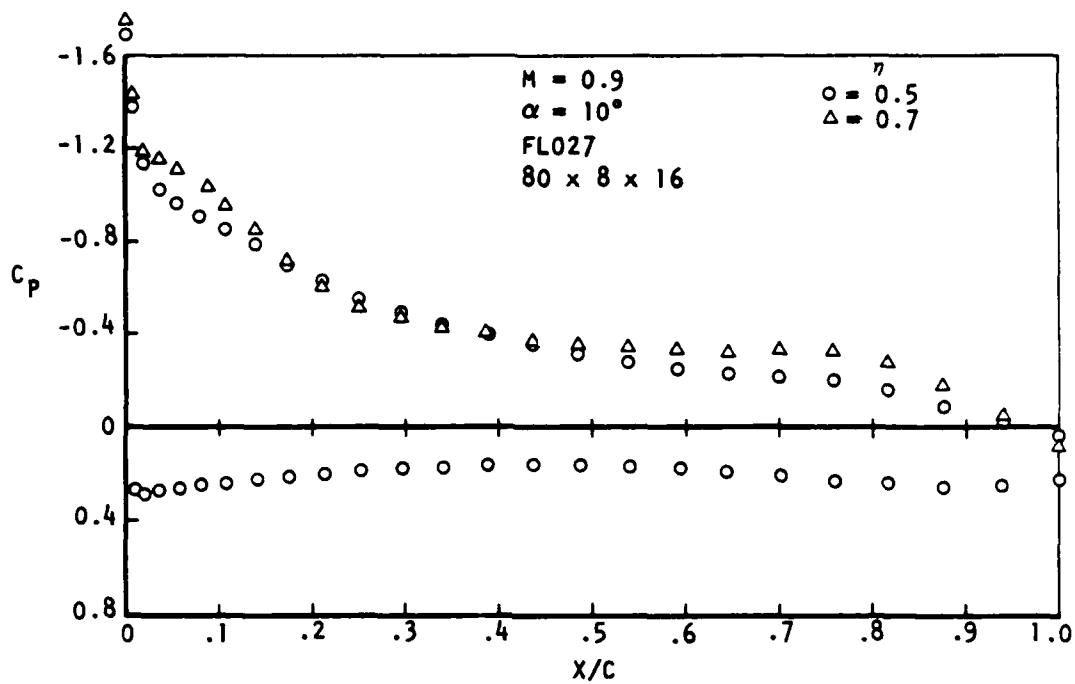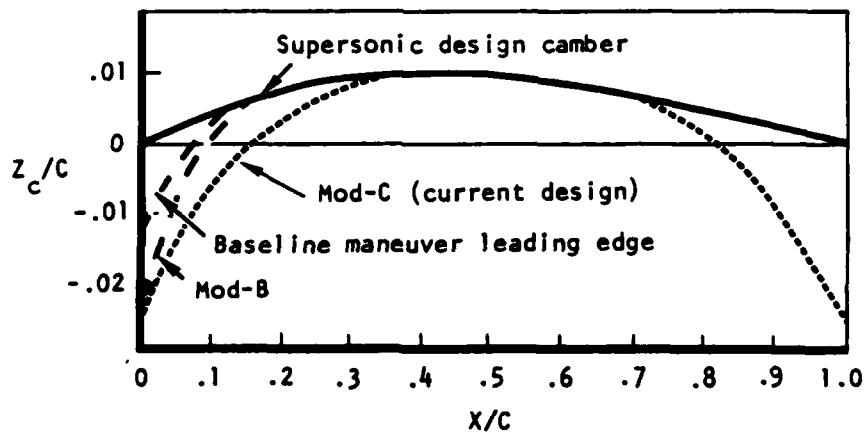Medium- and fine-grid solutions were obtained for the -B camber system. The wing section lift distribution is compared with the linear theory results in Figure 28. Linear theory calculations are shown for the total configuration (wing, body, canard, and aft tail) and for the wing-alone simulation with canard downwash.
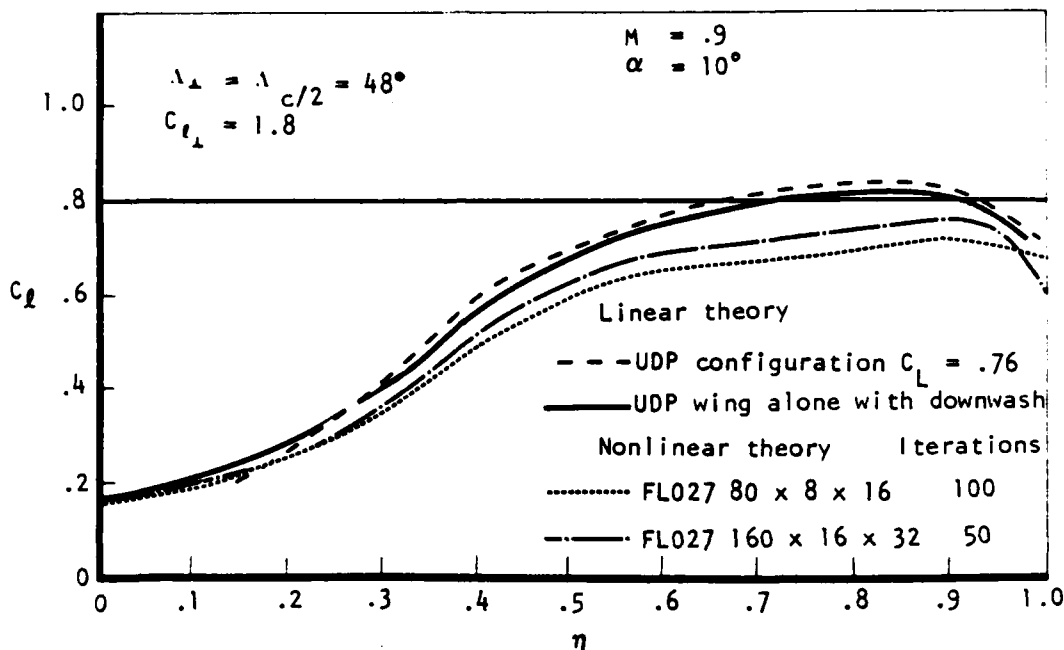
Figure 28. Section lift distribution, MOD-B.

Medium-mesh (80 by 80 by 16) pressure distributions are shown in Figure 29 for $\alpha = 10^o$, M = 0.9, for the -B modification. The leading edge peak has been reduced to the extent that separation does not occur. With the yawed wing integral boundary layer analysis, boundary layer characteristics were obtained for both laminar and turbulent initial conditions at the attachment line. In neither case was separation predicted. Results with the mesh density doubled (160 by 16 by 32) are shown in Figures 30 and 31 for 50- and 70-percent span, respectively. As noted, the leading edge peak decreased when the grid was refined. This behavior is attributed to the higher resolution available with the fine grid. Since this result was not expected, the indication is that any further modifications should be analyzed with the fine grid in order to make a proper judgement.

Figure 29.   Maneuver pressure distribution, MOD-B.

Figure 30.   Transonic pressure distribution, MOD-B, η = .5.

23

Figure 31. Transonic pressure distribution, MOD-B, η = .7.

The solution for configuration -B indicated a strong supersonic-to-supersonic swept shock, as noted in Figure 31. This shock extended from 55- to 90-percent span. Separation at the foot of the shock was predicted by the yawed wing viscous analysis.

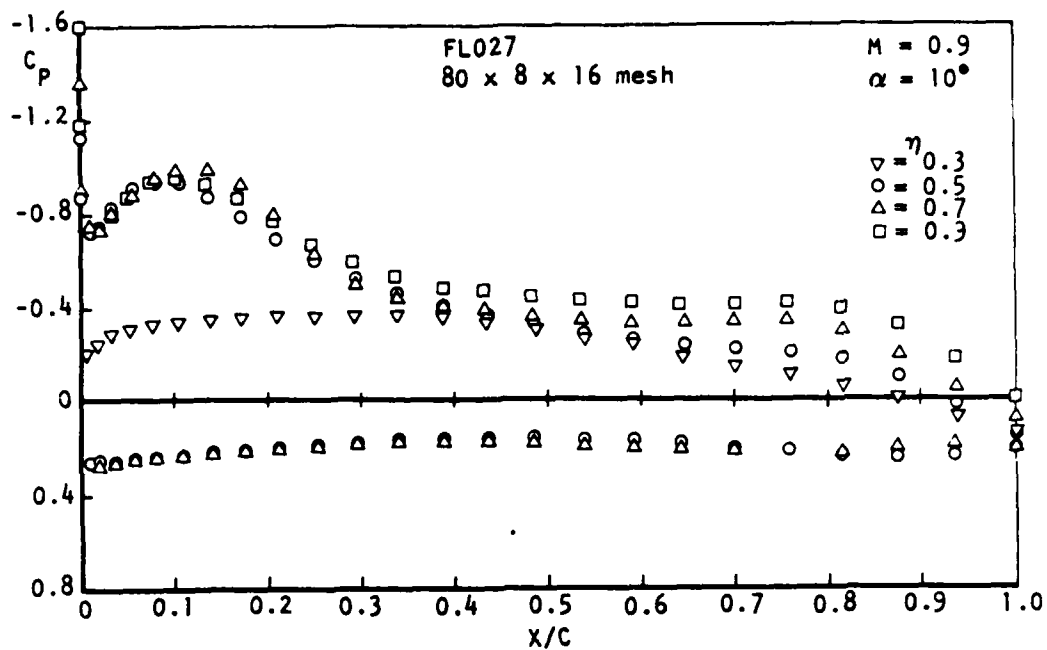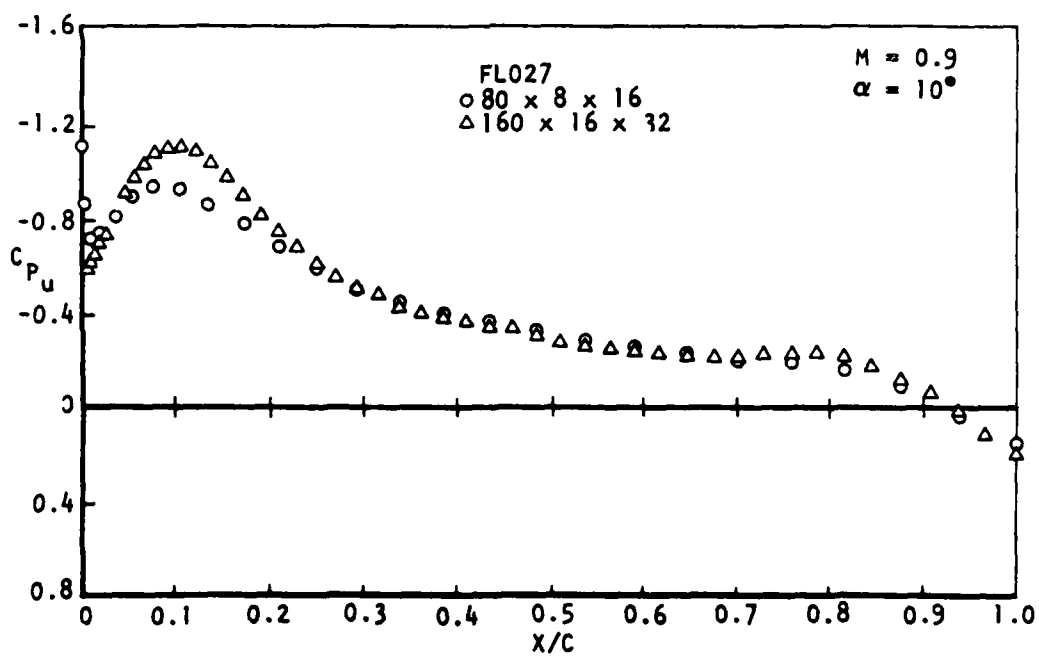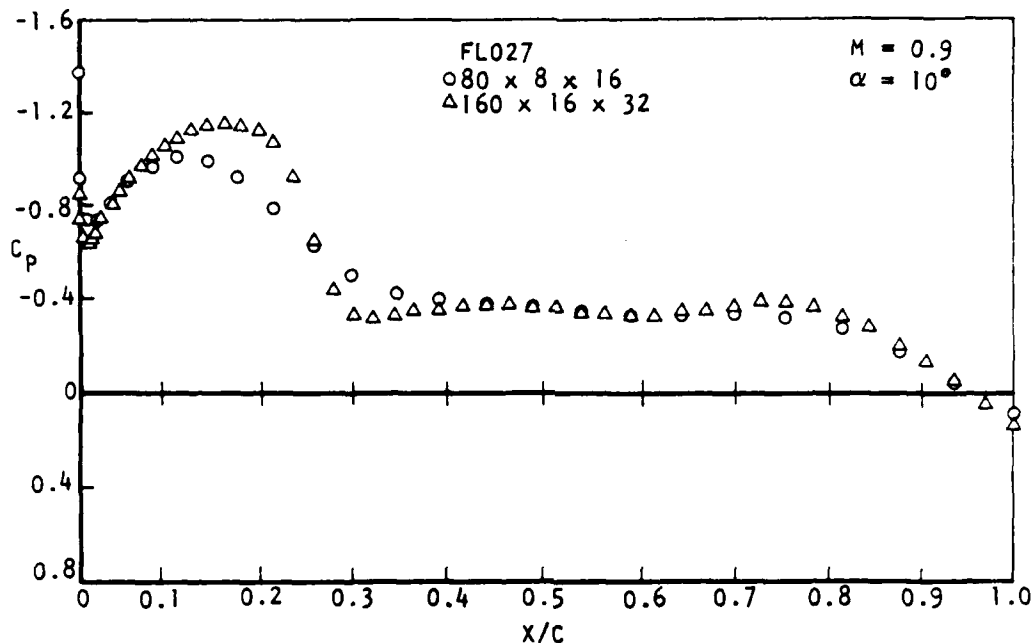Modifications were then made in an iterative cycle to weaken the outboard wing shock The 70-percent span station was used as a control point. The wing section was modified and analyzed with the transonic yawed wing program. The hinge line was moved progressively aft, and several leading edge deflections were analyzed. The objective was to derive an upper surface curvature that would weaken the shock. At 70-percent span, it was necessary to move the hinge line to 40-percent chord. After a satisfactory leading edge camber was derived for the control section, the other wing sections were constructed. Three equally spaced chordwise leading edge segments were assumed. The leading edge shape at the other span stations was constructed by deflecting the supersonic airfoils similarly. Further outboard (90-percent span), the hinge line was maintained at nominally 40-percent chord. The hinge line was also moved aft to 30-percent chord at 50-percent span. This selection resulted in a three-segment spanwise device, shown in Figure 32. This is primarily a consequence of the curved planform leading edge. This system could be replaced by a single hinge line over the outer 70 percent of the wing. The leading edge device at the side of the fuselage could be removed without substantially affecting transonic flow quality since the section lift is low for the inboard wing.

24
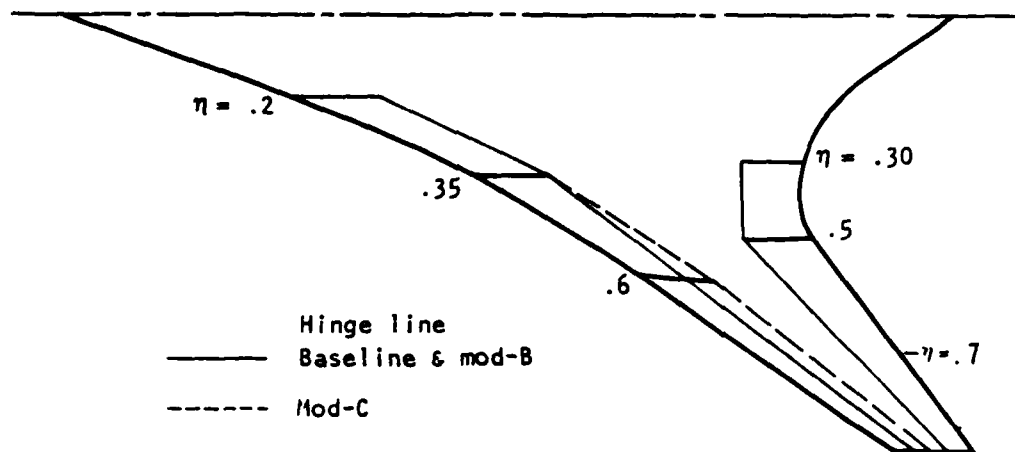
Figure 32. Variable camber system hingelines.

The revised camber system was analyzed with the three-dimensional transonic method. The shock on the outboard wing was weakened. The leading edge peak was increased relative to the previous design. Several three-dimensional design-analysis cycles were conducted to reduce the high leading edge velocities. The final solution (MOD-C) is shown in Figure 33. The leading edge peak was not entirely removed. This would require additional bending near the leading edge and/or increased leading edge radius.
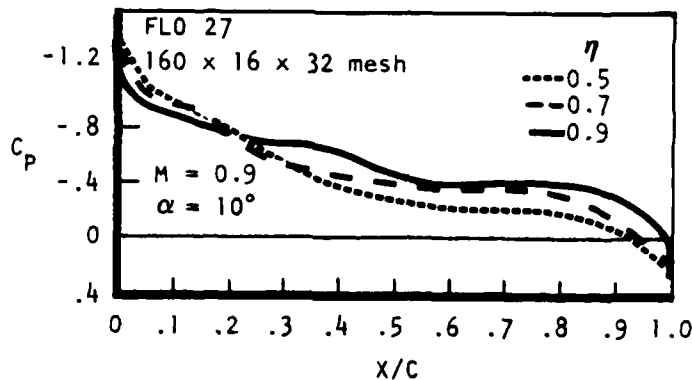
Figure 33. Maneuver pressure distribution for MOD-C design.

The final maneuver camber at η = 0.71 (MOD-C) is shown in Figure 27. The final twist distribution is shown in Figure 34. Since the leading and trailing edge deflections produced only a small net twist change, most of the required twist must be obtained from aeroelastic deflection. The final maneuver sections are shown in Figure 35.

A swept wing boundary layer calculation was made for the pressure distribution at 70-percent span. Transition due to cross-flow instability occurred at 1-percent chord. The calculated displacement thickness and wall shear stress angle, relative to the local streamline, are shown in Figure 36. The turbulent boundary layer was calculated with Bradshaws tapered wing method [11]. The calculation was made for full-scale flight conditions at M $\approx$ 0.9, 30,000 feet. Separation occured at 98-percent chord.
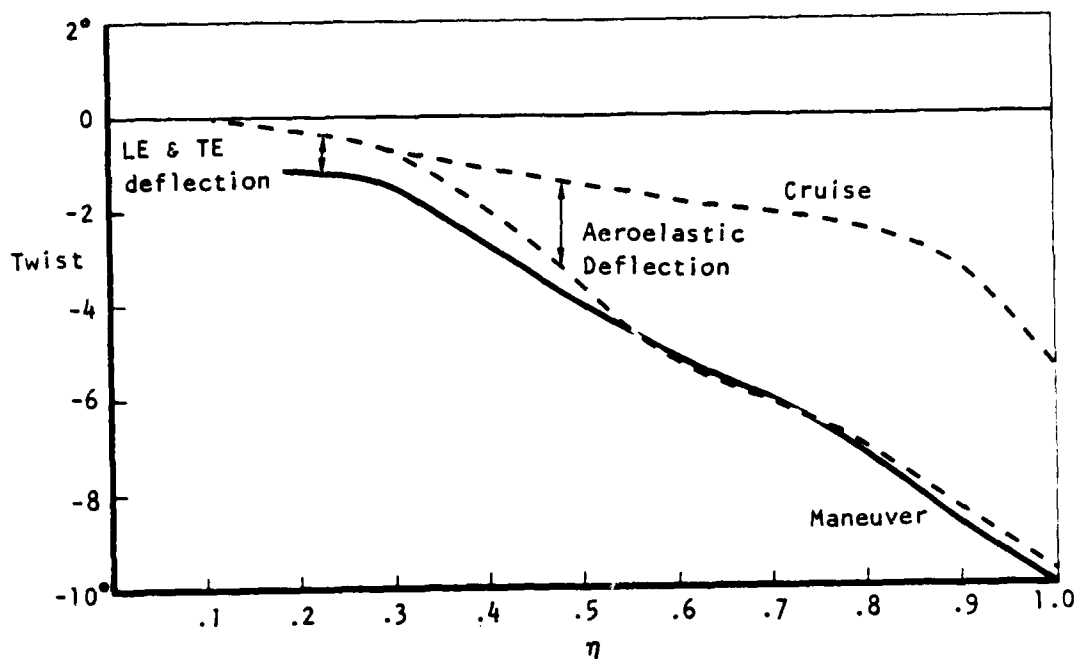
Figure 34.   Supersonic bias maneuver wing twist, MOD-C.
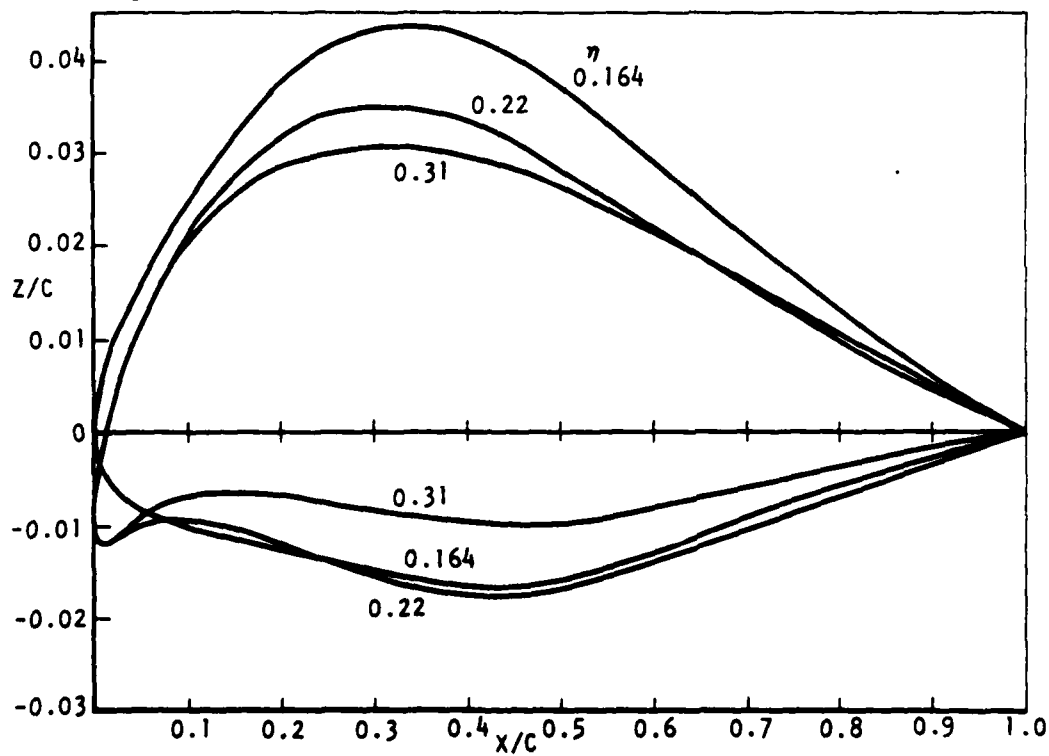
(a)   Inboard

Figure 35.   Maneuver sections MOD-C.

(b)   Center

(c)   Outboard
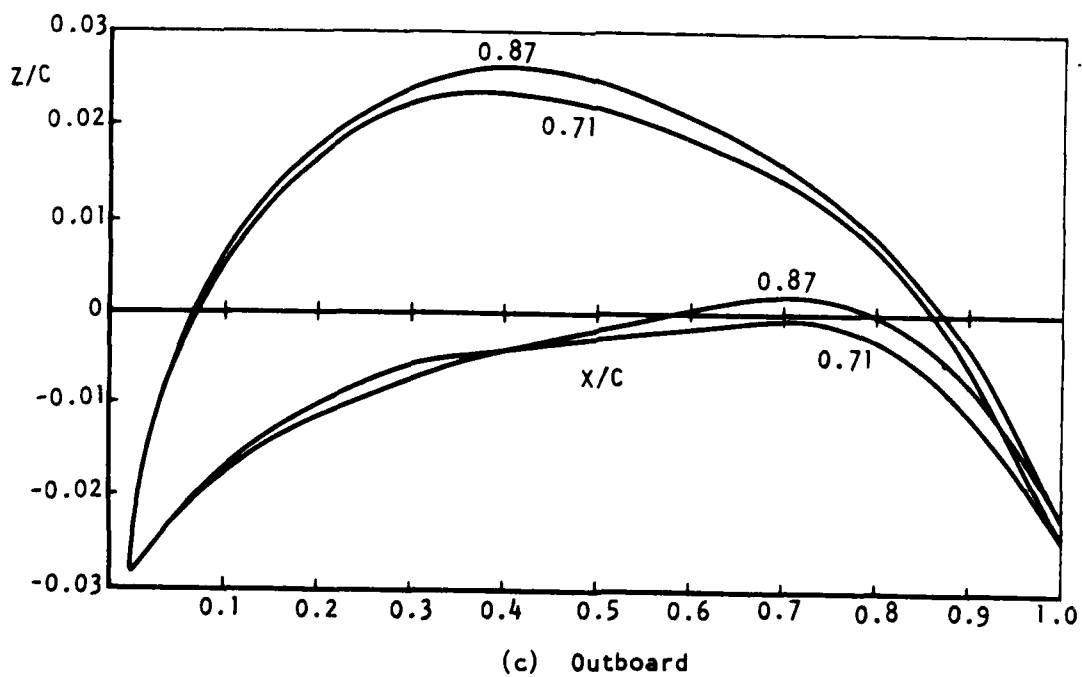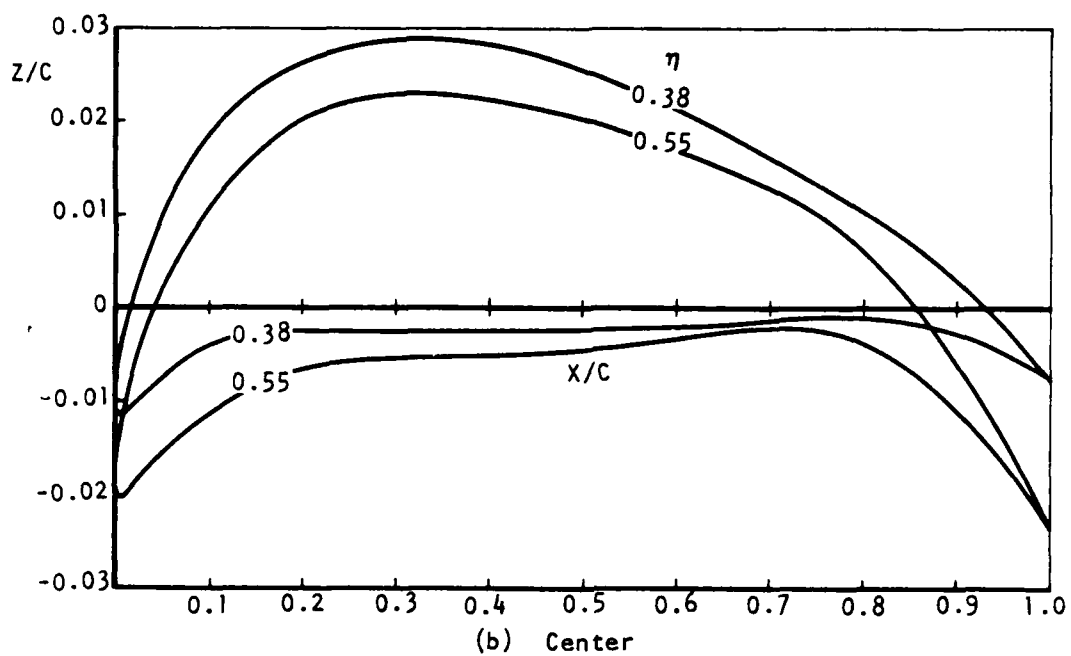
Figure 35.   Maneuver sections MOD-C. (Concluded)
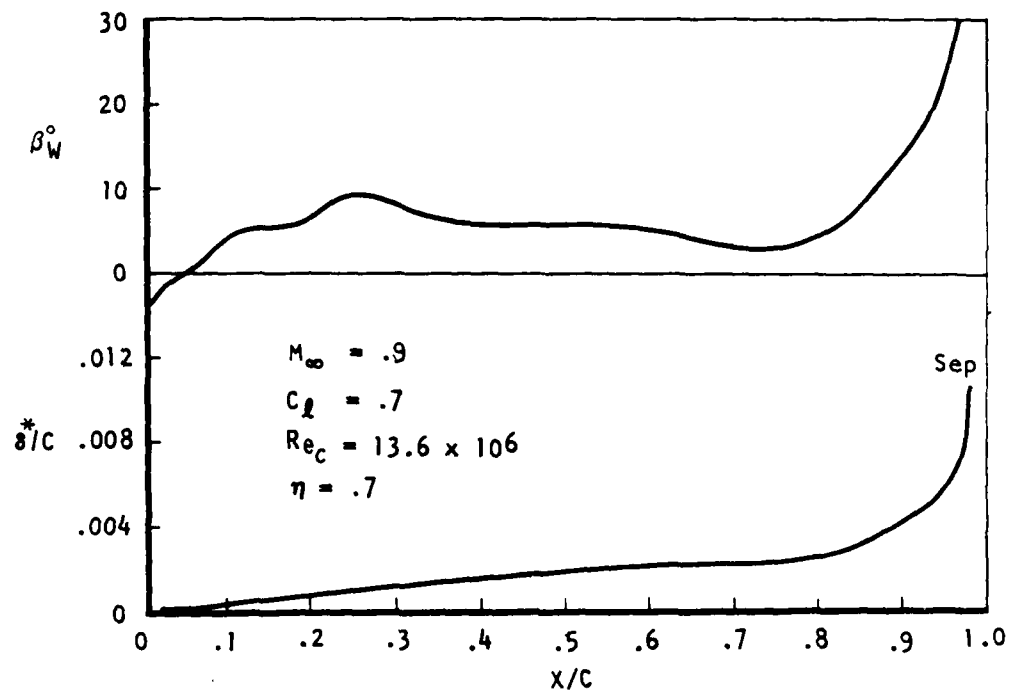
Figure 36.   Supersonic bias maneuver boundary layer characteristics.

TRANSONIC MANEUVER BIAS

BASELINE

The baseline configuration (Figure 37) and mission (Figure 38) selected for the transonic bias design are similar to these of the advanced HiMAT fighter [13].

$S_W = 298$ ft^2

$W_{TO} = 17064$ lb

$T/W_{TO} = 1.43$

SEP at .9M/30K/8g $= -131$ fps

$AR = 3.85$

— 35.3 ft —

— 45.7 ft —

8.8 ft
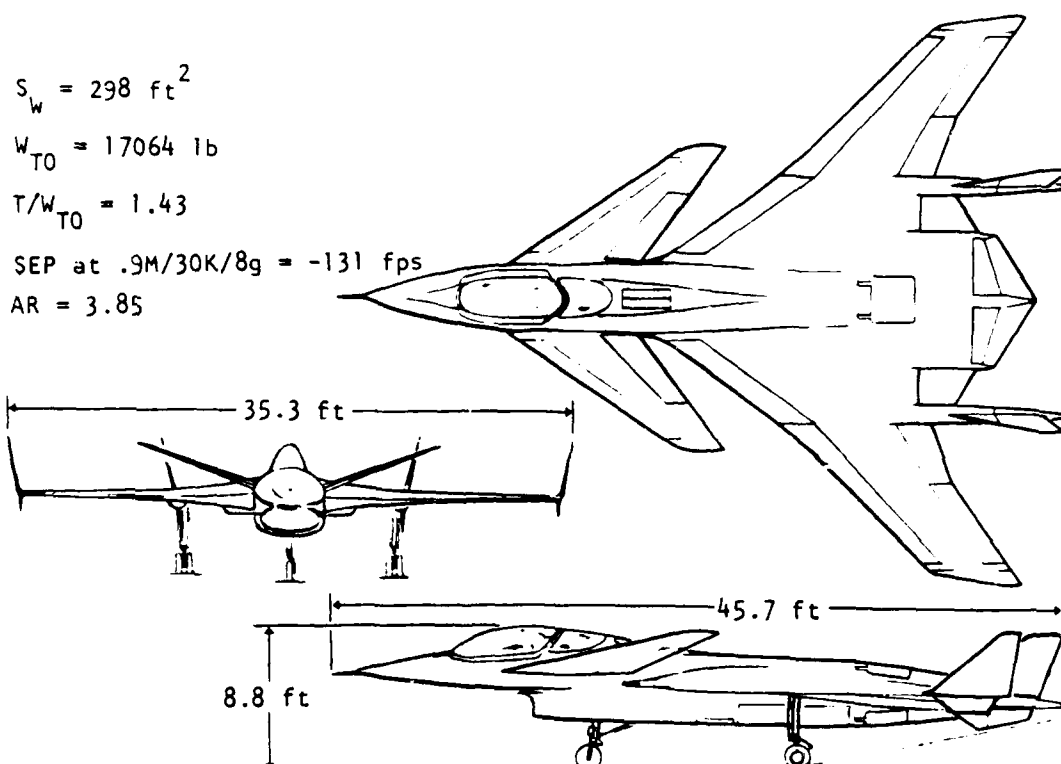
Figure 37. HiMAT fighter baseline

The advanced HiMAT fighter mission does not have a supersonic cruise requirement and has only minor supersonic flight consisting of an acceleration from best cruise mach number (BCM) to M = 1.4, 30,000, followed by a deceleration to M = 1.2, and two 360-degree, Ps = 0 turns at Nz = 8, M = 0.9. The mission radius is 300 nautical miles.

The transonic bias vehicle mission will be similar except that M = 1.6 cruise capability will be assumed. The configuration will thus require improved supersonic efficiency.
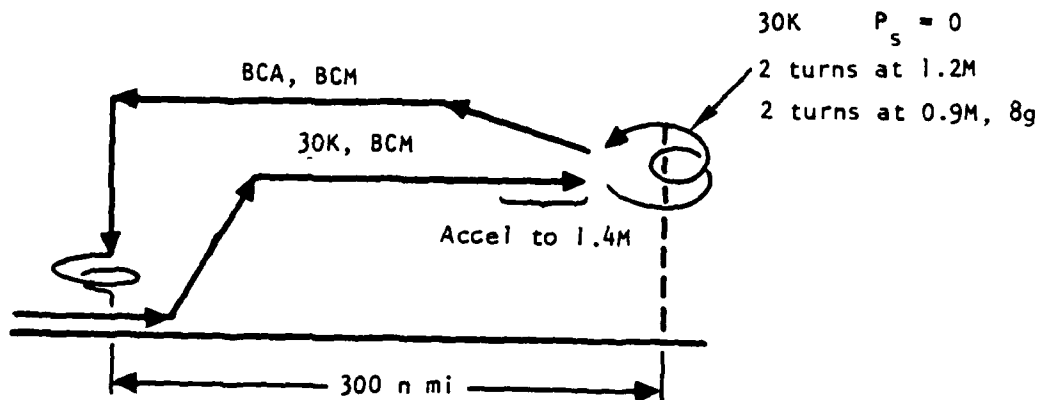
Figure 38. HiMAT fighter design mission.

CONFIGURATION DEVELOPMENT

The configuration modifications which established the maneuver bias baseline are summarized in the following. Most of the changes were directed toward reducing the supersonic wave drag.

The winglet was removed to reduce supersonic volume and camber drag and skin friction drag. The primary function of the winglet was to provide directional stability at high angles of attack. Analysis of the HiMAT dynamic stability characteristics (Figure 39) indicated there was sufficient margin to allow removal of the winglet without adverse effects relative to spin susceptibility.

The wing sweep was increased from 45 to 53.6 degrees to maintain a subsonic leading edge at M = 1.6. The reconfigured wing has an aspect ratio of 3.44. The maneuver drag-due-to-lift efficiency will be reduced as a result of wing planform modification and removal of the winglet. To maintain the 8 g capability of the HiMAT configuration, wing loading was reduced by increasing the reference area from 298 to 356 square feet. The 8 g condition at 30,000 feet corresponds to a lift coefficient of CL = 0.95.

To decrease the supersonic volume drag, the thickness for the inboard wing was reduced to 5 percent. The volume was recovered by adding a 20-inch-long fuselage plug at the center of gravity.

31

$$C_{\eta_{\beta\, DYN}} = C_{\eta_\beta} \cos\alpha - \left(\frac{I_z}{I_x}\right) C_{\ell_\beta} \sin\alpha \qquad\qquad LCDP = C_{\eta_\beta} - C_{\ell_\beta}\, \frac{C_{\eta_{\delta a}}}{C_{\ell_{\delta a}}}$$

INDICATES INCREASING ALPHA
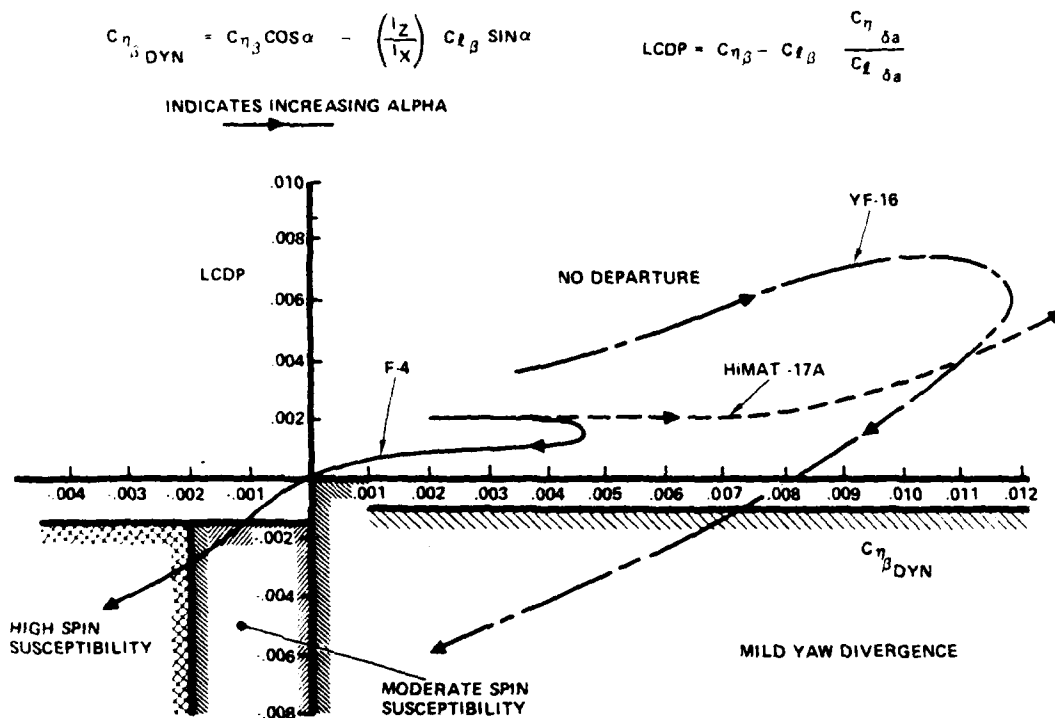
Figure 39.   Configuration effects on stability

The two-dimensional nozzle was replaced by an axisymmetric nozzle in order to eliminate propulsion effects on the wing design beyond basic sizing considerations.

The baseline maneuver *bias configuration* evolution is summarized in Figure 40. The relative canard size was retained when the wing area was increased. The projected canard span is 50 percent of the wingspan.

Having established tbe transonic bias configuration general arrangement, the wing design is initiated in accordance with Figure 41.

TRANSONIC MANEUVER DESIGN

The span load is first optimized with linear theory subject to constraints on the section loading and moment. This establishes the wing and canard section design conditions and indicates the magnitude of twist required.   Airfoils are designed using the transonic yawed wing analysis [10] for regions where sweep theory is appropriate; that is, the canard and outer wing. The sections are then installed on the configuration, and the camber and twist are adjusted using linear theory to maintain swept isobars. This initialization is then analyzed with nonlinear three-dimensional potential theory and modified using a design/analysis cycle.

WINGLETS
LARGE VERTICALS
HIGH AR
NOT OPTIMIZED FOR C_{D_W}

INCREASE WING SWEEP

REMOVE WINGLETS
SMALLER TAILS $\}$ LOWER S_{WET}

AXISYMMETRIC NOZZLE

DECREASE WING THICKNESS

$AR, \lambda, \wedge_{LE}$ 3.85, .25, 45°

S_W, S_C, S_V 298, 95, 50

$t/c = .07 \rightarrow .045$

$AR, \lambda, \wedge_{LE}$ 3.44, .25, 53.5

S_W, S_C, S_V 356, 121, 32

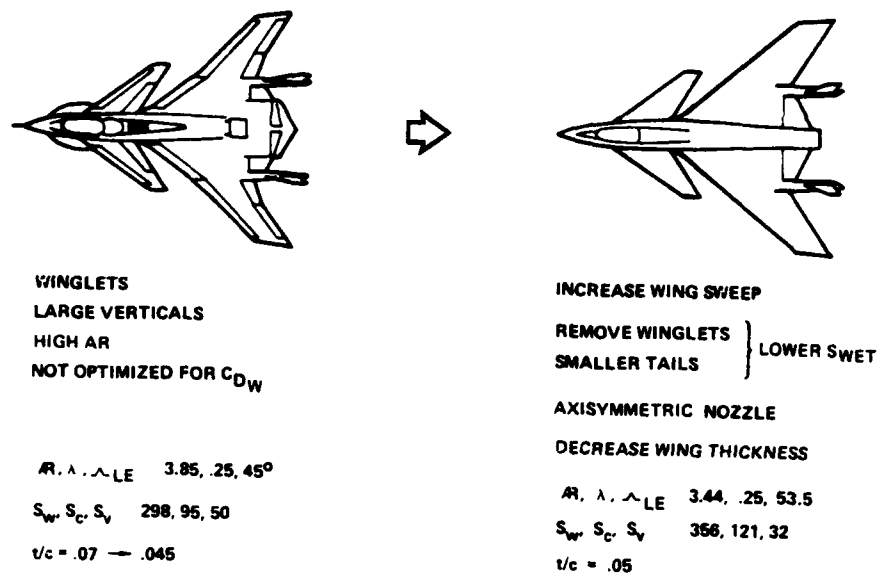$t/c = .05$

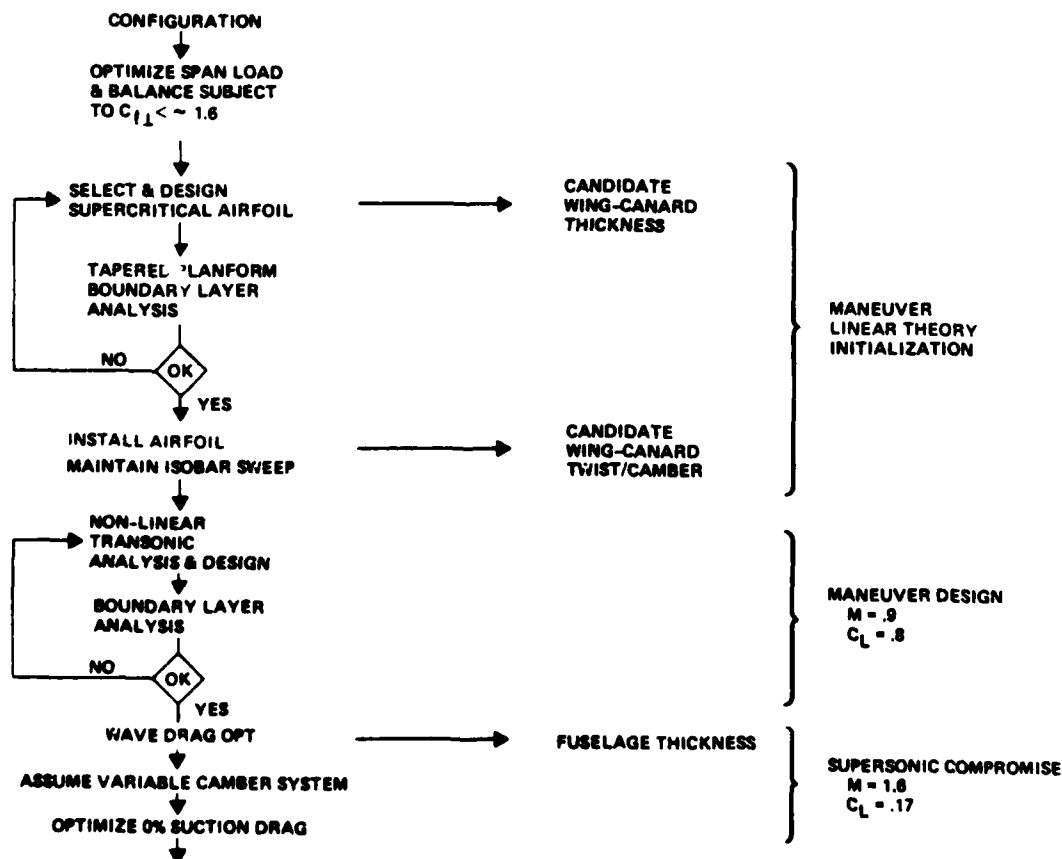Figure 40.   Maneuver bias configuration evolution.

Figure 41.   Maneuver bias design approach.

The maneuver point is $C_L = 0.95$ at $M = 0.9$, 30,000-foot altitude. The configuration will be designed at a $C_L = 0.8$. It is postulated that, as for the HiMAT, use of a slightly off-design condition results in better subsonic efficiency at low C_L and improves the potential for obtaining acceptable supersonic performance.

LINEAR INITIALIZATION

The linear theory inverse and optimization methods are used to determine an initialization for the transonic analysis/design cycle. In order to minimize drag, (1) the section lift distribution should be such that a transonic pressure distribution can be developed which has weak shocks and minor trailing edge separation, and (2) the span load should be optimized to reduce vortex drag. Linear theory is used to optimize the drag subject to constraints and determine a preliminary twist and camber. This process sets the transonic design condition for the development of airfoils for the three-dimensional design.

The constraints in the design process include specifying a section lift for the outboard wing and canard. Based on sweep theory and previous transonic airfoil designs, a section lift constraint of $C = 0.8$ is imposed. The midchord sweeps are approximately 45 degrees so that this limit corresponds to a perpendicular lift of $C = 1.6$. The linear theory design solutions are used to derive twist and camber for a given loading. The objective is to design for the minimum section lift but still require a practical twist distribution. To arrive at a preliminary twist, a chord-load shape representative of supercritical airfoils for the design condition is selected as a constraint function. A second chord-load distribution, a sine function, is used to adjust the moment without changing the section lift.

The design proceeds by specifying a loading and a center-of-pressure variation, then imposing a total moment constraint and solving for the twist and camber. The configuration is trimmed at the nominal CG (0.15c). The twist and camber are examined and, if they are not acceptable, the spanwise loading and center-of-pressure variation are modified. These are selected such that the isobars will be swept. Thus, for example, if the section lift is constrained to a low value, the twist required may be excessive. The section lift constraint is modified until both the wing and canard twist distributions are acceptable.

The constrained span loading is shown in Figure 42 for the final linear theory design. The wing and canard twist distributions had 9.5 and 8.5 degrees of washout, respectively.

TWO-DIMENSIONAL TRANSONIC DESIGN

With the design condition established, airfoils are developed for the canard and outboard wing (n 40%). Since the sweep for both regions was similar, only one airfoil was derived. The airfoil design was started from an airfoil with a design condition close to that required. Several design/analysis cycles were made with the transonic yawed wing program (10) to modify the upper surface curvature for acceptable flow characteristics.
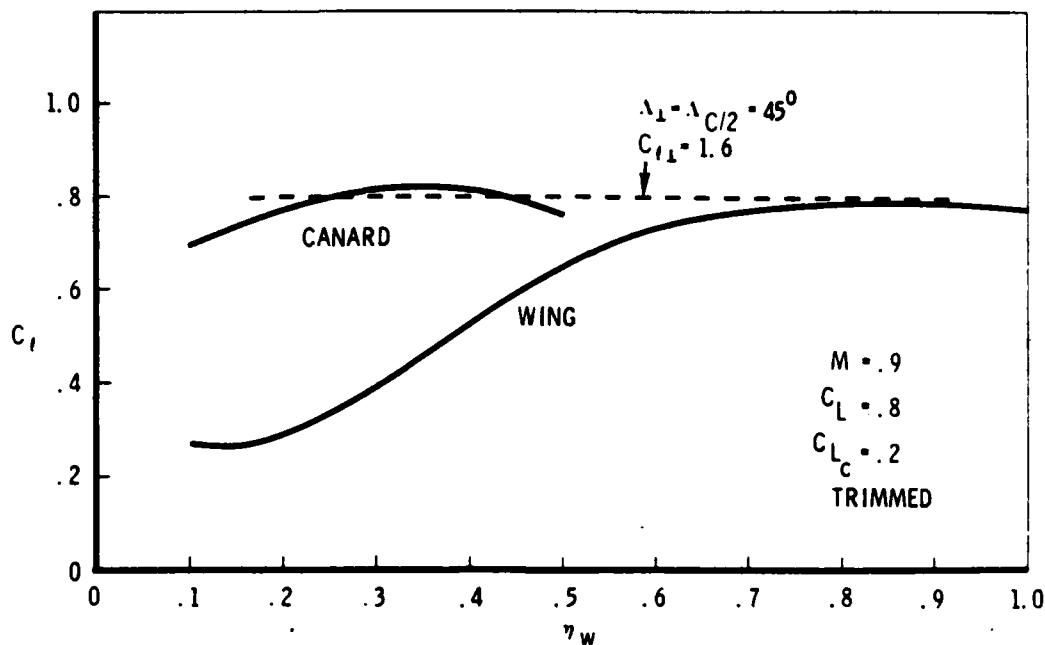
34

Figure 42. Linear maneuver design span loading.

An analysis was conducted for C_l = 0.75, M = 0.9, and Λ = 45. The airfoil that was developed is shown in Figure 43. The thickness ratio is 0.048. The plateau terminates in a weak shock at 50-percent chord. The upper surface displacement thickness for a chord Reynolds number of 20 million is shown in Figure 44. Some trailing edge separation is present.

THREE-DIMENSIONAL TRANSONIC DESIGN

The airfoil of Figure 43 was installed on the canard and outboard wing in preparation for the three-dimensional design cycle. Since sweep theory is approximate at best for a tapered low-aspect-ratio panel, the airfoil may be installed by either: (1) determining the streamwise chord load and obtaining an inverse with linear theory, or (2) correcting for three-dimensional effects with a twist distribution such that the desired lift distribution is maintained. Both are essentially equivalent for an untapered high-aspect-ratio wing. For this configuration, the second approach was used. A linear theory analysis indicated that the section lift did not change appreciably, so that the twist derived in the linear theory design cycle would be adequate.

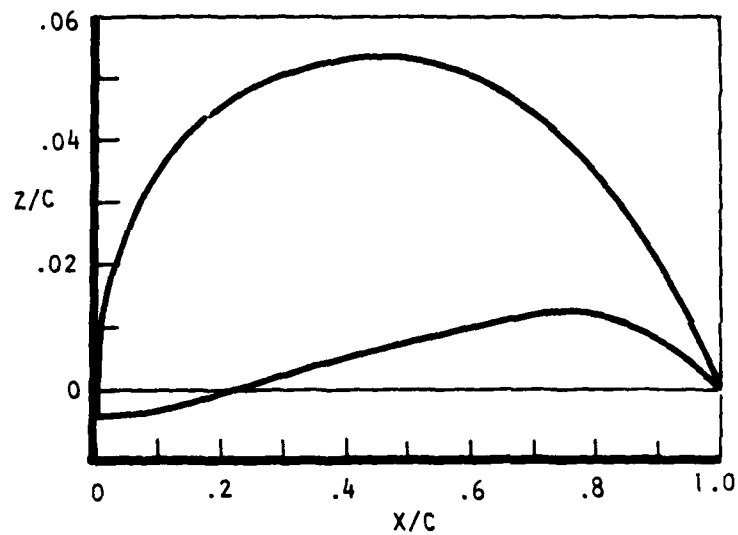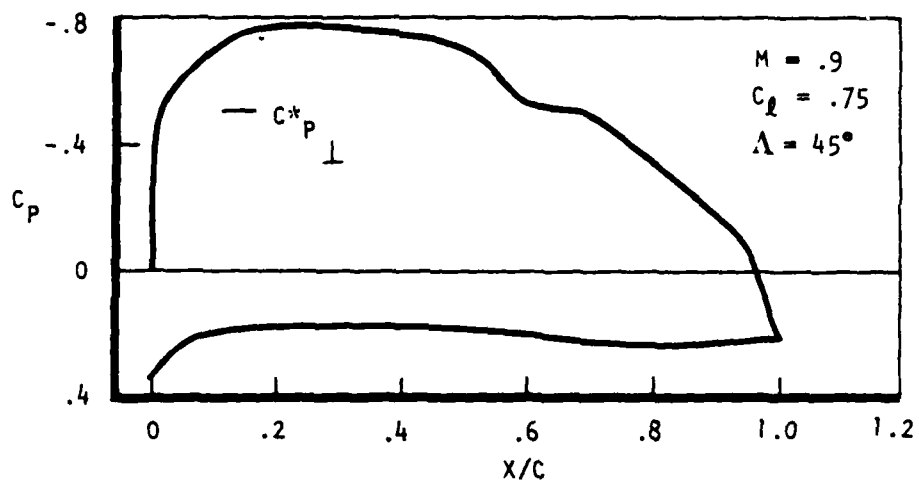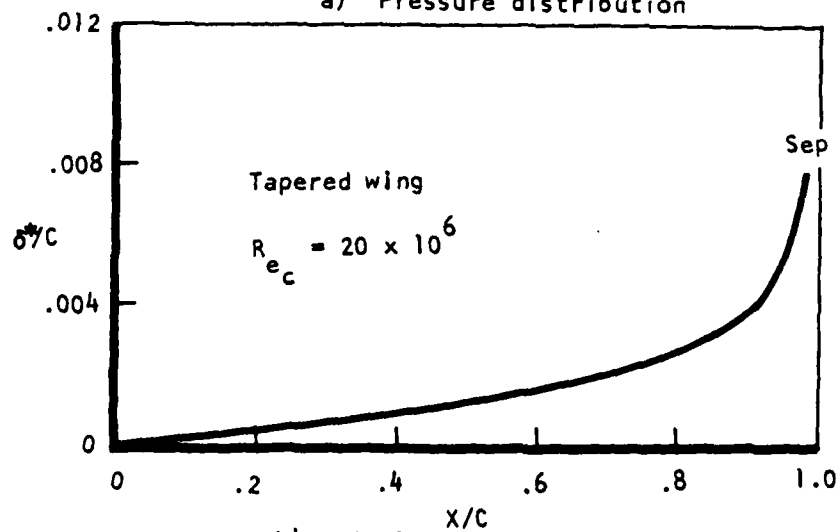Figure 43.   Maneuver bias candidate supercritical airfoil.

M = .9
C_ℓ = .75
Λ = 45°

C_P^* $\perp$

a)   Pressure distribution

Sep

Tapered wing

R_{e_c} = 20 × 10^6

b)   Displacement thickness

Figure 44.   Supercritical airfoil characteristics.

The wing isobars are shown in Figure 45. The analysis indicated unsweeping of the isobars at the tip. Therefore, an inverse was obtained for a pressure distribution with swept isobars. The pressures inboard of 80-percent span were not changed. The resulting camber is shown in Figure 46. This revised tip camber was used for the transonic initialization.
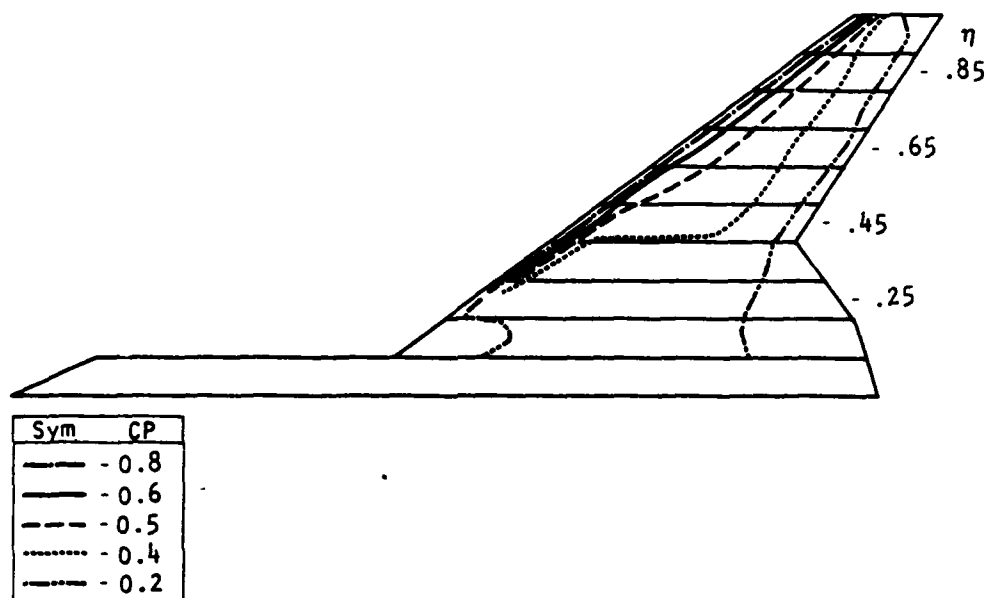

Sym	CP
—·—	-0.8
——	-0.6
———	-0.5
·········	-0.4
—··—	-0.2

Figure 45. Wing upper surface isobars-linear theory.

The inboard wing camber, n < 0.4, from the linear theory design was used without change along with the thickness derived for the outboard supercritical airfoil. For this region of the wing, sweep theory is not applicable; therefore, the linear theory design results provide the only means of initializing the transonic design.

The conservative full-potential FLO27 code [6] was used to analyze the wing. The downwash at α = 10° was calculated as described previously. The geometric wing twist, canard-induced downwash, and effective twist are shown in Figure 47. Upper surface pressure distributions are shown in Figure 48 for M = 0.9, α = 10° for a medium grid (80 by 8 by 16). No shocks are apparent at this level of analysis. The loading for the forward chordwise region has increased relative to the two-dimensional sweep theory result. This occurs as a result of the wing taper; that is, the higher leading edge sweep produces a more subsonic-type leading edge pressure distribution. This circumstance is advantageous since the local critical condition decreases from leading to trailing edge as a result of the change in isobar sweep. That is, higher velocites can be maintained without shocks as long as the flow component normal to the isobar is only slightly supercritical.
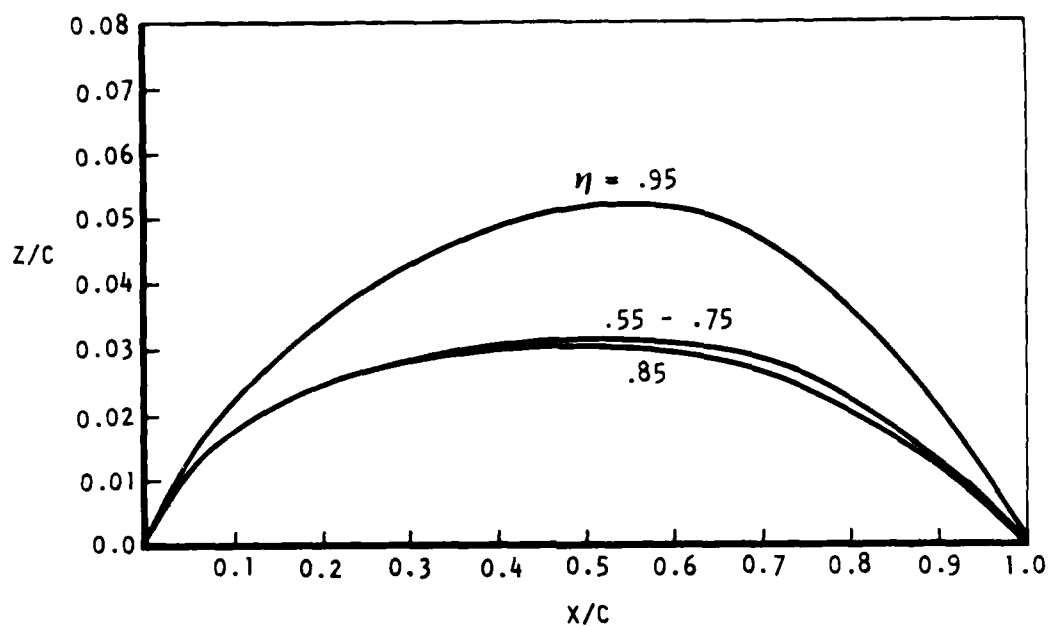
Figure 46. Camber modification for swept isobars.
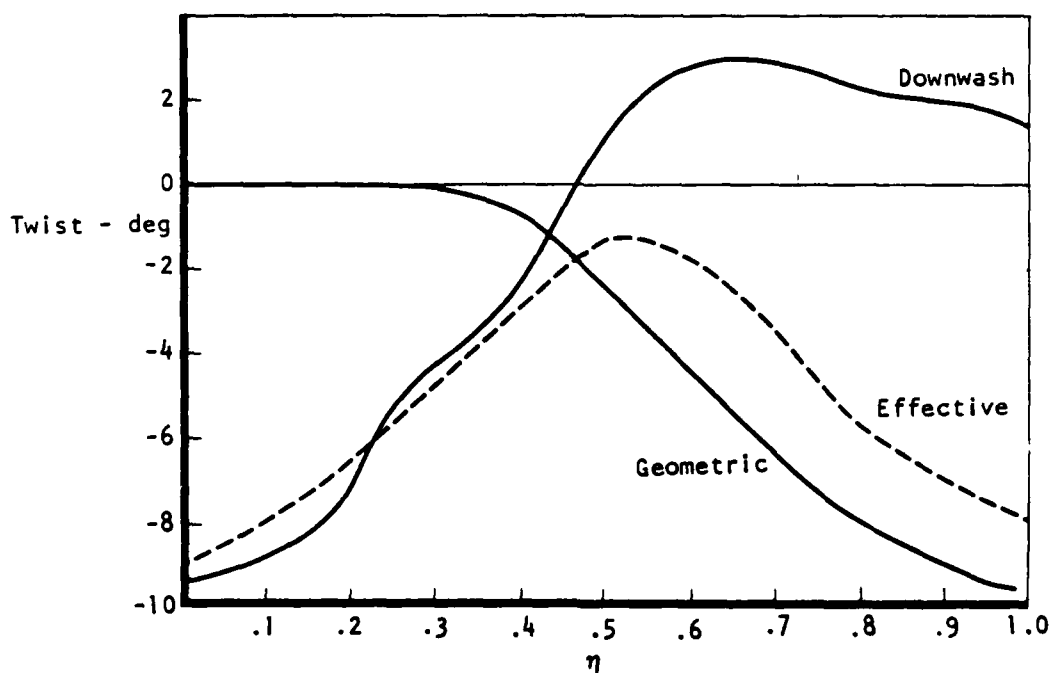
Figure 47. Maneuver wing twist, M = 0.9, α = 10°

38
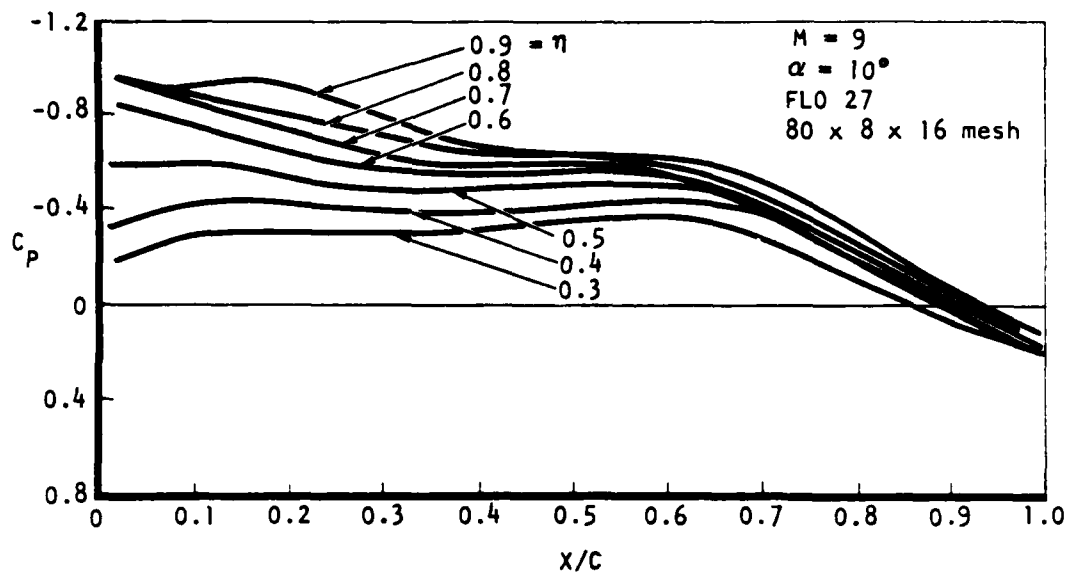
Figure 48.   Maneuver wing pressure distribution.

A tapered wing boundary layer analysis [11] was conducted for the pressure distribution at 70-percent span. The displacement thickness and wall flow angle are shown in Figure 49. Minor trailing edge separation is present.

Figure 49.   Wing upper surface boundary layer characteristics at η = .7.

The wing was modified to fine tune the pressure distribution at 90-percent span and to increase the inboard wing loading. The procedure to modify the design consists of (1) a trial-and-error approach where the curvatures are modified and the design is reanalyzed, or (2) an application of the CONMIN [7,8] optimization technique.

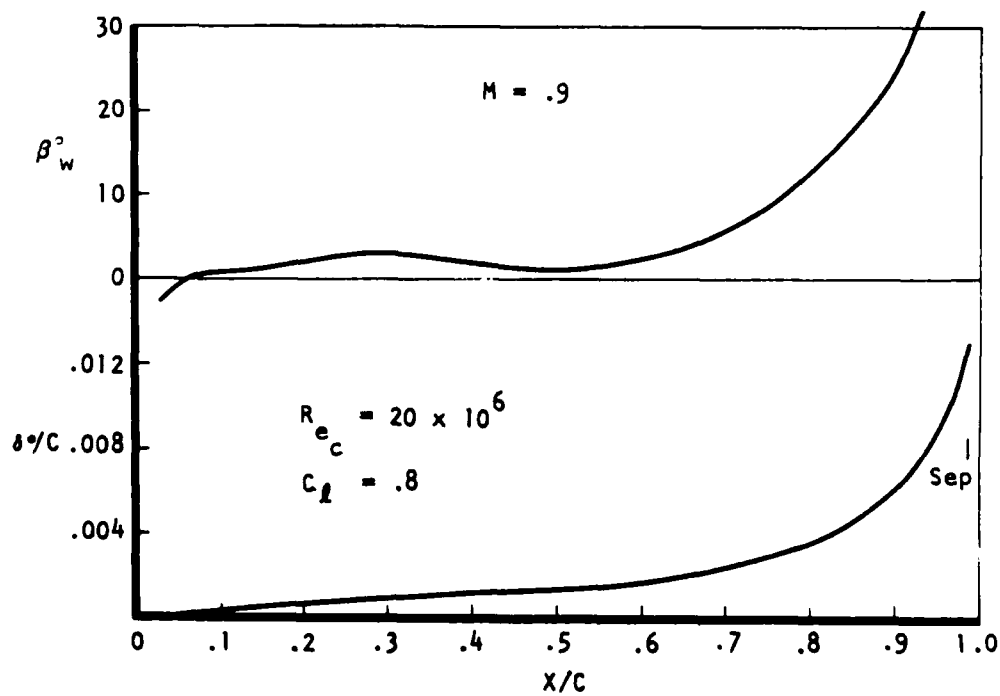The CONMIN optimization technique operates as follows. An objective function is selected which is to be minimized. This function may be any characteristic calculated by the analysis program, in this case FLO27. Usually, a design pressure distribution is specified over a portion of the wing. A set of perturbation functions is selected. The program modifies the specified wing sections to obtain the derivatives of the objective function with respect to the perturbation function coefficients. The gradient direction which minimizes the objective is calculated, and the wing sections are perturbed correspondingly. This procedure requires some iteration to arrive at a set of functions which produce feasible airfoils. Also, it is sometimes necessary to derive the desired pressure distribution in a stepwise manner; that is a separate optimization cycle for various regions of the airfoil. The design pressure distribution is satisifed in a least-squares sense.

The inboard wing loading was increased to improve the overall efficiency. The nonlinear analysis indicated that more loading could be carried inboard without producing strong unswept shocks. A flat-top-type pressure distribution was specified for the inboard wing (n < 0.4). Redesign was accomplished by application of the CONMIN/FLO27 method, followed by analysis with smoothed wing sections. The sections were modified to produce smooth camber distributions for variable camber considerations.

The wingtip region was also redesigned to maintain swept isobars. Outboard wing loading increased somewhat due to the inboard wing redesign. The tip (90-percent span) developed a localized high-velocity region. This area was redesigned to obtain a relatively constant spanwise pressure distribution. The final wing pressure distribution is shown in Figure 50.
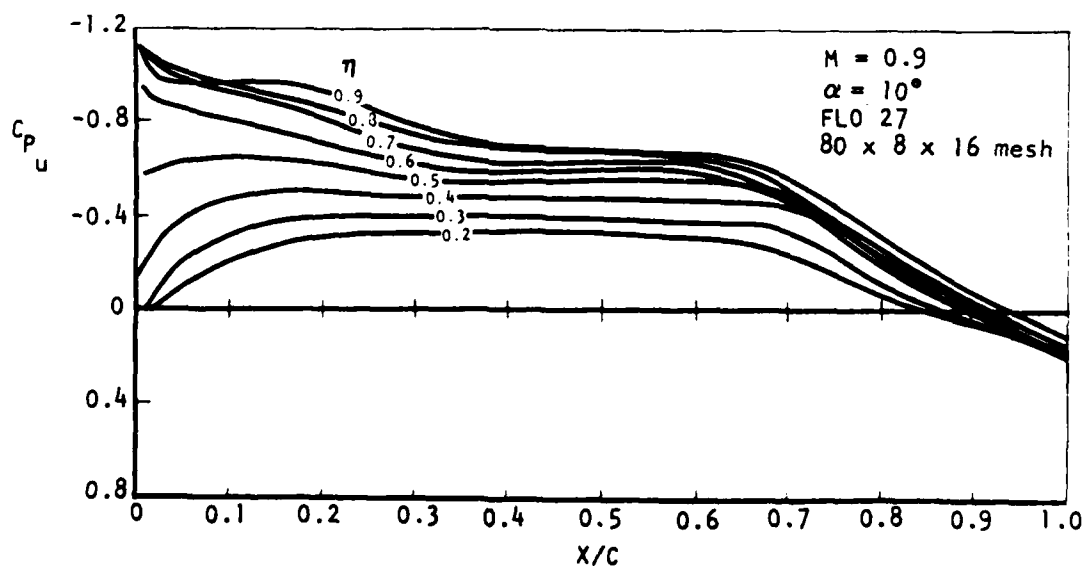

Figure 50. Modified maneuver wing pressure distribution.

The canard development paralleled that of the wing. A correction to the camber was made with linear theory to obtain swept isobars at the tip. The geometric and effective twist at $\alpha = 10^0$ are shown in Figure 51. The wing-induced upwash is small. A FLO 27 analysis of the canard, extended to the flow centerline, is presented in Figure 52 for $M = 0.9$, $\alpha = 10^0$. The flow quality is acceptable, in that no shock is indicated. A boundary layer calculation for the 70-percent distribution predicted separation at 95-percent chord. This was further forward than the wing separation point. The pressure distributions are similar, but the average sweep is higher; i.e., $\bar{\Lambda} = 46.5$ for the canard versus $\bar{\Lambda} = 45^0$ for the wing.

Modifications were made to the inboard canard sections to reduce the expansion that occurs just before the final recompression. The modification results in a flatter upper surface distribution, as shown in Figure 53 The intent was to prevent an overexpansion and shock near the trailing edge at off-design conditions.

Nonlinear results for the wing and canard section lift are compared with linear theory in Figure 54. The linear theory calculation was made for the wing body-canard. The nonlinear loading spanwise center of pressure has moved outward relative to linear theory.

The twist distributions are shown in Figures 47 and 51. The wing and canard sections are shown in Figures 55 and 56, respectively.

SUPERSONIC PERFORMANCE

Drag-due-to-lift is minimized for supersonic cruise by use of a variable camber system. A volume wave optimization is restricted to the fuselage in order to preserve to transonic wing flow quality.

DRAG-DUE-TO-LIFT

The supersonic performance obtained by a variable camber system was investigated for $M = 1.6$ cruise conditions. The camber derived from the transonic design is used as a constraint in the linear theory optimization. Various combinations of leading and trailing edge segments of the wing and canard are selected as variables. The linear theory optimization program determined the deflections and twist distributions for a given lift and moment.

The variable camber system initially includes wing leading edge device, trailing edge flaps, a variable incidence canard, or a leading edge device and canard flap. The simulation is shown in Figure 57.

At $M = 1.6$ and 50,000 feet, the cruise lift is $C_L = 0.1$. The solutions are obtained for a trimmed condition at this point. An unconstrained supersonic optimum was determined in order to evaluate the variable camber system penalty. The drag-due-to-lift (0-percent suction) is shown in Figure 58 along with the flat-plate variation.

41
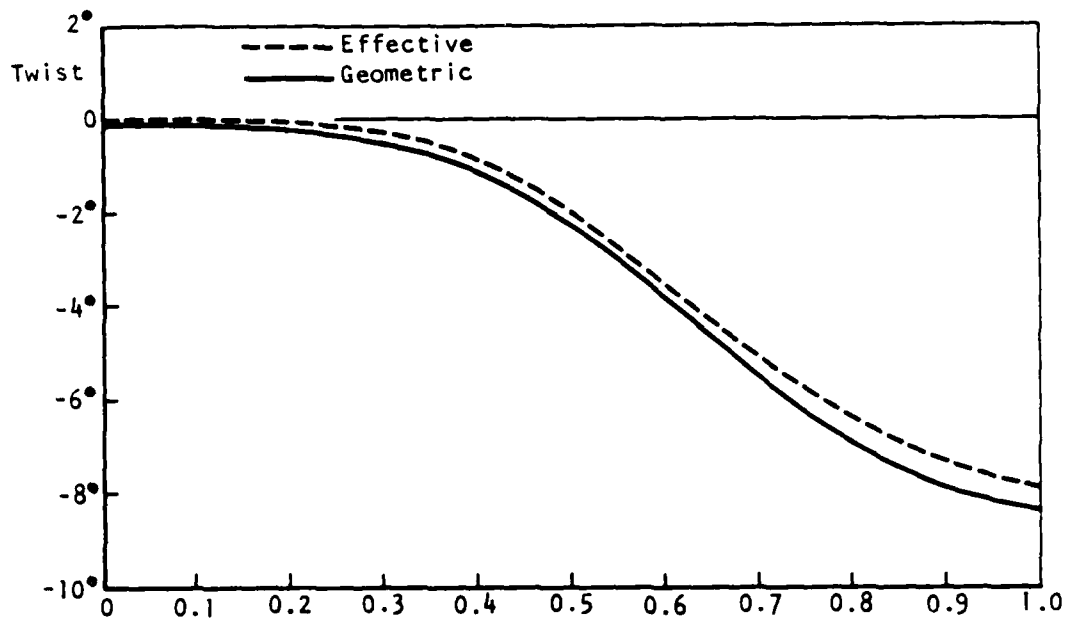
Figure 51. Maneuver bias canard twist.
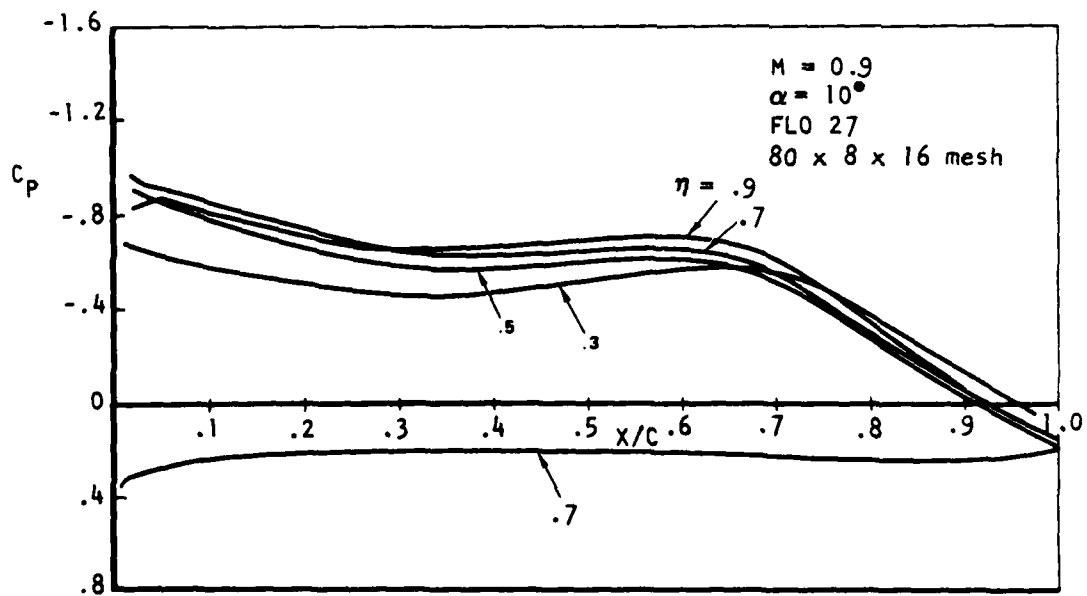
Figure 52. Maneuver canard pressure distribution.

Figure 53. Modified maneuver canard pressure distribution.

Figure 54. Maneuver bias section lift distribution

(a) Inboard

(b) Center

Figure 55. Maneuver bias wing sections

Figure 55.   Maneuver bias wing sections. (concluded)

Figure 56.   Maneuver bias canard sections.

45

Figure 57. Maneuver bias variable camber system.

Figure 58. Maneuver bias zero suction drag due to lift at M = 1.6.

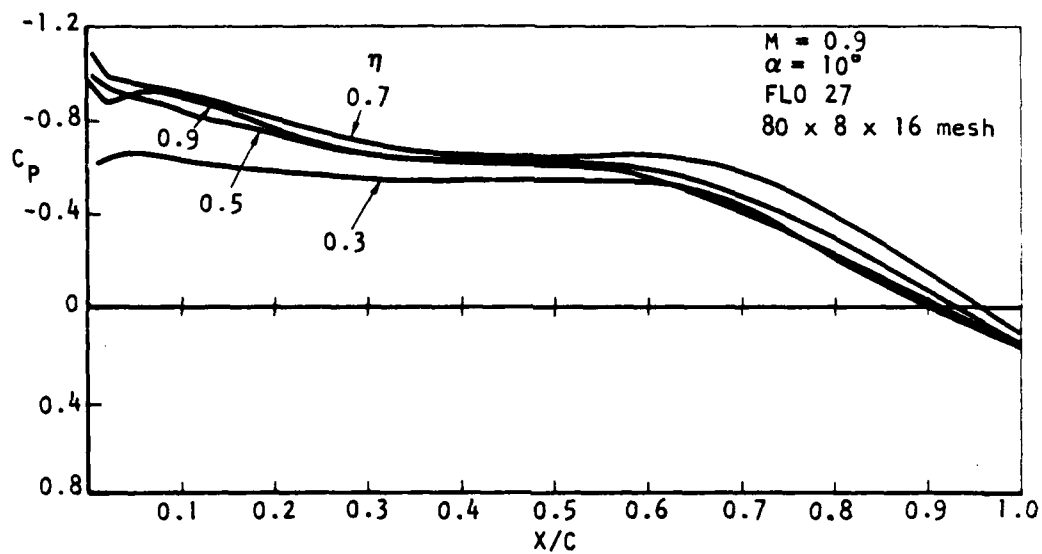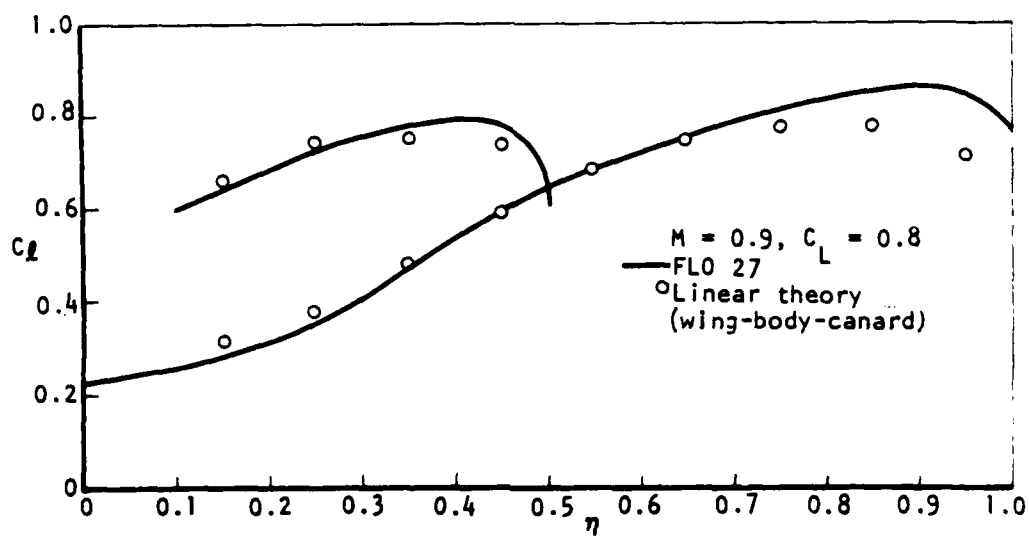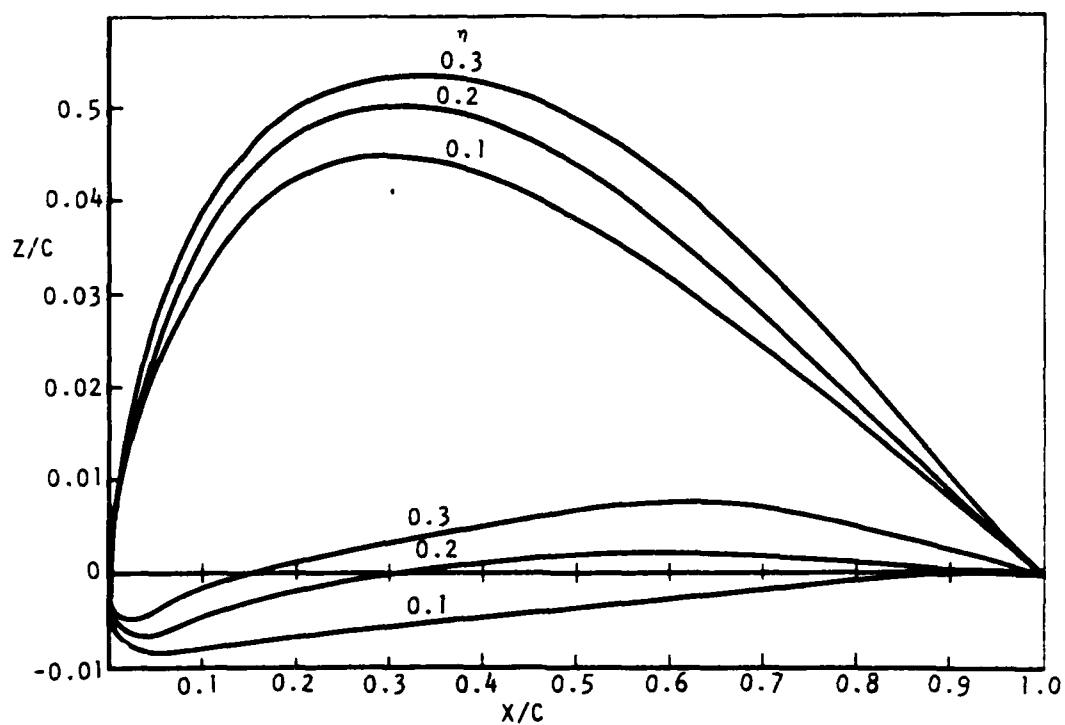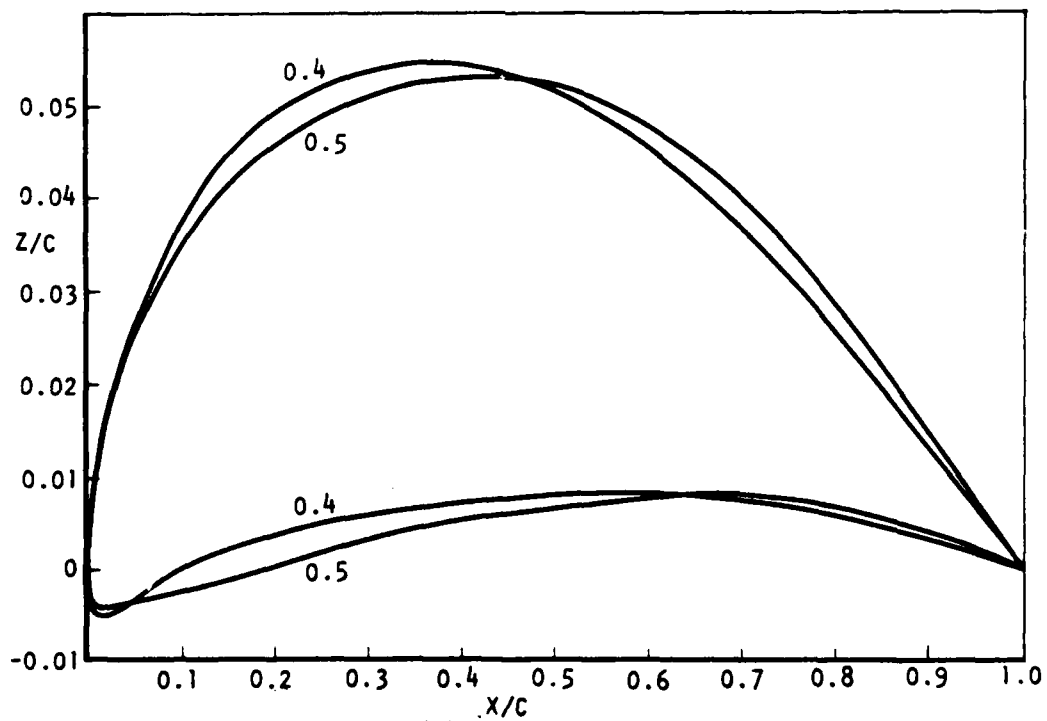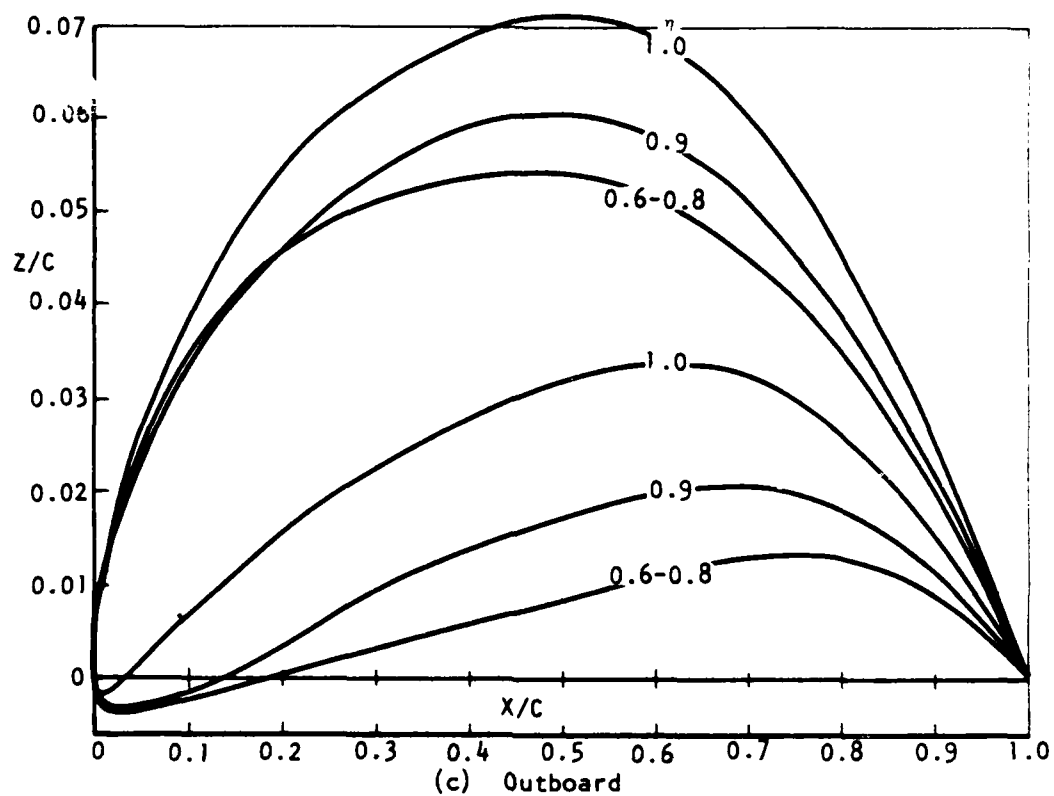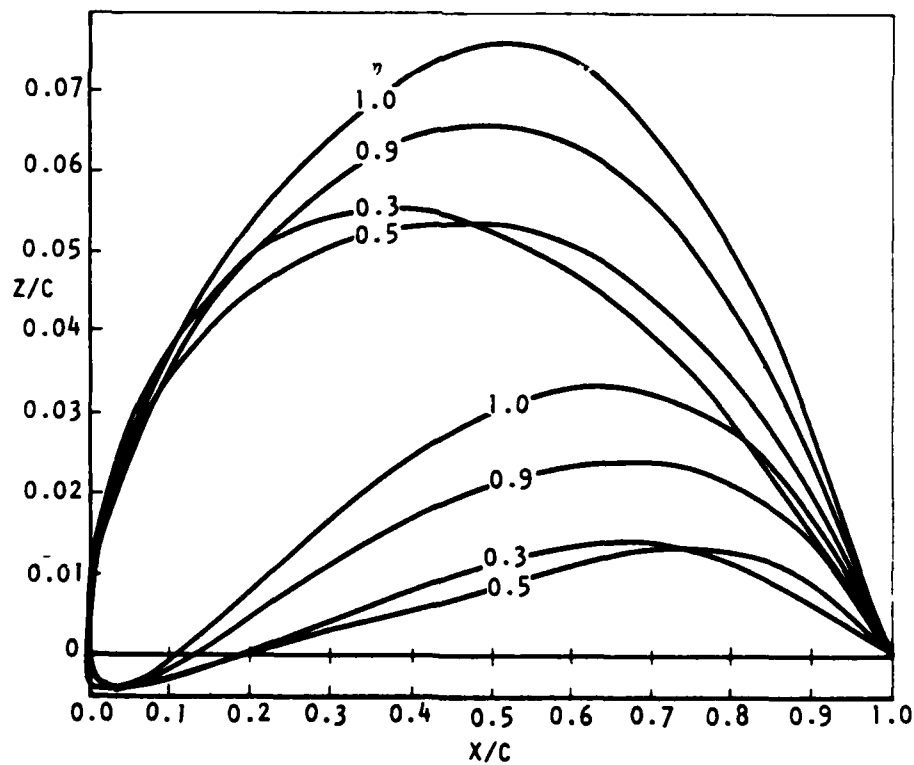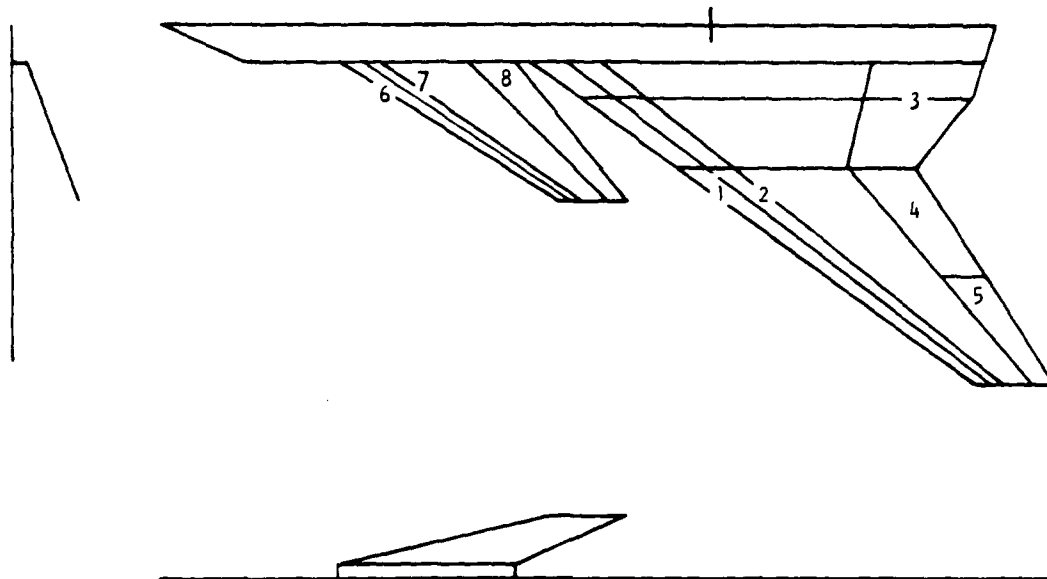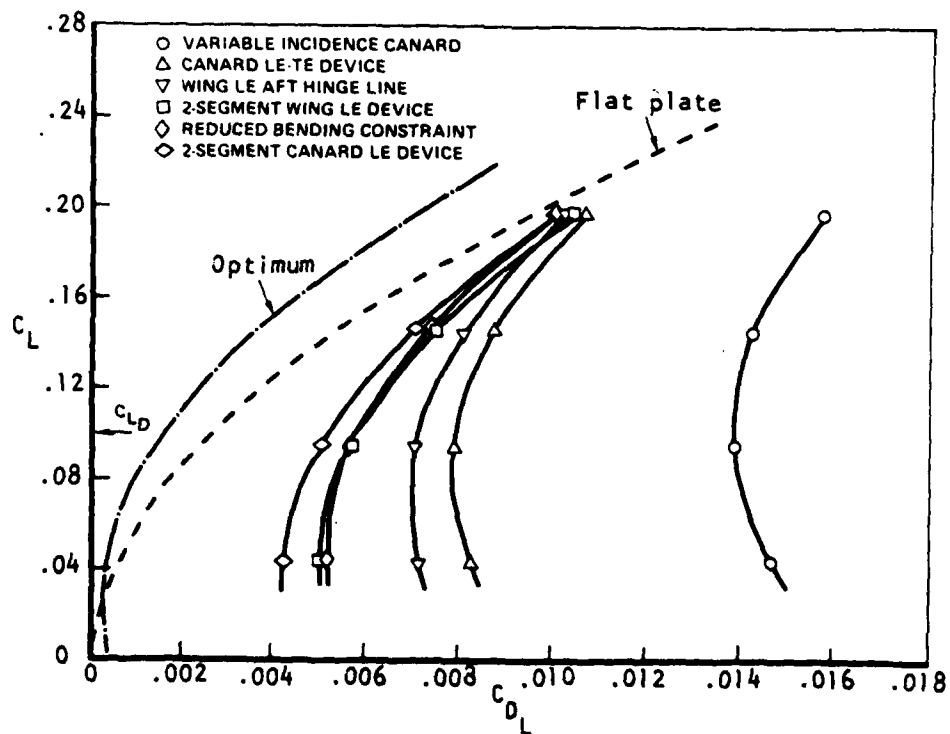The procedure to derive the supersonic camber is straightforward. A set of flaps is selected, including a combination of leading and trailing edge devices. The drag is minimized with the linear theory optimization technique. The twist is constrained, as required, to obtain a smooth bending requirement. Several solutions are usually required to obtain the sensitivity of drag to: (1) the chordwise extent of the variable camber devices, and (2) the number of elements in each variable camber segment; that is, single-segment flap or smooth chordwise bending (multiple segments).

The wing leading edge device extended initially to 20-percent chord and was assumed to deflect as one segment. An optimization was obtained with no twist constraints. The maneuver camber was input as a set of constraints. The wing twist distribution exhibited spanwise discontinuities because of the variation in trailing edge flap deflections. The wing twist was smoothed and constrained in subsequent solutions. The twist differential between maneuver and cruise was approximately 5 degrees at the wingtip.

Further optimizations were performed to investigate variable camber systems for the canard. First, a variable incidence canard was assumed. The drag polar is shown in Figure 58. Next, a 20-percent leading edge device and a 30-percent canard flap were considered. The twist at the canard root was constrained to the maneuver value. As shown in Figure 58, a substantial improvement in drag-due-to-lift was obtained.

The hinge line of the wing leading edge device was changed to allow the tip region to be uncambered. The hinge line extends from 15-percent chord at the root to 30-percent chord at the tip. The drag polar is shown in Figure 58. A two-segment wing leading edge device was then assumed, as indicated in Figure 57. The optimization produced deflections for panels 1 and 2 of 7 and 3 degrees, respectively. The reduction in drag-due-to-lift is shown in Figure 58.

The twist increment required by aeroelastic deformation was constrained in the previous solutions to a net differential of 5 degrees at the wingtip. An optimization was obtained for a twist differential of approximately 7 degrees, corresponding increased wing bending. The solution sought to unload the tip region. With less twist, the solution compensated by increasing the trailing edge flap deflections. The drag was slightly higher than the previous solution. This result indicated that the bending requirement could be reduced without any drag penalty. The wing twist was constrained to the distribution shown in Figure 59 with a 4-degree differential at the tip. The drag polar is shown in Figure 58. The elevon and aileron deflections were now of reasonable magnitude, -6.4 and -7.4-degrees, respectively.

A two-segment canard leading edge device was then assumed. Also, the hinge line was moved aft at the tip to more effectively uncamber this region. The canard leading edge device hinge line extends now from 20-percent chord at the root to 30-percent chord at the tip. The drag polar is shown in Figure 58 for the final optimization.

Substantial supersonic cruise drag-due-to-lift penalities (above optimum) remain for a leading and trailing edge system on both the canard and wing. Elimination of canard variable camber devices further decreases lifting efficiency. Aeroelastic bending requirements are moderate as indicated by the twist characteristics shown in Figure 59.
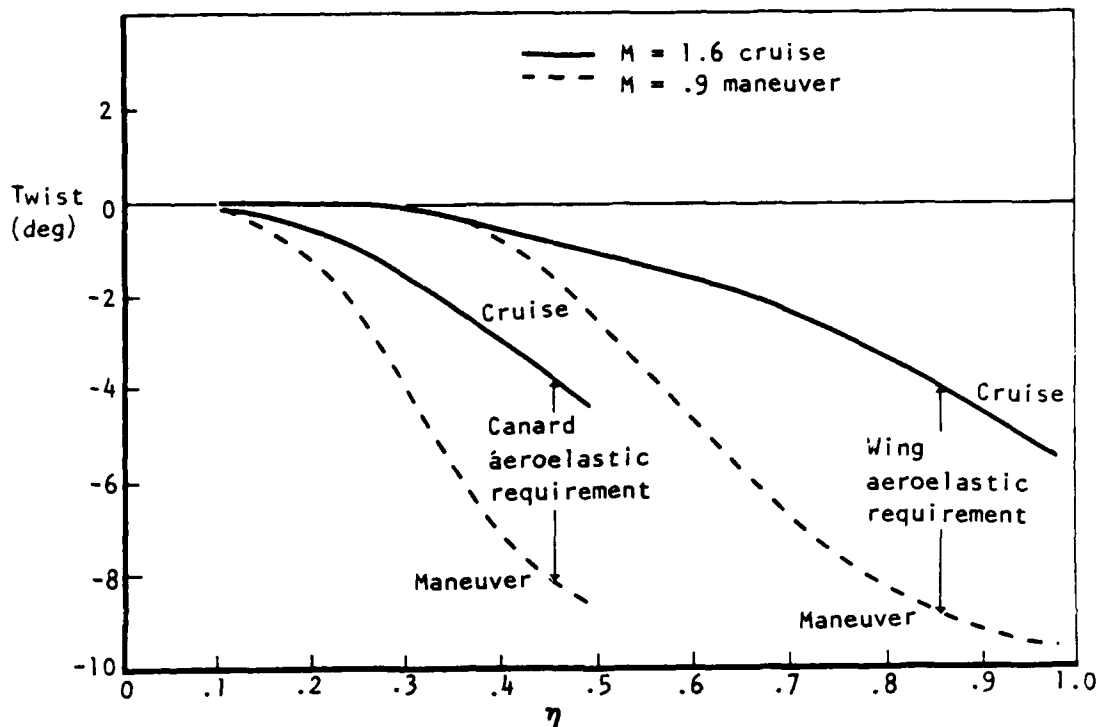
Figure 59.   Maneuver bias twist requirement for supersonic cruise

WAVE DRAG

A wave drag analysis of the maneuver bias configuration (Figure 40) was conducted with the method of Reference 3. Wave drag is compared with that for the HiMAT fighter in Figure 60. This wave drag reduction is due primarily to the increased wing sweep and reduction of the inboard wing thickness.

Several supersonic wave drag optimizations were obtained, and they indicated that the wave drag below M = 1.6 could be reduced by redistributing the fuselage volume to the region between the wing and canard. By adding volume during the optimization process, the engine cross-sectional area constraints could be held and wave drag reduction could still be obtained.

The baseline fuselage was retained for the maneuver bias configuration. It is felt that this represents the smallest impact on transonic maneuver performance. Large changes in volume distribution and possible wing-body blending are, at this time, considered to be in the domain of compromise designs.

Figure 60.   Maneuver bias supersonic wave drag.

SECTION IV

CRUISE/MANEUVER COMPROMISE

BASELINE

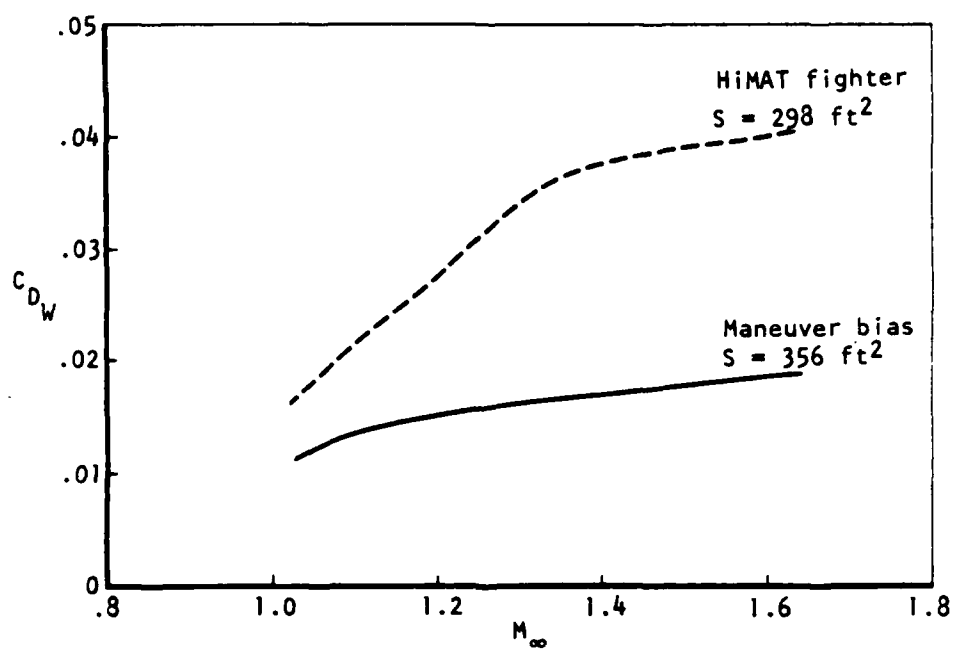An existing Rockwell ATS configuration was used as a starting point for deriving a compromise configuration. Vehicle size, powerplant, airframe propulsion system integration, etc, were established from this arrangement. Efficient $M = 1.6$ cruise and a midmission sustained 3.5 g, $M = 0.9$, maneuver at 30,000-foot altitude were the principal design criteria. The mission used in sizing the air-to-surface tactical fighter is indicated in Figure 61.

Maneuver requirement
- $n_z = 3.5$ $P_s = 0$
- $M = 0.9$
- $h = 30,000$ ft

M = 1.6, BCA

BCM, BCA

BCM, BCA

Loiter
20 min
@ S.L.

5% total
fuel
reserves

Base

- (1) $360°$ A/B turn ($M = 1.6$)
- Drop stores

M = 1.6, BCA

Target

200 n mi

FEBA

350 n mi
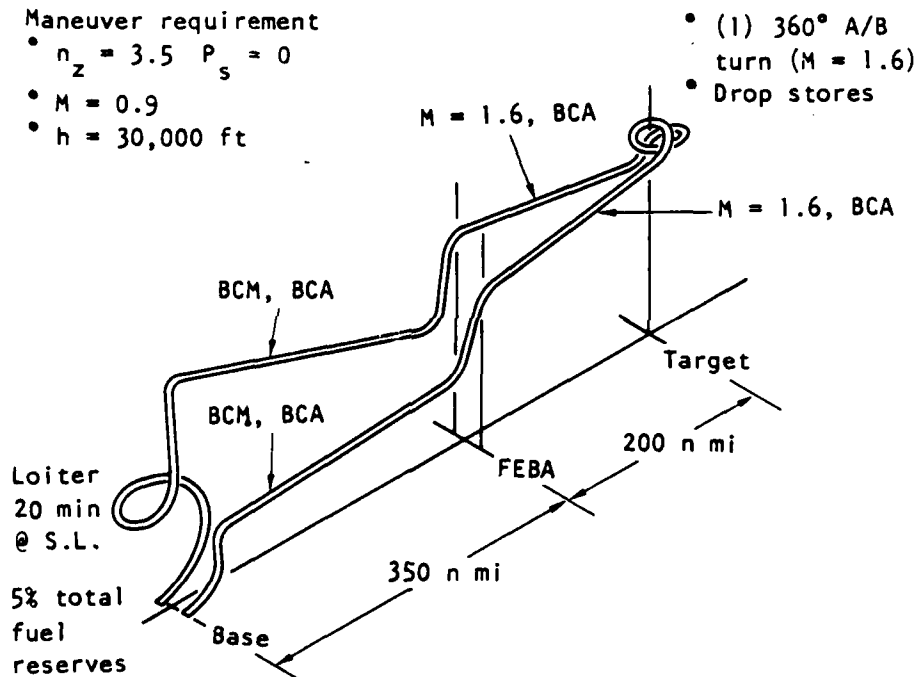
Figure 61. Compromise design mission.

CONFIGURATION DEVELOPMENT

A comparison of the supersonic and maneuver bias design drag-due-to-lift efficiency of Figure 62 indicates the technique of increasing the camber and twist of a low-design C_L wing (using a deflectable leading/trailing edge system and aeroelastic tailoring, respectively) is a preferred approach compared to reducing the camber and twist of a high-design C_L wing. On the basis of this finding, the supersonic bias wing-canard-tail was scaled to provide a midmission maneuver wing loading of 80 ($W/S = 80$) and was incorporated into the compromise vehicle definition. A summary of the compromise arrangement evolution in conjunction with pertinent geometric characteristics is presented in Figure 63.

Figure 62. Bias design lifting efficiency comparison.

Figure 63. Compromise configuration evolution.

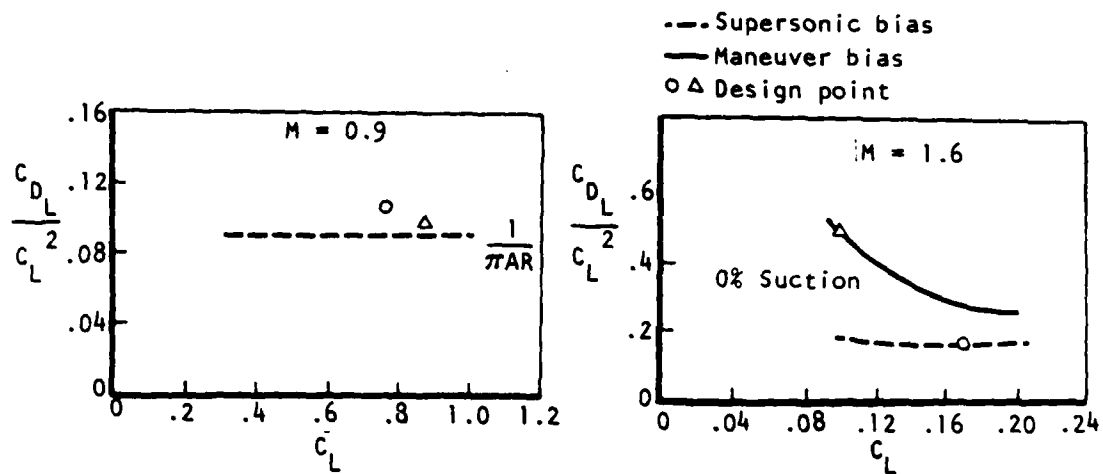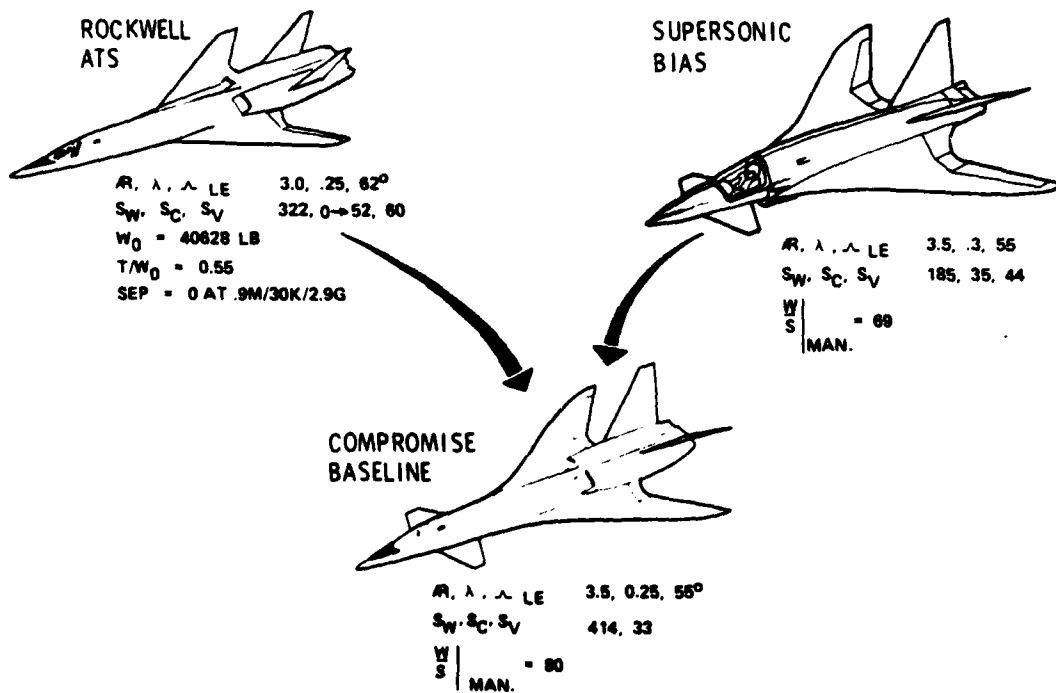Although the present study is primarily concerned with wing design, low-speed, high-lift characteristics and static longitudinal stability were established in order to refine the empennage size and wing location of the compromise baseline. Takeoff lift and balance is presented in Figure 64. A limit trimmed C_L of 1.48 at 15-degree angle of attack is indicated for 20-percent chord wing trailing edge flap with deflections of 20-degrees inboard and 10-degrees outboard (10-degrees were reserved for roll control). Canard overtrim provides a trimmed lift increment of 0.07, assuming a canard sectional $C_{\ell MAX} = 1.2$. The longitudinal stability of the compromise vehicle is presented in Figure 65. A 15%c statically unstable balance was used in order to reduce supersonic trim drag penalties.
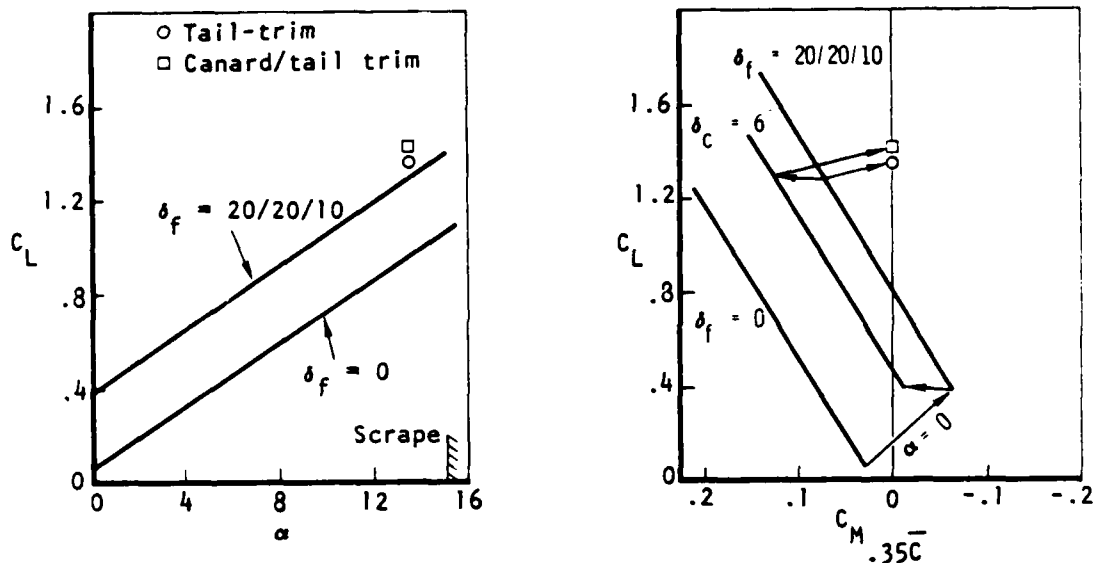
Figure 64. Low-speed trimmed characteristics, M = 0.2.

Having established the compromise configuration general arrangement, the wing design is initiated in accordance with Figure 66. The approach is based on modification of the supersonic bias design cycle to significantly increase the supersonic design C_L in excess of that required for cruise in recognition of the higher wing box camber required for good transonic maneuver flow quality. An iteration loop to locally increase the box camber has been incorporated in the maneuver design to further facilitate a compromise between the supersonic cruise and transonic maneuver points. The basic camber philosophy is to limit its magnitude in order to realize modest supersonic cruise drag-due-to-lift penalties, but at the same time to reduce the variable camber system chord extents, number of elements, deflections, etc, required to attain a controlled supercritical maneuver flow.

52

$$S_{REF} = 414.5 \text{ ft}^2, \ CG = 0.35\bar{c}$$

Canard
△ On
◇ Off

dC_M/dC_L   vs   Mach number

C_{L_α}   vs   Mach number
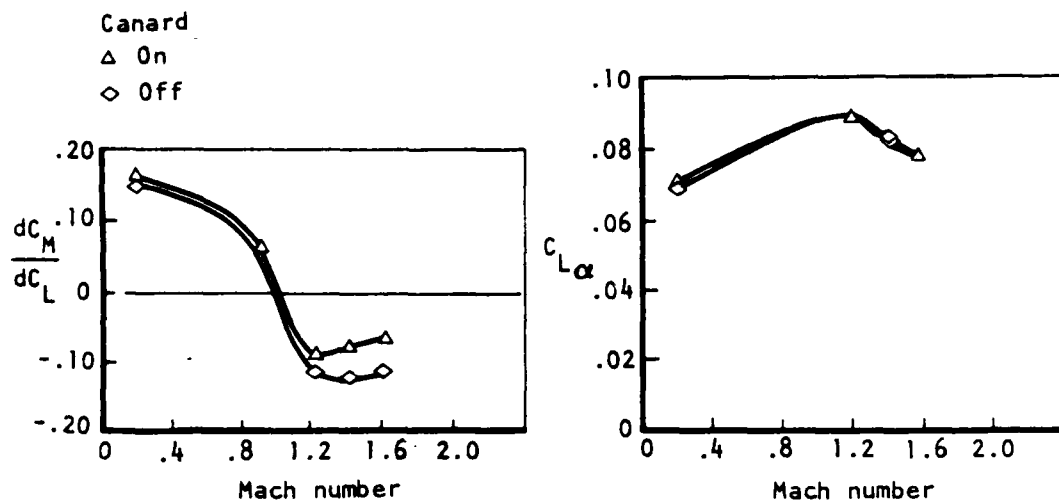
Figure 65. Effect of mach number on longitudinal stability.

CONFIGURATION

WAVE DRAG OPT ──────▶ THICKNESSES DISTRIBUTION

OPTIMIZE 0%
SUCTION DRAG ──────▶ CAMBER
& TWIST

SUPERSONIC
DESIGN
M = 1.6
C_L = .21

ASSUME
VARIABLE CAMBER ──────▶ CONSTRAINED OPT
SYSTEM   CAMBER
& TWIST

MODIFY VARIABLE
CAMBER SYSTEM

TRANSONIC
NON-LINEAR
ANALYSIS

NO

OK?

YES

BOUNDARY
LAYER
ANALYSIS

MODIFY WING
BOX CAMBER

MANEUVER DESIGN
M = .9
C_L = .77

EVALUATE BOX COMPROMISE
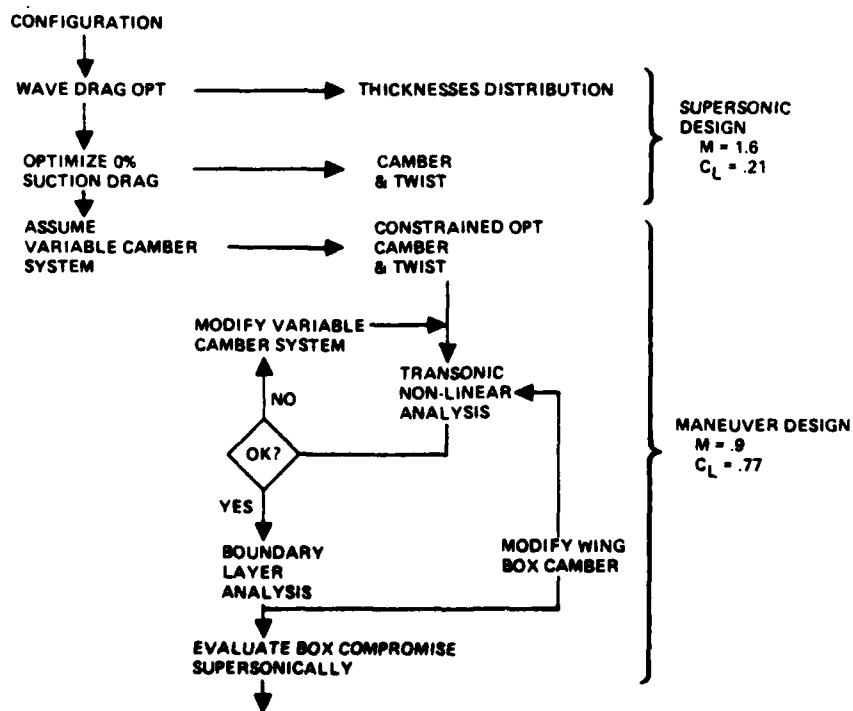SUPERSONICALLY

Figure 66. Compromise design approach.

53

SUPERSONIC DESIGN

Constant-volume supersonic wave drag optimization was performed, and the results are presented in Figure 67 for design mach numbers of M = 1.2, 1.4, and 1.6. The compromise baseline and supersonic bias design are shown for comparison purposes. The solution removed the wing trailing edge blending in the process of deriving the wing section definition. The M = 1.4 design generally provides the lowest overall wave drag levels as a result of requiring fewer wing constraint points to obtain a practical solution and is competitive with the supersonic bias design. The M = 1.4 optimized fuselage geometry and wing sections are presented in Figures 68 and 69, respectively. Cockpit, nacelle capture area, and 4-percent minimum wing thickness constraints were observed in addition to constant wing-body volume.
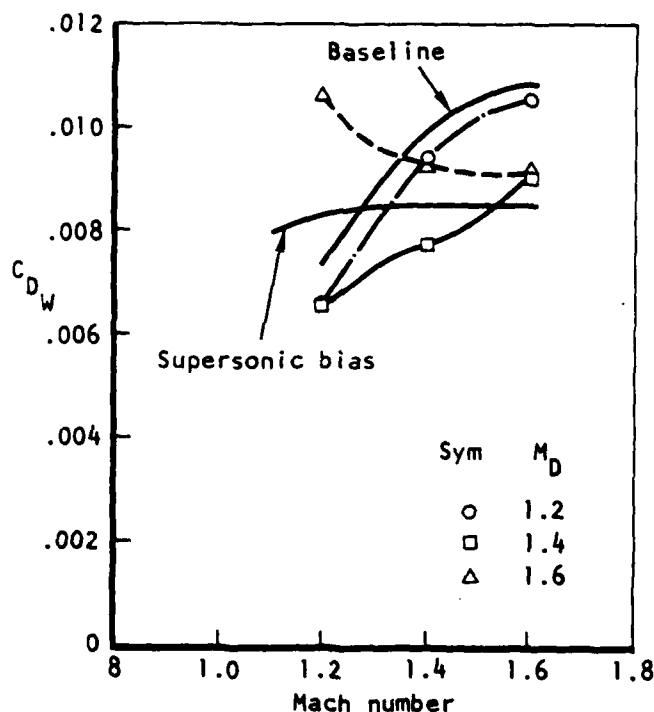

Figure 67. Compromise design wave drag optimization.

The trimmed zero-suction drag-due-to-lift was optimized at M = 1.6 and C_L = 0.206, which is 25-percent higher than required for cruise in recognition of the higher wing box camber required for transonic maneuver. The results are presented in Figure 70 and are compared to the flat-plate original ATS configuration. The goal of modest supersonic drag-due-to-lift penalty relative to the uncompromised supersonic bias design is realized. The associated supersonic design twist and camber are presented in Figure 71. The results vary smoothly with peak camber and twist values of 1.1 percent and -4.6 degrees, respectively, at the wingtip.

Figure 68. M = 1.4 optimum fuselage.

······ Original contour ⎫ Constant
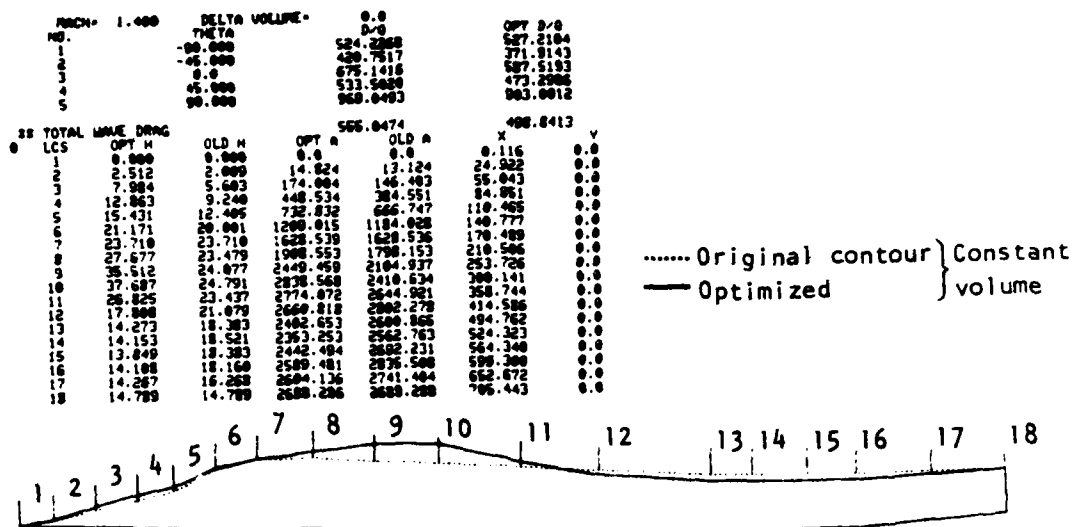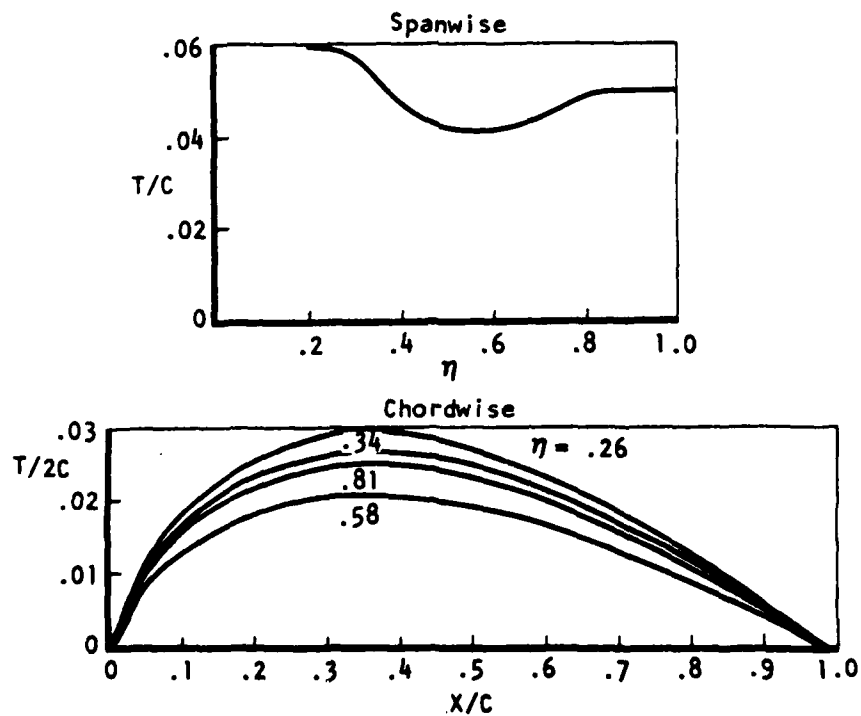—— Optimized ⎬ volume
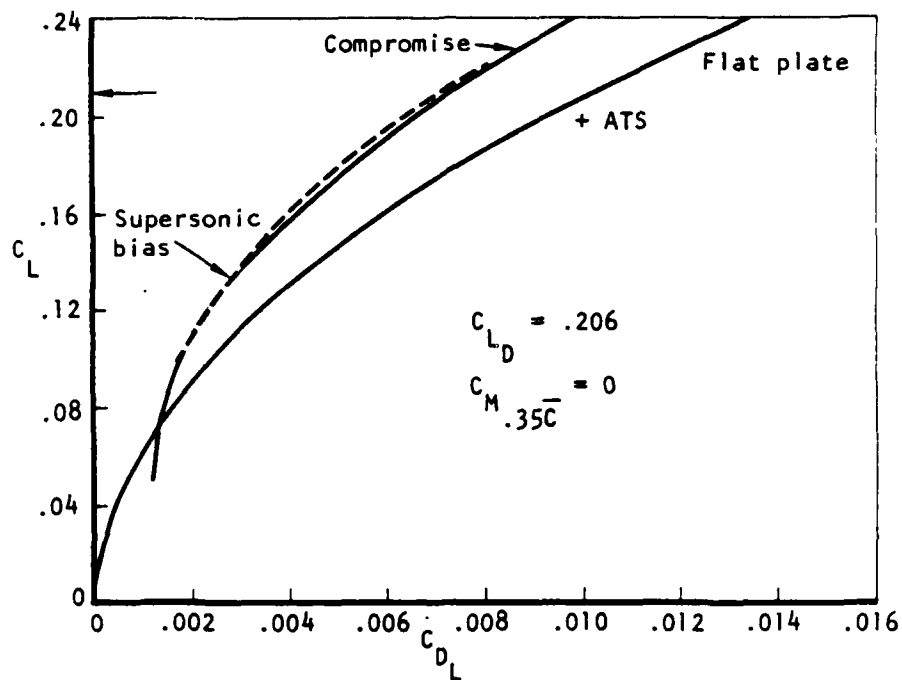

Figure 69. M = 1.4 optimum wing thickness.

Figure 70. Compromise zero suction drag due to lift at M = 1.6.
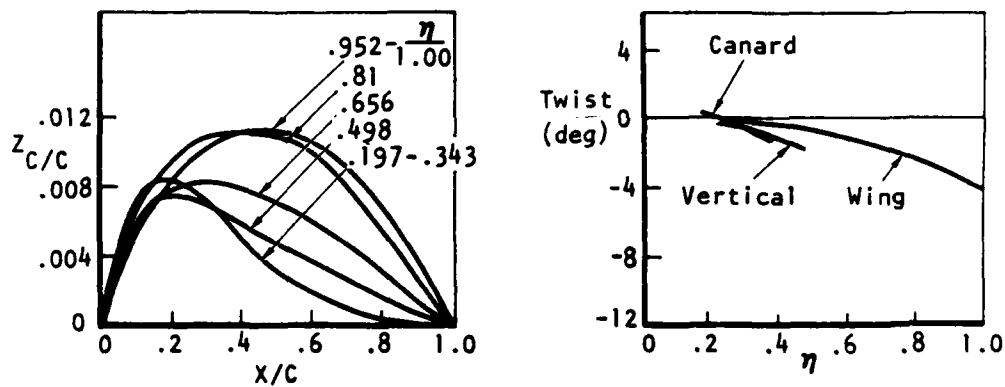
Figure 71. Compromise supersonic twist and camber design,
M = 1.6, C_{LD} = 0.206.

TRANSONIC MANEUVER DESIGN

A variable camber system for use at transonic maneuver conditions was incorporated into the candidate supersonic design in accordance with Figure 66.

A three-chordwise-element/two-spanwise-segment leading edge device of 20-percent chord extent inboard and 30-percent chord extent at the tip was selected in conjunction with a single-chordwise-element/three-spanwise-segment 20-percent chordtrailing edge flap for the study. A sketch of the leading/trailing edge flaps is presented in Figure 72. A basic goal of the variable camber devices is to achieve a satisfactory maneuver flow quality with a system that is substantially simpler than that employed for the supersonic bias design. The canard was constrained to the supersonic design twist and camber.

Figure 72. Linear optimum leading and trailing edge deflections,
M = 0.9, C_{LD} = 0.40.

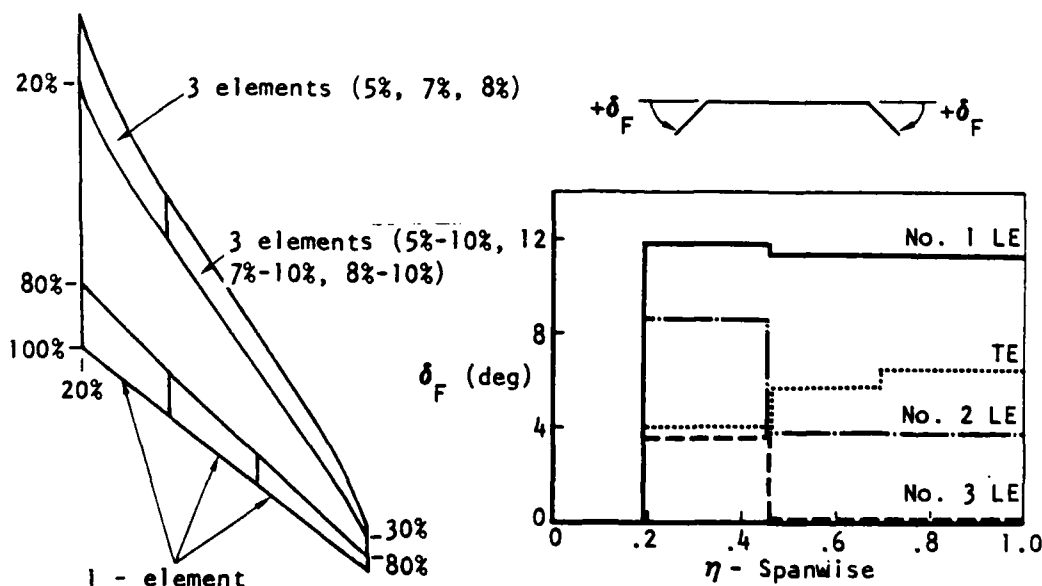A linear zero-suction drag-due-to-lift flap optimization was performed at M =
0.9 and C_L = 0.40. The purpose of this step is to develop candidate maneuver
wing section definitions for subsequent use in nonlinear transonic relaxation analysis
refinement. The resulting maneuver deflections and twist/camber are presented in
Figures 72 and 73, respectively. Examination of the results indicate a maximum
leading edge deflection of 12 degrees and a 4- to 6-degree trailing edge deflection.
The results further indicate the potential of using a two-chordwise-element leading
edge device in the outboard 55 percent of the wing span. Maximum camber of 2.5
to 4 percent of local wing chord and a twist angle of -9 degrees at the wingtip are
indicated. The twist difference between supersonic cruise and maneuver is optimally
provided by aeroeleastic tailoring since the desired leading and trailing edge
deflections result in minor net twist. The increment in wing box twist required
from structural deflection is consistent with that attained during the HiMAT RPRV
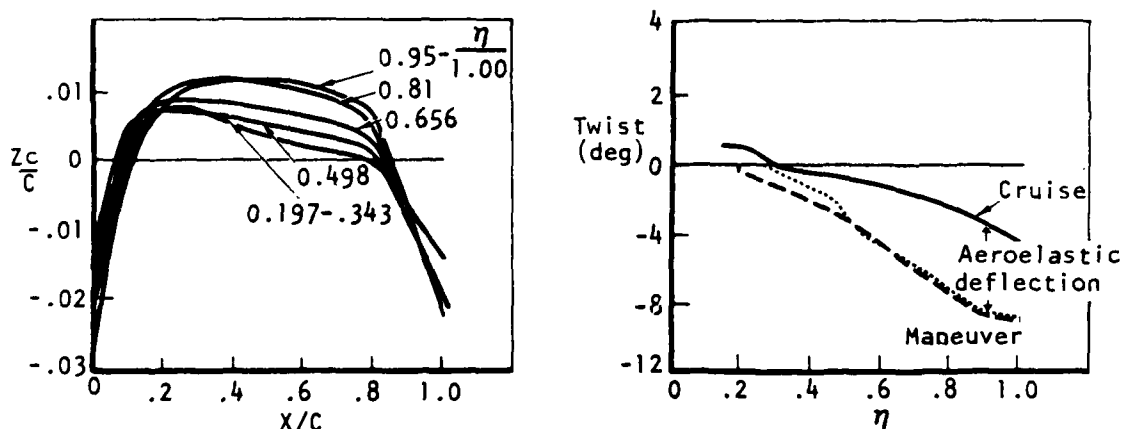development.

Figure 73. Candidate maneuver wing twist and camber,
M = 0.9, C_{LD} = 0.40.

A linear theory assessment of the candidate transonic design maneuver span loading is presented in Figure 74. A limit perpendicular sectional lift of 1.8 was observed based on past transonic design experience.
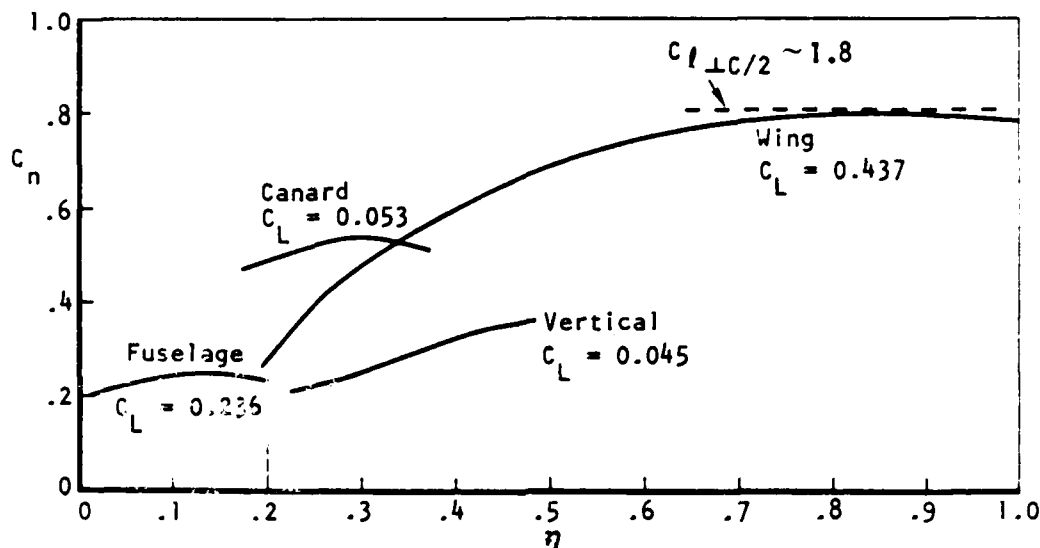

Figure 74. Linear theory span load at maneuver design point,
M = 0.90, C_L = 0.77, α = 10.46°

Transonic assessment of the candidate maneuver configuration was based on the modified small-disturbance analysis of Reference 9 in order to incorporate the impact of the fuselage. The transonic interference of the canard on the wing is approximated by twisting the wing for the canard downwash/upwash field. This interference is evaluated using a mixed linear analysis in which tangential flow boundary conditions are specified on the canard-body and $C_{P_{NET}}$ = 0 on the wing plane. The resulting twist correction is presented in Figure 75 and was used to adjust the candidate transonic wing design twist of Figure 73. The simplified body input definition was used in conjunction with a fully conservative, modified, small-disturbance formulation [9] and a 61 by 28 by 20 inner and 30 by 19 by 12 outer mesh. The resulting maneuver quality is presented in Figure 76. Excessive flow acceleration occurred on the upper wing surface at the trailing edge flap hinge line. The flap chord extent was increased from 20 to 25 percent, and the outboard flap segment deflection was decreased from 6.4 to 4 degrees, to reduce this effect. The resulting airfoil section and maneuver flow quality are presented in Figures 77 and 78.
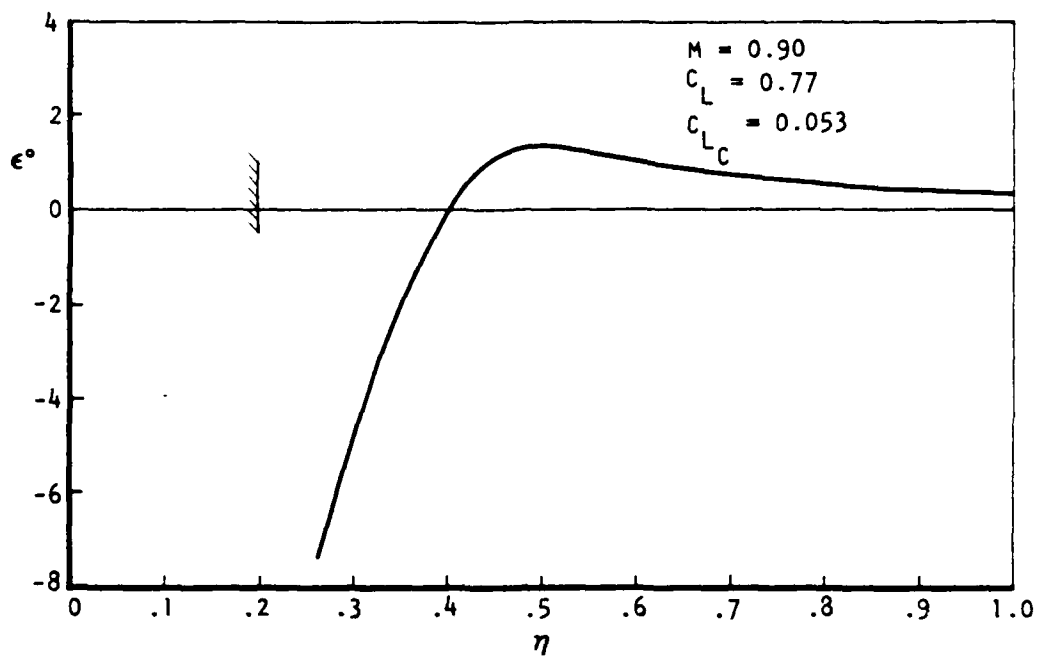
Figure 75. Canard induced wing downwash.

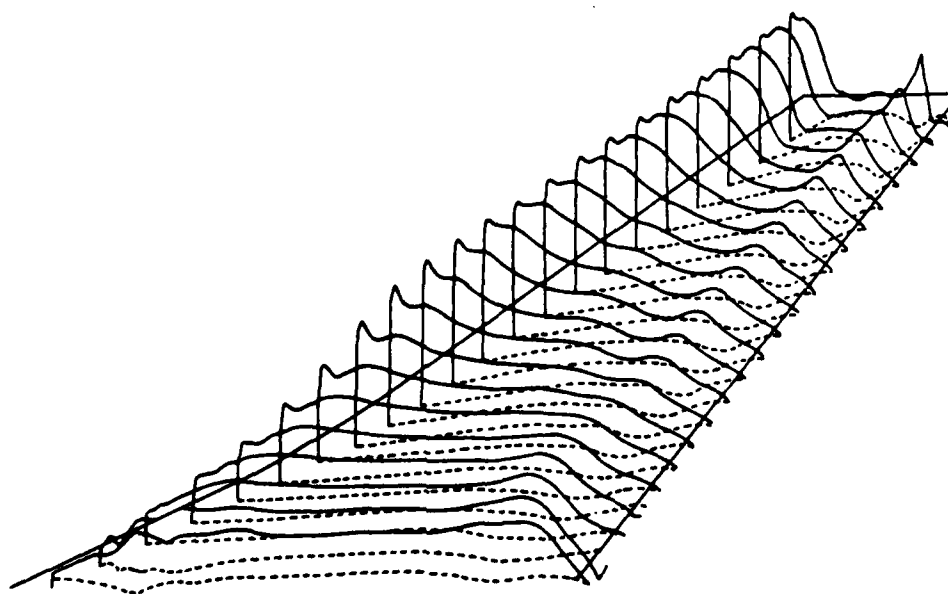Figure 76. Initial compromise wing maneuver flow,
M = 0.9, = 10.46°.

MESH
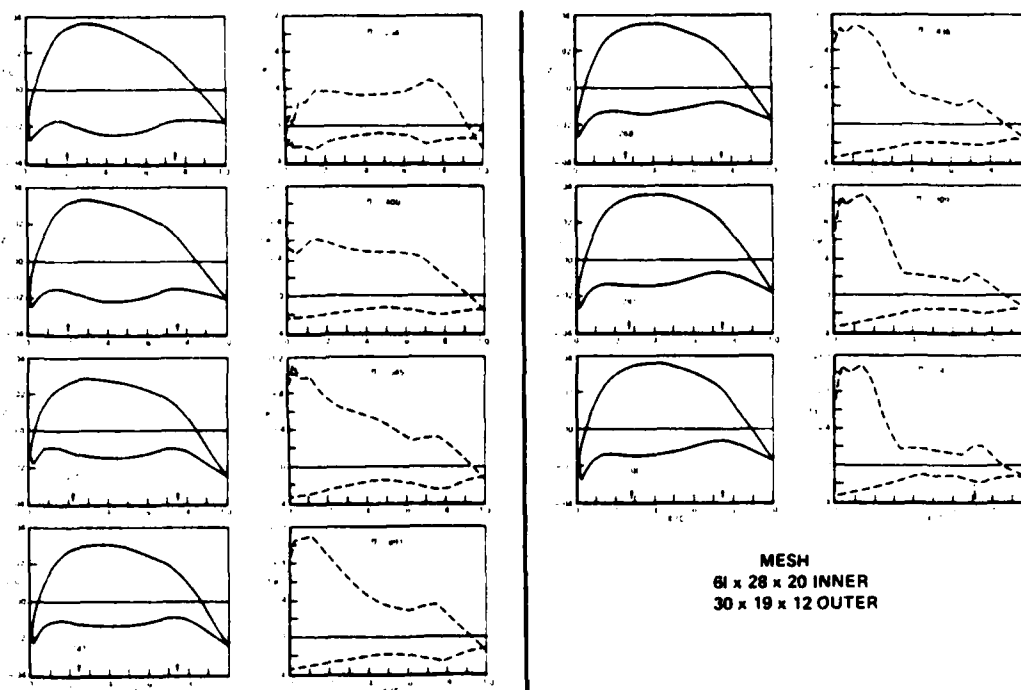**6l x 28 x 20 INNER**
30 x 19 x 12 OUTER

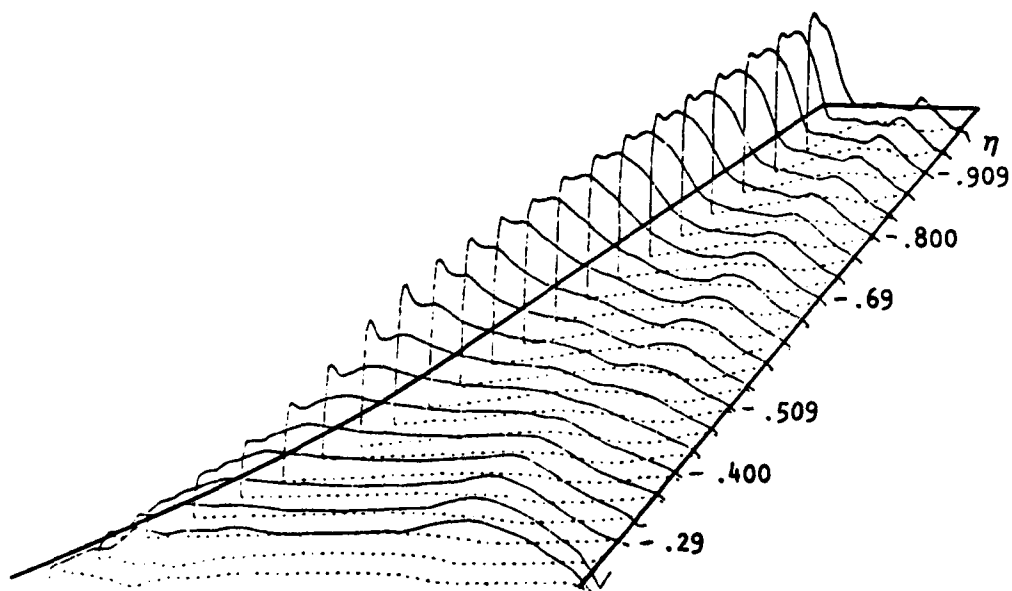Figure 77. Compromise wing maneuver point characteristics,
M = 0.9, = 10 deg.

Figure 78. Compromise wing maneuver flow, M = 0.9, = 10°.

61

Increased leading edge flap deflection was considered in an effort to reduce the peak suction pressure and shock strength in the wing outboard region ($\eta > .85$). The flow quality was not significantly improved. Increased loading of the inboard portion of the wing (by increasing the leading edge flap deflection and wing incidence) was attempted in order to reduce the angle of attack. This effort was not particularly successful in reducing the outboard wing leading edge loading. Additional wingspan box camber will apparently be required in the outer 15 percent of the wingspan to improve the maneuver flow quality in this region.

The status transonic maneuver twist-and-flap-deflection schedule are presented in Figure 79. A two-element, 20-percent chord leading edge and one-element, 25-percent chord trailing edge device achieves the compromise design goal of a substantially simpler system than developed for the supersonic bias design. It is emphasized that the deflectable surfaces considered throughout this study employ localized smoothing at the hinge line to eliminate camber discontinuities and associated overacceleration of the flow.
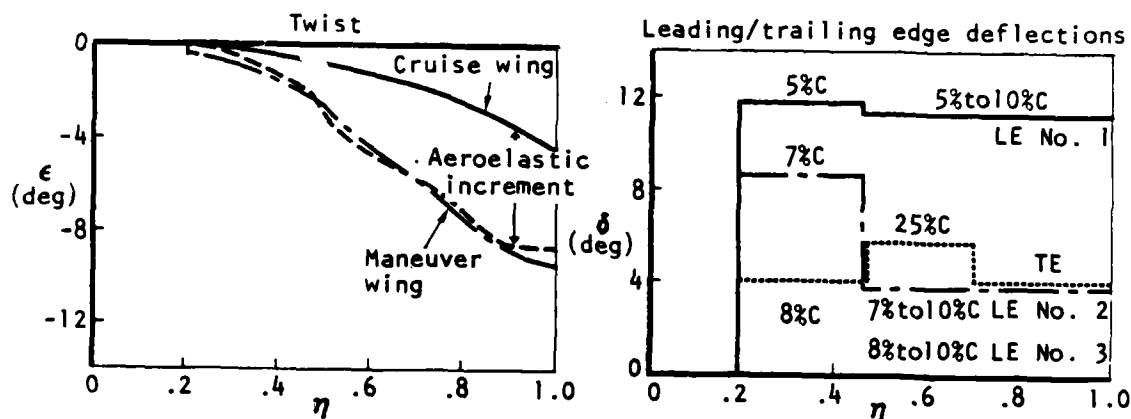

Figure 79. Compromise wing maneuver twist and variable camber
deflections, M = 0.9, α = 10 deg.

62

Viscous evaluation of the status maneuver wing flow was based on a three-dimensional finite-difference boundary layer analysis [9]. Infinite-yawed wing side edge approximations and X:Y:Z mesh of 23:11:20 were used. The wing leading edge sweep and unit Reynolds number produced an essentially fully turbulent flow as a result of cross-flow transition. Normal displacement thickness results are presented in Figure 80 for maneuver flight condition of M = 0.9 and 30,000-foot altitude. Use of the separation wall stress (normal to the local element line) criteria resulted in a systematic weakening of the adverse pressure gradient in the tip region (η = 0.982), indicated by the dotted line of Figure 80. Efforts to maintain attached flow closer to the trailing edge resulted in the pressure distribution labeled redesign goal, which was successful in limiting separation to approximately the last 5 percent of the root chord. Although further efforts to weaken the adverse pressure gradient at the inboard trailing edge (by decreasing the flap deflection to 2 degrees) were successful, improved boundary layer recompression was not indicated. Owing to the uncertainty of specifying wing side edge boundary conditions, the analysis was not pursued further.
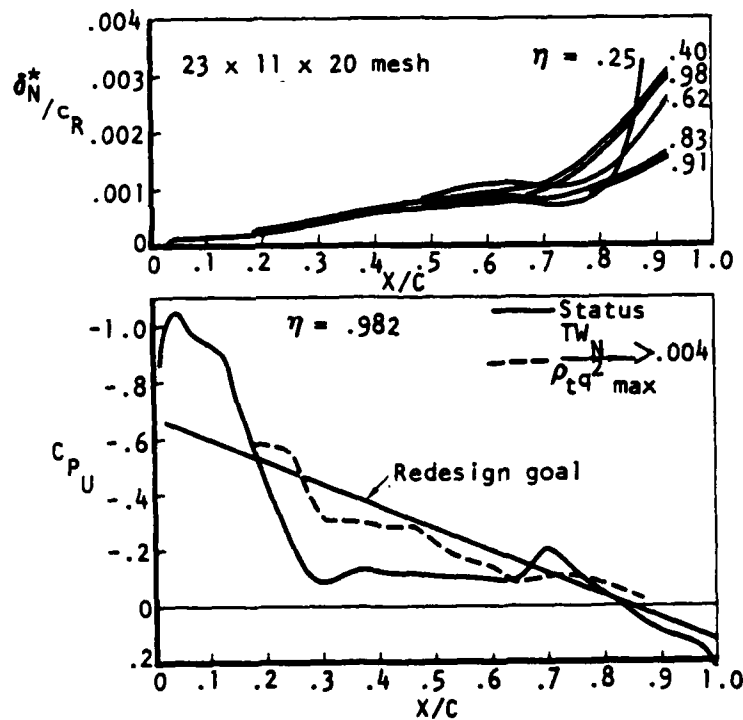

Figure 80. Maneuver point boundary layer evaluation,
M = 0.9, H = 30K, R_{CR} = 43 x 10^6.

SECTION V

DESIGN COMPARISONS

The supersonic bias, maneuver bias, and compromise designs of the present study are compared to each other and the HiMAT RPRV, HiMAT advanced fighter, and ATS in Figure 81. Planform parameters, transonic maneuver design characteristics, and vehicle size class are indicated.

Configuration	$S_w/S_c \sim Ft^2$	R_w	Λ_{LE}	λ	$\frac{W}{S}\big|_{man}$	Maneuver N_Z	Maneuver C_L **	Design C_L Wing/canard	$W_{TO} \sim LB$
HiMAT RPRV	58/ 17.4	3.85	45	.25	53	8	1.18	.75/.25	3370
HiMAT Fighter	298/89	3.85	45	.25	47	8	1.05	.8/.2	17000
Supersonic Bias	185/35	3.5	56	.3	69	4	.77	.7/.05	15700
Maneuver Bias	356/121	3.44	53.5	.25	39	8	.95	.6/.2	17000
ATS	322/0 → 52	3.0	62	.25	85.8	2.9	.70	—	40628
Compromise	414/47.7	3.5	55	.25	80	3.5	.77	.45/.05	—

*1/2 Fuel without armament
**M = 0.9, h = 30,000 ft, q = 357 lb/ft^2

Figure 81. Design comparisons.

The maneuver bias design was derived from the advanced fighter derivative of the HiMAT RPRV by degrading the maneuver CL through increasing the wing sweep 10 degrees in order to improve supersonic volumetric efficiency (Figure 60).

The supersonic bias and compromise designs were derived from the supercruise and ATS configurations, respectively, by reducing the wing sweep and increasing the aspect ratio in order to improve transonic maneuver efficiency. A 10-percent higher maneuver C_L was achieved while maintaining supersonic volumetric efficiency (Figures 10 and 67) and increasing the supersonic cruise lifting efficiency (Figure 70).

A major result derived from the present study is indicated in Figure 82, which compares the maneuver and supersonic drag-due-to-lift efficiency of the various designs. The use of deflectable leading and trailing edge devices to decamber a high design C_L wing results in substantial supersonic cruise drag due-to-lift penalties. Cambering a low-design C_L wing for transonic maneuver produced reasonable flow quality, as judged by boundary layer calculations and the absence of strong shocks.

Comparison of the compromise and supersonic bias designs indicates equivalent levels of aerodynamic performance can be achieved with a substantially reduced variable camber system complexity (Figures 27 and 79). An increased maneuver C_L = 0.05 is forecast for the compromise vehicle from horizontal tail trim considerations resulting from the 4-percent unstable longitudinal stability level at M = 0.90.

Finally, the results of Figure 82 indicate that a family of wing designs exist in which increased supersonic camber penalties are accepted by increasing the design C_L in order to build in larger amounts of wing box camber for increased transonic maneuver capability.
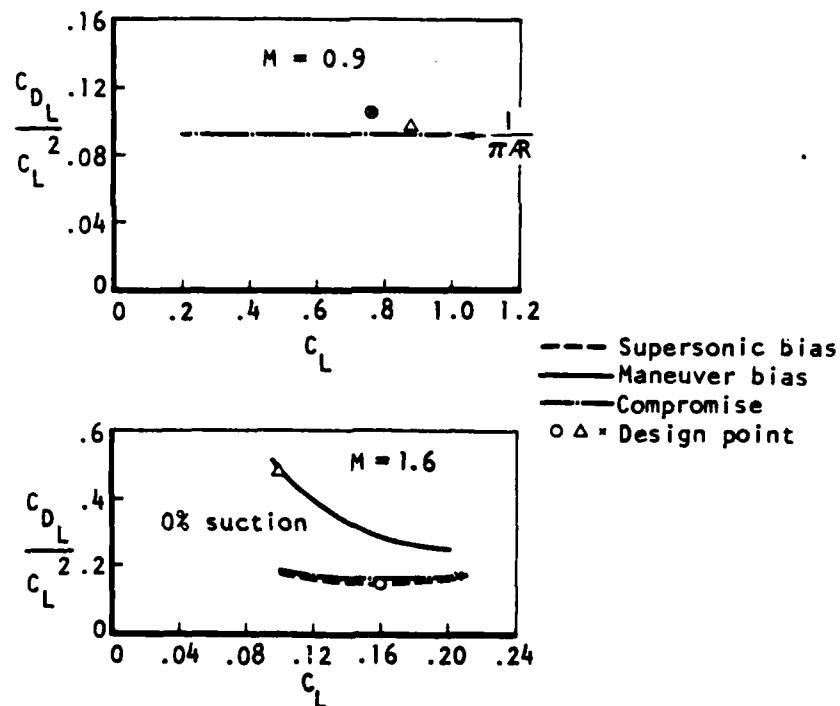

Figure 82. Aerodynamic lifting efficiency.

SECTION VI

CONCLUSIONS

1. Supersonic cruise efficiency emphasizes increased wing sweep with corresponding higher perpendicular sectional lift for a given maneuver condition.

2. Transonic maneuver efficiency emphasizes decreased wing sweep, increased wing aspect ratio, and reduced wing loading.

3. At the maneuver condition, the design section lift has been increased relative to current designs. That is, the perpendicular section lift where a weak shock, minor trailing edge separation condition can be maintained has been increased to allow higher transonic efficiency with a higher wing sweep for supersonic considerations.

4. Cruise/maneuver point camber matching is best satisfied through the use of both leading and trailing edge devices.

5. Cruise/maneuver point twist matching is best satisfied aerodynamically using aeroelastic tailoring.

6. The approach of decambering a high-design C_L wing results in large supersonic drag-due-to-lift penalties and a relatively complicated variable camber system.

7. Judgment of maneuver flow quality is more subjective than desired for performing variable camber system trade-offs.

8. A number of computational deficiencies were found during the present study. The more noteworthy were a lack of a transonic multisurface capability, reliability of transonic drag predictions, and uncertainties concerned with specifying wing root chord conditions for boundary layer analysis.

9. Experimental validation of the compromise design approach, methodology, and performance is required.

REFERENCES

1. Dunn, K., "Rockwell Unified Distributed Panel Program," Rockwell Document TFD-75-713, 1975.

2. Bonner, E., Clever, W., and Dunn, K., "Aerodynamic Preliminary Analysis System Part I - Theory," NASA CR-145284, April 1978.

    Divan, P., Dunn, K., and Kojima, J., "Aerodynamic Preliminary Analysis System Part II - User's Manual and Program Description," NASA CR-145300, April 1978.

3. Bonner, E., "Wave Drag Optimization of a Three Dimensional Thickness Distribution of Fixed Planform," Rockwell Document TFD-75-260, March 1975.

4. Clever, W., "Wing Twist and Camber Optimization Program," Rockwell Document TFD-78-532, July 1978.

5. Bauer, F., Garabedian, P., Korn, D., and Jameson, A., "Supercritical Wing Sections II," Lecture Notes on Economics and Mathematical Systems, Springer-Verlag, New York, 1975.

6. Jameson, A., and Caughey, D.A., "A Finite Volume Method for Transonic Potential Flow Calculations," AIAA 3rd Computational Fluid Dynamics Conference Proc, pp 35-54, June 1977.

7. Vanderplaats, G.N., "CONMIN - A Fortran Program for Constrained Function Minimization," NASA TM X-62,282, 1973.

8. Hicks, R., and Henne, P.A., "Wing Design by Numerical Optimization," AIAA Paper 77-1247, 1977.

9. Mason, W.H., et al, "An Automated Procedure for Computing the Three Dimensional Transonic Flow Over Wing-Body Combinations, Including Viscous Effects," AFFDL-TR-77-122, February 1977.

10. Bonner, E., "Prediction of Infinite Yawed Wing Transonic Viscous Characteristics," Rockwell Report NA-76-441, August 1976.

11. Bradshaw, P., "Calculation of Three-Dimensional Turbulent Boundary Layers," J. Fluid Mechanics, Vol 46, Part 3, pp 417-445, 1971

12. Child, R.D., et al, "Design and Analysis of a Supersonic Penetration/Maneuvering Fighter," Rockwell RePort NA-75-118, April 1975.

13. Gingrich, P.B., Child, R.D., and Panageas, G.N., "Aerodynamic Development of the Highly Maneuverable Aircraft Technology Remotely Piloted Research Vehicle," NASA CR-143841, June 1977.

END

DATE
FILMED
3-82

DTIC